WESTFÄLISCHE
WILHELMS-UNIVERSITÄT
MÜNSTER

Westfälische Wilhelms-Universität Münster

Soft Gluon Resummation for Heavy Particle Production at the Large Hadron Collider

Author:

Vincent Michel Theeuwes

Supervisor:

Jun. Prof. Dr. Anna Kulesza

Completed: September 23, 2015

Updated version: March 24, 2016

Theoretische Physik

Soft Gluon Resummation for Heavy Particle Production at the Large Hadron Collider

Inaugural-Dissertation

zur Erlangung des Doktorgrades

der Naturwissenschaften im Fachbereich Physik

der Mathematisch-Naturwissenschaftlichen Fakultät

der Westfälischen Wilhelms-Universität Münster

vorgelegt von

Vincent Michel Theeuwes

aus Nijmegen

- 2015 -

Abstract

With the discovery of the Higgs boson in Run 1 of the LHC and the measurements of Run 2 eagerly awaited, precision prediction of production cross sections are essential to the progression of particle physics. In this light, we present possible improvements to the current predictions for processes both of the Standard Model and beyond. We focus on the inclusion of higher order logarithmic terms originating from the emission of soft and collinear gluons by means of threshold resummation. These corrections are explored in the context of different types of processes: $gg \rightarrow ZH$, squark and gluino production and $2 \rightarrow 3$ processes. For $gg \rightarrow ZH$ production the scale uncertainty is significantly reduced due to the inclusion of contributions at next-to-leading logarithmic accuracy in the resummation. When these contributions for the gluon initial state are added to the total $pp \rightarrow ZH$ cross section, this results in an overall reduction of the scale uncertainty by a factor two. The resummation for the squark and gluino production is performed at next-to-next-to-leading logarithmic accuracy and results in significant enhancements in the cross section. Additionally the scale dependence is mostly reduced with respect to the result at next-to-leading logarithmic accuracy. The exception is the gluino pair production which has a minor increase in scale dependence. Finally we extend the resummation formalism to $2 \rightarrow 3$ processes by means of the example of $pp \rightarrow t\bar{t}H$. For this process we present the the numerical results for absolute threshold resummation. In addition the resummation formalism for differential cross sections is presented.

Contents

1 Introduction

Through mankind's search to explain the world around them, even at the most fundamental level, the Standard Model (SM) was proposed. The SM describes the elementary particles and their interactions. It was formulated in the 1970s in its current form. The elementary particles of this version of the SM are six leptons and six quarks, which interact through the exchange of gauge bosons resulting in the electroweak and strong forces. The electroweak model was proposed by Weinberg, Glashow and Salam [1–3]. The model of the strong interaction was constructed by Fritzsch, Gell-Mann, Leutwyler, Gross, Wilczek and Weinberg [4–6]. All the masses of the massive particles (except neutrinos) are provided through the Higgs-mechanism [7–9], which will be explained in greater detail in Chapter 2. This same mechanism also results in the Higgs boson, which was discovered in 2012 [10, 11].

The collider experiments confirm the SM at great accuracy. However, we know that the SM is not the complete theory for physics at a fundamental level. This is because there are still phenomena that cannot be explained by the SM, for example gravity and dark matter. Therefore, theories beyond the Standard Model (BSM) still need to be explored.

The details of the SM that are still unknown are the exact couplings of the recently discovered Higgs boson. The new Large Hadron Collider (LHC) run, which started in 2015 at higher energy and luminosity, should help to improve the experimental precision of the Higgs boson results. However, this also requires an improvement in the theoretical calculations. A deviation of the properties of the Higgs boson could imply a more complex Higgs sector with multiple Higgs bosons or couplings to new particles in loops. Greater precision in determining the properties of the Higgs boson will therefore allow us to confirm or exclude certain BSM theories.

Another way in which we can confirm or exclude BSM theories is through new particle searches. One example of an extension of the SM that adds a large number of particles that are yet to be discovered is supersymmetry (SUSY) [12, 13]. SUSY introduces an extra symmetry between fermions and bosons and therefore adds a partner to every particle we currently know of. More will be explained about this theory in Chapter 3. In SUSY the particles with the largest production cross section are the colored particles, squarks and gluinos. These are the super partners of the quarks and gluons respectively. These particles are typically heavy, with masses of the order of TeV.

In quantum field theory cross sections are computed through perturbation theory, order by order in the coupling. The cross section at leading order (LO) is the cross section calculated with the lowest order in the couplings. However there are different couplings in the SM. Therefore we can compute up to next-to-leading order (NLO) in quantum chromodynamics (QCD) or in the electroweak theory. In this thesis we will focus on QCD corrections, which are described by the interactions between colored particles. Due to the size of the strong coupling and the fact that it increases for low scales colored particles are not detected alone, but form showers containing multiple emissions of colored particles. The fact that one can only detect showers, which are detected as a jet, means that we cannot distinguish between a quark and a quark that emits a gluon collinearly. Therefore not only the loop diagrams with the same initial and final

state particles need to be computed at higher orders, but also the emission of massless colored particles.

In these perturbative calculations the higher order terms in the coupling are neglected. Therefore, an estimation of the uncertainty this procedure introduces is needed. In the fixed order calculations a renormalization scale has to be used. The renormalization scale is introduced when canceling the effects due to the divergences at the ultraviolet momenta scales. In addition the factorization between the short distance hard process and the long distance description of the proton introduces another scale. These scales can be chosen freely and therefore the dependence on each of them should cancel up to the order at which the computations are done. The scale dependence is now an indicator of the potential size of the higher order contributions to the cross section. Other uncertainties are also introduced due to the description of the partons within the proton on the basis of fits to the experimental results and the size of the coupling which is fitted along side the description of the proton.

In the perturbative calculations of production cross sections there occur certain types of terms that can become large in certain regions of the phase space. One of the regions in which these large contributions occur is near threshold. In the threshold limit extra emitted gluons are forced into the soft limit. Soft emitted gluons provide large logarithmic contributions in this threshold variable. One possible definition of threshold is absolute threshold. Absolute threshold occur when the partonic center of mass energy is close to the kinematic restriction for the on-shell production of the final state particles (the sum of their masses). In the case of processes with two massive final state particles there is an additional enhancing effect near the absolute threshold called Coulomb correction. These Coulomb corrections originate from the exchange of a gluon between two slow moving colored particles. These different large contributions can spoil the perturbative nature of the series. Therefore the perturbative expansion should be reformulated near threshold in order to take these terms into account better. This reformulation is known as resummation and will be described in detail in Chapter 4.

The threshold contributions are important for a variety of processes. For SUSY particle production the effects near absolute threshold are important as the masses of the SUSY particles are very high compared to the hadronic center of mass energy at the LHC. This automatically brings the process close to threshold. Additionally for processes with gluons in their initial state the threshold effects are also important. This is because the gluons in the protons have a large probability to have only a small fraction of the proton momentum. Therefore the particles are brought close to threshold without requiring heavy particles in the final state.

In this thesis we will explore the usage of threshold resummation for soft-gluon emission for a variety of processes and study at different possible ways of defining the threshold variable. In Chapter 2 we will introduce the SM and discuss the basics of the Higgs boson and its properties. SUSY will be introduced in Chapter 3. The general structure of resummation will be explained in Chapter 4. In Chapter 5 resummation will be applied to gluon-induced Higgs Strahlung. The more advanced case of squark and gluino production will be treated in Chapter 6. The final case that will be treated is three particle production, where the techniques will be demonstrated by means of $t\bar{t}H$ production. This can be found in Chapter 7. Finally we will conclude and summarize in Chapter 8.

2 The Standard Model

In order explain the world at the most fundamental level, the SM was proposed. The starting point for the construction of the SM is a general Lagrangian for free fermions:

$$\mathcal{L} = i\bar{\psi}\left(x\right)\gamma^{\mu}\partial_{\mu}\psi\left(x\right) - m\bar{\psi}\left(x\right)\psi\left(x\right) \tag{2.1}$$

where ψ is the fermion field. For this Lagrangian we can require invariance under certain local symmetries, $\psi\left(x\right) \rightarrow e^{i\alpha^{a}\left(x\right)T^{a}}\psi\left(x\right)$. Here T^{a} is the generator of the gauge group that describes the local symmetry. Due to the requirement of invariance under these local symmetries, we need to introduce the gauge boson fields, $A_{\mu}^{a}\left(x\right)$, and a covariant derivative $D_{\mu} \equiv \partial_{\mu} - ig_{1}A_{\mu}^{a}\left(x\right)T^{a}$. The gauge boson fields transform as $A_{\mu}^{a}\left(x\right) \rightarrow A_{\mu}^{a}\left(x\right) + \frac{1}{g_{1}}\partial_{\mu}\alpha^{a}\left(x\right) + f^{abc}A_{\mu}^{b}\alpha^{c}$. Lastly in order to give the particles masses we need to introduce a scalar field with a vacuum expectation value, this will be explained in more detail in Section 2.1. Which fields and symmetries need to be introduced is determined through observations.

For the SM the local symmetry is $U(1) \times SU(2) \times SU(3)$. Here $SU(3)$ invariance leads to the gluons and the strong interactions. $SU(2)$ invariance leads to the W-field and finally $U(1)$ invariance leads to the B-field. The W- and B-fields mix due to electroweak symmetry breaking resulting in the massive W- and Z-bosons and the massless photon which are the mediators of the electroweak interactions.

These symmetries allow us to describe the fields of the SM in terms of their representations with respect to the symmetry group. The representation of the different SM particles can be seen in Table 2.1. For example the representation **3** of quarks means they are in a triplet configuration with the three different colors. These quarks can be changed from one color to another through interaction with the $SU(3)$ associated boson (the gluon). The singlet representation (**1**) means that this particle does not interact through this force carrier.

2.1 Higgs physics

The Higgs mechanism [7–9] (more formally called the Brout–Englert–Higgs mechanism) produces the electroweak symmetry breaking that provides the particles with their masses. The mass term in Equation 2.1 seems to be invariant under local symmetries. However, there is a problem for the $SU(2)$ symmetry. As shown in Table 2.1, the W-field only interacts with the left handed component of the fermions. The mass term can be rewritten into $m\bar{\psi}\left(x\right)\psi\left(x\right) = m\bar{\psi}_{L}\left(x\right)\psi_{R}\left(x\right) + m\bar{\psi}_{R}\left(x\right)\psi_{L}\left(x\right)$. As the left- and right-handed components change differently under the $SU(2)$ transformation, this mass term is not invariant under the local $SU(2)$ transformation. In addition the boson mass terms ($A^{\mu}A_{\mu}M^{2}$) are not invariant under any of the symmetries. As we know that there are massive fermions and massive bosons, we need some effect to generate these terms.

In order to solve this issue, we will introduce a new scalar field. This field is an $SU(2)$ doublet, ϕ, allowing for an interaction term between the left- and right-handed fields:

$$\mathcal{L} = -y\bar{\psi}_{L}\phi\psi_{R} = -y\left(\bar{\psi}_{u}, \bar{\psi}_{d}\right)_{L}\begin{pmatrix} \phi_{u} \\ \phi_{d} \end{pmatrix}\psi_{R} = -y\bar{\psi}_{u,L}\phi_{u}\psi_{R} - y\bar{\psi}_{d,L}\phi_{d}\psi_{R} \tag{2.2}$$

Particle representations		
Name	Symbol	$(SU(3), SU(2), U(1))$
Quarks		
Left-handed quark doublet	$Q = (u_L, d_L)$	$\left(\mathbf{3}, \mathbf{2}, \frac{1}{6}\right)$
Right-handed up-type quark	u_R	$\left(\mathbf{3}, \mathbf{1}, \frac{2}{3}\right)$
Right-handed down-type quark	d_R	$\left(\mathbf{3}, \mathbf{1}, -\frac{1}{3}\right)$
Leptons		
Left-handed lepton doublet	$L = (\nu_L, e_L)$	$\left(\mathbf{1}, \mathbf{2}, -\frac{1}{2}\right)$
Right-handed charged lepton	e_R	$(\mathbf{1}, \mathbf{1}, -1)$
Gauge bosons		
Gluons	g	$(\mathbf{8}, \mathbf{1}, 0)$
W-bosons	W	$(\mathbf{1}, \mathbf{3}, 0)$
B-boson	B	$(\mathbf{1}, \mathbf{1}, 0)$
Higgs		
Higgs boson	H	$\left(\mathbf{1}, \mathbf{2}, \frac{1}{2}\right)$

Table 2.1: The representations of the SM particles. Each of the quarks and leptons has 2 heavier families in addition. The fermions are split into left- and right-handed parts as only the left-handed part couples through the weak interaction (W). The W- and B-bosons are the interaction eigenstates. After symmetry breaking these will mix to form the mass eigenstates $W^{\pm}$, Z and the photon γ. Due to this the $U(1)$ representation labeled by the eigenvalue of the hypercharge generator Y is related to the electric charge $Q = T_3 + Y$, where T_3 is the third component of the $SU(2)$ isospin. Right-handed sterile neutrinos can also be added to the SM, but they do not couple to any particles.

This only provides an interaction term. In order to provide a mass term we need the scalar field to have a vacuum expectation value (VEV). This VEV needs to be generated by the potential of this new scalar field. How to obtain this VEV will be presented later in this section. In this manner we can expand our field around the VEV as $\phi = \langle\phi\rangle + h$, with $\langle\phi\rangle$ the VEV. By expanding the field near the VEV we are breaking the $SU(2) \times U(1)$ symmetry. This results in a mass and interaction term in the form:

$$\mathcal{L} = -y\bar{\psi}_L\phi\psi_R = -\frac{yv}{\sqrt{2}}\bar{\psi}_{d,L}\psi_R - yh_u\bar{\psi}_{u,L}\psi_R - yh_d\bar{\psi}_{d,L}\psi_R \tag{2.3}$$

with

$$\langle\phi\rangle = \frac{1}{\sqrt{2}}\begin{pmatrix} 0 \\ v \end{pmatrix} \tag{2.4}$$

This method provides us with a mass term with a mass $m = yv/\sqrt{2}$. The mass term for the ψ_u field can be generated through the charge conjugate of the field ϕ^c.

Next the mass term for the gauge bosons needs to be generated. This is done by means of the kinetic term for the field ϕ, using the covariant derivative $D_\mu = \partial_\mu - \frac{i}{2}g_1 B_\mu - ig_2 A^a_\mu T^a$, with B the $U(1)$ field and A^a the three $SU(2)$ fields. The kinetic term for a scalar field is given by $(D^\mu\phi)^\dagger D_\mu\phi$. If the kinetic term is expanded in terms of the VEV, the lowest order term results in

$$\frac{1}{2}(0,v)\left(\frac{g_1}{2}B_\mu + g_2 A^a_\mu T^a\right)\left(\frac{g_1}{2}B^\mu + g_2 A^{b,\mu}T^b\right)\begin{pmatrix} 0 \\ v \end{pmatrix} = \frac{1}{2}V_\mu M^2 V^\mu \tag{2.5}$$

where we have defined a mass matrix M^2 in the basis of the four fields B and A^a. Diagonalizing this matrix results in the four eigenstates: the massless photon $A_\mu = \frac{1}{\sqrt{g_1^2+g_2^2}}\left(g_1 A^3_\mu + g_2 B_\mu\right)$, the Z-boson $Z_\mu = \frac{1}{\sqrt{g_1^2+g_2^2}}\left(g_2 A^3_\mu - g_1 B_\mu\right)$ with mass $m_Z = \frac{v}{2}\sqrt{g_1^2 + g_2^2}$ and the W-bosons $W^\pm_\mu = \frac{1}{\sqrt{2}}\left(A^1_\mu \mp iA^2_\mu\right)$ with mass $m_W = \frac{v}{2}g_2$.

The above only works under the condition that the scalar acquires a VEV. The most general Lagrangian for a complex scalar field is given by:

$$\mathcal{L} = (D^\mu\phi)^\dagger D_\mu\phi - V(\phi) = (D^\mu\phi)^\dagger D_\mu\phi - \mu^2\phi^\dagger\phi - \frac{\lambda}{4}\left(\phi^\dagger\phi\right)^2 \tag{2.6}$$

where $\mu^2, \lambda \in \mathbb{R}$. For the potential to be bounded we need $\lambda > 0$. However, μ^2 has two possibilities:

- If $\mu^2 \geq 0$ there is only one minimum located at 0, this potential will not have a VEV.

- If $\mu^2 < 0$ the minimum is located at $|\phi| = \sqrt{\frac{-2\mu^2}{\lambda}}$, this assumption provides our potential with a VEV and can result in the mass generation.

Other than the masses this mechanism also produces one massive scalar called the Higgs boson. This boson is the degree of freedom that is left over from the Higgs field, after three degrees of freedom are absorbed for the longitudinal components of the W- and Z-bosons. The Higgs boson interacts with every massive elementary particle proportional a coupling strength to their mass. This is because the Higgs boson originates from the same effect that provides the particles with their mass, the Higgs field. An overview of the different production and decay processes for the Higgs boson will be presented next. In Sections 2.2 and 2.3 a more detailed discussion of the theoretical status for the relevant production processes for this thesis will be given. A full overview of the theoretical status of the Higgs analysis can be found in [14–16].
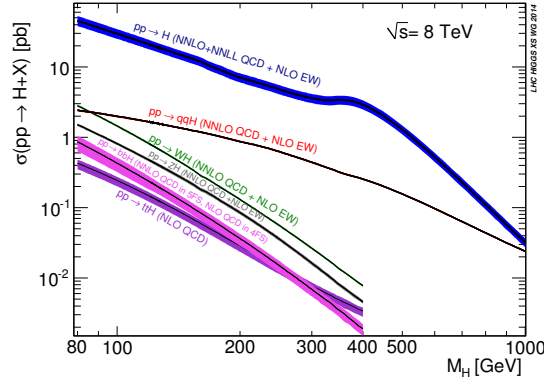
Figure 2.1: SM Higgs boson production cross sections. This is presented for a center of mass energy of 8 TeV at the LHC. These are the up to date results used for the at the experimental collaborations of the LHC. [17]
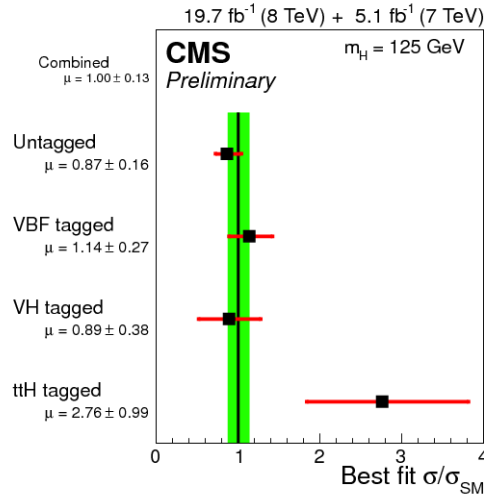
Figure 2.2: The experimental results for the Compact Muon Solenoid (CMS) collaboration, studying the different production processes of the Higgs boson. This includes the theoretical uncertainty in green and the experimental uncertainty in red. [18]

2.1.1 Production channels

The interaction of the Higgs boson is strongest with particles that have a large mass, as can be seen in the previous section the Yukawa coupling is proportional to the mass, $y = m\sqrt{2}/v$. This means that the largest cross sections are production channels where the Higgs boson is emitted by one of the heavy particles in the SM. The heaviest particles are the top quark and the W- and Z-bosons. An overview of the size of the different contributions to the production of Higgs bosons can be seen in Figure 2.1. The different production processes will be discussed in the order of the size of the cross section. Note that even though some processes have smaller cross sections than the other processes, they are all needed in order to properly study the different properties of the Higgs boson. An example of the current status of the Higgs analysis for the different production channels can be seen in Figure 2.2.

Gluon fusion: Gluon fusion is the dominant Higgs production channel. It is a loop-induced $2 \rightarrow 1$ process, where the initial state gluons fuse into a top quark loop which emits the Higgs

Figure 2.3: Some examples of diagrams for the different types of Higgs production channels. In (a) the gluon fusion process is shown, in (b) an example of vector boson fusion is shown, in (c) Higgs strahlung is shown with a Z-boson in the final state and in (d) an example of Higgs radiated off top quarks is shown.

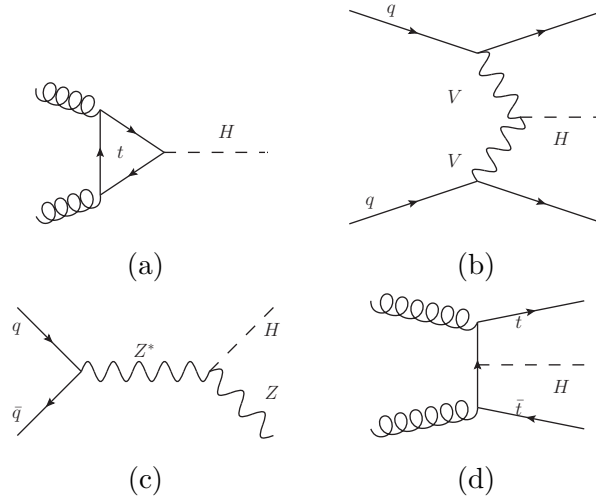boson. The LO diagram is shown in Figure 2.3(a). In the SM the top quark loop is the dominant contribution, however any massive particle that interacts strongly and has its mass generated by the Higgs mechanism can be in the loop. If a BSM theory alters the SM coupling between the top quark and the Higgs one expects a change in the experimental result of this production channel. Also if the model adds new massive colored particles that obtain their mass through the Higgs mechanism, there should be a difference in the cross section of this production channel.

Vector boson fusion: Vector boson fusion is the next most dominant channel. It involves the emission of a vector boson by the two initial state quarks of the proton. These two vector bosons then fuse into a Higgs boson. This results in a $2 \rightarrow 3$ process with a Higgs boson and two quarks in the final state. An example of a Feynman diagram for this process is displayed in Figure 2.3(b). The two quarks can be observed as two hard jets, one in the forward and one in the backward direction. Vector boson fusion is an important production process for determining the coupling strength between the vector bosons and the Higgs boson.

Higgs strahlung: Higgs Strahlung involves the production of a vector boson and a Higgs boson. At LO this involves a quark and anti-quark pair from the initial state protons interacting to form an off-shell vector boson. This vector boson becomes on-shell through the emission of a Higgs boson. The Feynman diagram for this process can be seen in Figure 2.3(c). This process is also an important channel for the analysis of the coupling strength between the vector bosons and the Higgs boson. The theoretical status of Higgs Strahlung will be discussed in more detail in Section 2.2 as this process is one of the two Higgs production processes that are important for this thesis.

Higgs radiation off top quarks: The last Higgs production process that will be discussed here is Higgs radiation off top quarks. This process is similar to top anti-top production. The only difference is the added Higgs boson which is emitted by one of the final state top quark or the exchanged top quark. One of the Feynman diagrams that contributes to this process is
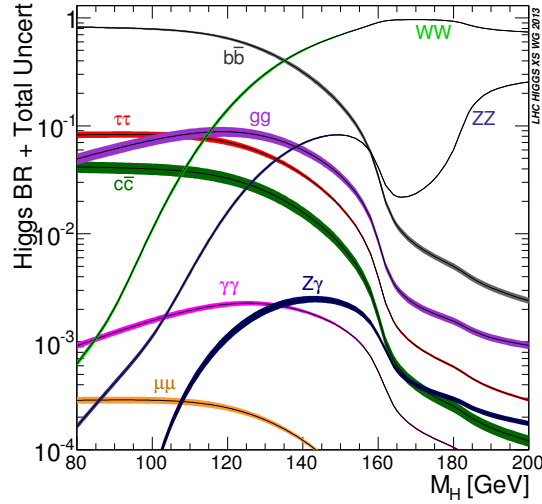
Figure 2.4: SM Higgs decay branching ratios for all the different possible decay products. The theoretical uncertainties are included as a band around each line. [17]

given in Figure 2.3(d). As the Higgs boson is always emitted off a top quark, this is a very important production channel for the analysis of the interaction between the Higgs boson and the top quark. This production process will be discussed in greater detail in Section 2.3.

2.1.2 Decay channels

In Figure 2.4 an overview for the different decay mode fraction of the total decay width of the Higgs boson can be seen. In the region of the discovered Higgs boson there are many different decay modes that are all important. This region for the Higgs mass (120-140 GeV) is a region in which it was harder to discover or exclude the Higgs boson. However, through hard work on both the experimental and the theoretical side the Higgs boson was in fact discovered in this region [10, 11]. The decay modes in which this discovery was made are Higgs to two photons, two Z-bosons, two W-bosons and two tau leptons. In addition the contribution from Higgs production in association with a vector boson, where the Higgs boson decays to a bottom anti-bottom pair, contributed. The two main contributions that led to the discovery were the decay to two photons and the decay to two Z-bosons (which then decay to four charged leptons). These contributions may not have the largest branching ratios, but they have the least influence from background channels that make the measurement more difficult.

Now that the Higgs boson has been discovered, this region has its advantages. The variety in the decay modes that are important allows us to study the Higgs decay into all these different modes. Most of these decay modes allow for a direct analysis of the coupling between the Higgs boson and the decay products. However, the decay into a pair of photons and the decay into a pair of gluons allow for a study of the Higgs coupling to the heaviest charged and colored particles of the model. For the SM the photon pair decay channel is dominated by a top quark or a W-boson loop and the gluon pair decay channel is dominated by a top quark loop as it is for the similar production mechanism. For a BSM theory these decays can also involve the new heavy particles in the loop. An example of the current status of the Higgs analysis of the different decay channels can be seen in Figure 2.5.
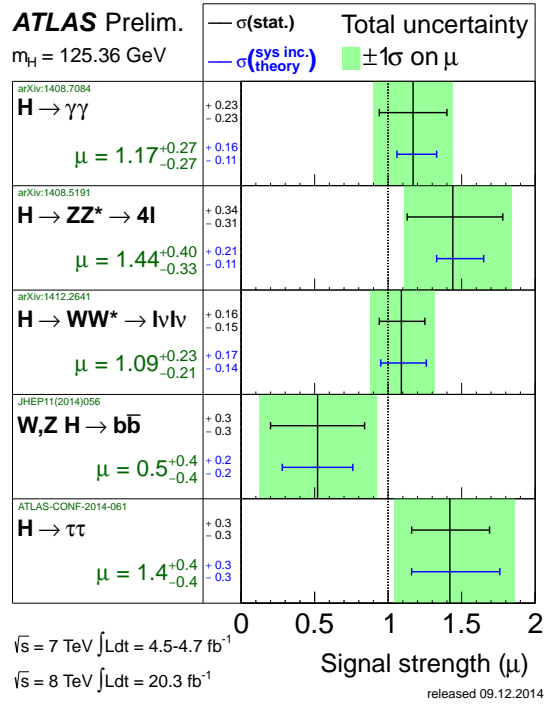
Figure 2.5: The results of the A Toroidal LHC Apparatus (ATLAS) collaboration at LHC for the different Higgs decay channels. This includes the 7 and 8 TeV measurements of the ATLAS collaboration. The total experimental and theoretical uncertainty is presented as a green band. [19–23]

2.2 Theoretical Status of Higgs Strahlung

At LO the Higgs Strahlung cross section can be separated into a Drell-Yan process $q\bar{q} \to V^*$ for the production of an off-shell vector boson and the decay of this off-shell vector boson into a Higgs boson and an on-shell vector boson. This can be written for the partonic cross section, $\hat{\sigma}$, as:

$$\hat{\sigma}_{q\bar{q} \to HV}(\hat{s}) = \int_0^{\hat{s}} dk^2 \hat{\sigma}^{DY}(q\bar{q} \to V^*(k)) \frac{d\Gamma}{dk^2}(V^*(k) \to HV) \tag{2.7}$$

with $\sqrt{\hat{s}}$ the partonic center of mass energy. This relation still holds at NLO in the coupling constant of QCD, and was calculated in [24–26]. An example of these types of corrections can be seen in Figure 2.6(a). At next-to-next-to-leading order (NNLO) this relation also holds approximately and therefore the NNLO corrections are dominated by the Drell-Yan corrections. These were evaluated in [27–29]. Corrections of this type are as in Figure 2.6(b). The Drell-Yan contributions to the cross section at N^nLO are of the order $g^4\alpha_s^n$, with g the electroweak coupling and $\alpha_s = g_s^2/(4\pi)$ for g_s the strong coupling, resulting in an increase of approximately 30% with respect to LO.

As was stated, the Drell-Yan convolution is approximate at NNLO. One of the additional contributions is through the emission of the Higgs boson off a top quark loop. This contribution is of the order $y_t g^3\alpha_s^2$ and results in a correction at the percent level [30]. An example of such a correction can be seen in Figure 2.6(c).

The NLO electroweak corrections do not factorize into Drell-Yan like production and decay. This is because at the NLO level the box diagrams already contribute. The NLO electroweak corrections have been calculated in [31] and result in corrections of the size $-(5-10)\%$.

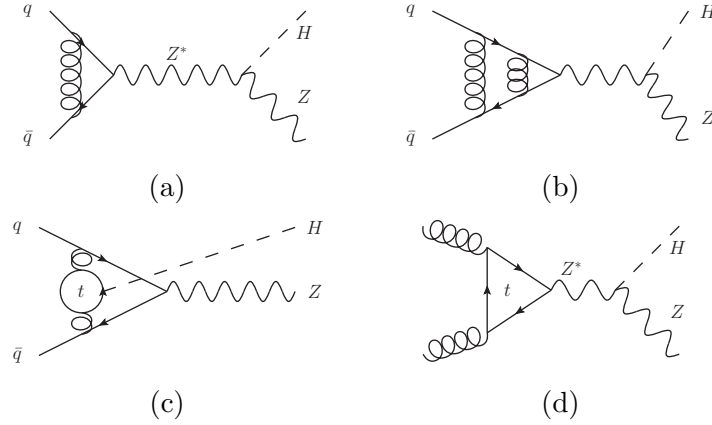Figure 2.6: Examples of different types of corrections to the $pp \to HZ$ process. In (a) an example of a one-loop diagram is presented, in (b) an example of a two-loop contribution for a Drell-Yan contribution, an additional contribution with a Higgs emitted from a top mass loop is shown in (c) and finally (d) shows a gluon initial state contribution.

The final type of corrections only apply to the HZ final state. For a Z-boson as a vector boson the gg initial state is also possible as can be seen in Figure 2.6(d). However, this is a loop induced process of the order $y_t^2 g^2 \alpha_s^2$ as it cannot have an interference contribution with respect to LO. Therefore this results in a NNLO contribution for the HZ final state. The contribution of $gg \to HZ$ is at partonic level the first contribution of its kind, meaning a "partonic LO". This means there are no additional terms logarithms of the scale to cancel the scale dependence of this process. This results in a large scale uncertainty for this specific initial state. This large scale uncertainty gives rise to a uncertainty for the HZ final state larger than for the HW final state, where this initial state does not exist at this order. In order to reduce this uncertainty and improve the prediction, the NLO QCD corrections to this process were calculated. The calculation was done in the heavy top mass limit effective field theory, because the exact solution is beyond the current capabilities of the calculation methods. Based on the top mass dependence of the NLO correction factor for $gg \to H$, it is argued that this approximation can be used. These corrections are of the order $y_t^2 g^2 \alpha_s^3$ and contribute at next-to-NNLO (N^{3}LO) level [32]. For the $gg \to HZ$ process the resummation will be discussed in Chapter 5.

2.3 Theoretical Status of Higgs Radiation off Top Quarks

The LO computation for $pp \to t\bar{t}H$ production was originally studied in [33–35], however these results have a large theoretical uncertainty due to the scale dependence of the strong coupling constant and parton distribution functions (PDFs). The NLO computations result in reasonable corrections of around 20% at the LHC and a strong reduction of the scale dependence [36–39].

In order to more precisely compare to experimental results, the NLO computation was matched to parton showers. This was done using the framework of a variety of programs for comparison: aMC@NLO [40], PowHel [41] and the POWHEG-Box [42].

Finally, the NLO electroweak corrections to the cross section were calculated in [43, 44]. These result in contributions of the order of -1% for the inclusive cross section and -10% for the tail in the transverse momentum distribution.

The fact that the process is a $2 \to 3$ process with two mass scales in the final state severely complicates the calculation of higher order corrections, therefore the calculation of the NNLO corrections is beyond the current capabilities of our field. However, it is still important to improve precision of the predictions and to estimate the size of higher order corrections. In order to accomplish both these points we can perform threshold resummation for $2 \to 3$ processes and specifically $pp \to t\bar{t}H$ production.

3 Supersymmetry

As stated in the introduction, we know that the SM cannot be the final theory and more physics must lie BSM. One example of such a theory is SUSY [12, 13]. In this chapter we will explain the basic concepts of SUSY and its motivation. For a more detailed explanations of SUSY it is recommended to look at [45].

3.1 Why supersymmetry?

Hierarchy problem: The reason SUSY was originally proposed in the context of the SM was in order to resolve the hierarchy problem. In the SM the masses of most particles are protected by a symmetry, that is to say that if their mass is set to zero we gain an extra symmetry. For example if we set the fermion mass to zero we gain an exact chiral symmetry. This symmetry means that the corrections to the mass will always be proportional to the mass itself, as the correction to the mass also needs to be zero. If the correction is non-zero we violate the new symmetry through the correction term. This fact prevents the corrections to the mass from becoming too large, as the corrections are of the order of the mass and proportional to the mass. This means the largest divergence one can have with respect to the energy cut-off is logarithmic. However, the Higgs boson is the only SM particle to not have such a symmetry, so the corrections can be significant. An example of this is the fermionic correction:
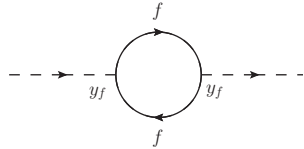
which results in

$$\Delta m_H^2 = \frac{y_f^2}{16\pi^2} \left[-2\Lambda_{UV}^2 + 6m_f^2 \log\left(\frac{\Lambda_{UV}}{m_f}\right) + \ldots \right] \tag{3.1}$$

where y_f is the Yukawa coupling between the Higgs boson and the fermion f and Λ_{UV} is a cut-off on the momentum of the fermion in the loop. This cut-off can be interpreted as the scale at which this model is no longer valid, so the scale at which new physics occurs. If, for example, the SM holds up until the Planck scale, where gravity starts to become important, this would lead to a correction to the squared mass of the order of $\left(10^{19}\text{GeV}\right)^2$ and the observed squared mass is of the order of $\left(10^2\text{GeV}\right)^2$. This means that our Lagrangian parameter μ^2 needs to be tuned to 34 digits in order to cancel against the contribution from the correction. This would require an astonishing coincidence.

Alternatively this calculation can be done in dimensional regularization instead of using a cut-off scale. In this case there will still be a corrections of the new physics with the highest mass. This new physics will always provide corrections proportional to the squared mass of the new

particle. Even if the particle does not couple directly to the Higgs boson, it will still happen at higher orders. Therefore the Higgs boson mass corrections are sensitive to the highest masses of the model.

However there is a way to resolve this coincidence. This is often done through means of a symmetry in particle physics. If we calculate the correction from a complex scalar particle loop:
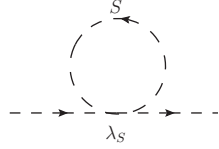

this correction results in:

$$\Delta m_H^2 = \frac{\lambda_S}{16\pi^2} \left[\Lambda_{UV}^2 - 2m_S^2 \log\left(\frac{\Lambda_{UV}}{m_S}\right) + \ldots \right] \tag{3.2}$$

Therefore if we introduce two new complex scalars for every fermion with $\lambda_S = y_f^2$, the term proportional to Λ_{UV}^2 will be canceled. This is exactly what SUSY does, it creates a symmetry between bosons and fermions. This symmetry adds two scalars for every fermion, due to the difference in degrees of freedom between fermions and scalars. Note that this does not cancel the logarithmic term, however this is much more manageable than a quadratic term. In our previous example and using the top mass for the fermion in the loop this leads to 2-3 digits that need to be "fine tuned".

Stability bound [46–48]: Other than the lack of explanation for gravity and dark matter, there could be another reason to believe there is BSM physics. Using renormalization group equations we can calculate the running of the quadratic Higgs coupling, λ in Equation 2.6. There are two problems that can occur for the quadratic Higgs coupling. First if the Higgs mass is too large, the coupling can become too large. This destroys the perturbative nature of our model and is often called the triviality bound. On the other hand if the Higgs mass is too small the quadratic Higgs coupling can become negative for large scales. If the quadratic coupling becomes negative our minimum is no longer a global minimum, but a local one. This means our universe is not stable anymore. What can however happen is that the minimum is unstable, but the decay time is larger than the age of our universe. This scenario is called meta-stable. In Figure 3.1 it can be seen that, for the Higgs mass of 125 GeV, there are no problems with the triviality bound. However, for large scales the Higgs mass is below the stability bound. This implies that we are in a meta-stable universe if there is no new physics before the Planck scale. Whether we should require a stable or meta-stable universe is still a matter of taste. If we should require the universe to be stable the value of the Higgs mass could possibly give the indication that there is some BSM physics between what we know now and the Planck scale. This new physics would need to modify the running of the quadratic Higgs coupling in a way in which it stays positive.

Dark matter: As was stated earlier one of the major points the SM lacks is a valid candidate for dark matter. SUSY is capable of providing such a candidate under the assumption that we introduce an extra symmetry called R-parity. The motivation for introducing this symmetry will be mentioned in Section 3.3. We will not go into more depth for dark matter other than stating that SUSY can provide a candidate as this is not the focus of this thesis.
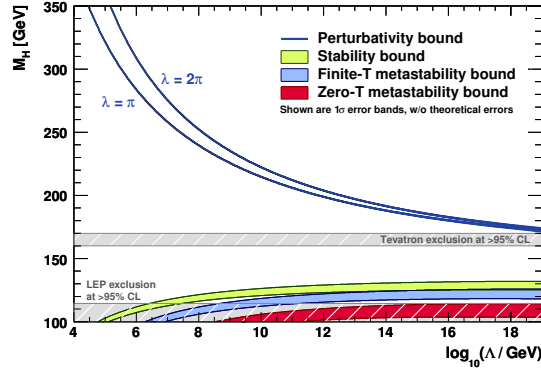
Figure 3.1: For a given value of m_H, the scale at which the stability or perturbativity (triviality) bound will be reached can be seen. Two different different definitions of the triviality bound can be seen as the upper lines. Different definitions for the (meta)stable universe can be seen as the lower three regions. The uncertainty band for the (meta)stability bounds are determined by means of experimental uncertainties. [46]
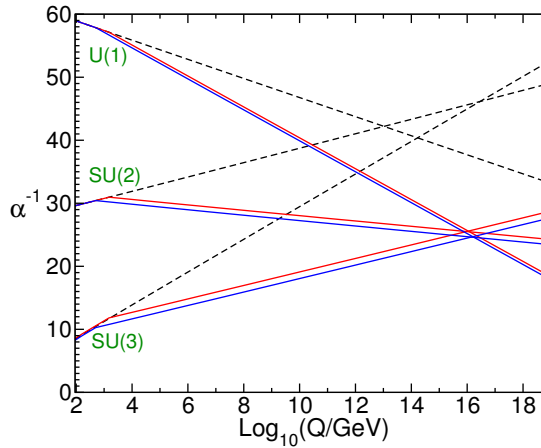
Figure 3.2: The running coupling constants $\alpha^{-1} = 4\pi g^{-2}$ as a function of the logarithm of the energy scale. This shows that the SM does not have the couplings unify at one scale, but the Minimal Supersymmetric Standard Model (MSSM) does. [45]

Grand unification [49]: Historically speaking a feature through which physicists grew more interested in SUSY for the SM was the possibility of combining it with Grand Unification Theory (GUT). GUT is a theory, where all of the gauge couplings of the SM $U(1) \times SU(2) \times SU(3)$ are unified at one scale into one coupling with one group, for example $SU(5)$ though this has been excluded for the SM. If the couplings are plotted for a running scale, in the SM they do not meet in one point. By including SUSY contributions in this calculation, the coupling do meet in one point. This can be seen in Figure 3.2.

3.2 What is supersymmetry?

Now that we have established some of the reasons to introduce SUSY, we can start to explore what exactly SUSY is. Here we will focus on SUSY with only one SUSY generator ($N = 1$), therefore every particle will have only one superpartner. However, a general supersymmetric theory can have more than one SUSY generator.

As was stated before SUSY introduces an extra symmetry between fermions and bosons:

$$Q \left| \text{Boson} \right\rangle \propto \left| \text{Fermion} \right\rangle \qquad Q \left| \text{Fermion} \right\rangle \propto \left| \text{Boson} \right\rangle \tag{3.3}$$

This transformation changes a boson into a fermion and vice versa, therefore the transformation itself needs to be fermionic in nature. The possible form of this symmetry in an interacting quantum field theory is strongly restricted by the Haag-Lopuszanski-Sohnius extension [50] of the Coleman-Mandula theorem [51]. For realistic theories with chiral fermions that transform differently, there is only one possible extension of the Poincaré group. This possible extension results in fermionic operators that have anti-commutation relations and for SUSY these are given by:

$$\left\{ Q, Q^\dagger \right\} \quad \propto \quad P^\mu \tag{3.4}$$

$$\{Q, Q\} = \left\{ Q^\dagger, Q^\dagger \right\} \quad = \quad 0 \tag{3.5}$$

This results in a transformation that commutes with the momentum operator and the gauge transformations, therefore the fermions and bosons coupled through this transformation need to have the same mass and quantum numbers. These particles can then be combined into supermultiplets with the same quantum numbers. Within these supermultiplets there need to be the same amount of bosonic and fermionic degrees of freedom. These supermultiplets can be categorized into two types: a Weyl spinor and a complex scalar field or a gauge boson field and a Majorana spinor. A Weyl spinor is either the left- or right-handed component of a spinor. We need to split the fermions into a left- and right-handed component due to the difference in the amount of degrees of freedom between a complex fermion and a complex scalar. Therefore for every SM fermion (except the neutrino) we obtain two complex scalars, as was mentioned earlier this will help resolve the hierarchy problem.

As there are no pairs of fermions and bosons in the SM that have the same quantum numbers, SUSY introduces new particles. These new particles (also called sparticles) are labeled by adding an s- in front of the particle names for the new scalar bosons and adding -ino at the end for the new fermions. The problem is that if these new particles indeed had the same mass as the SM particles we would have discovered them already, therefore SUSY needs to be broken allowing the new particles to have a different mass. In fact SUSY breaking is required to provide masses to all particles. This is because the symmetry breaking mechanism in the Higgs sector that provides the particles with their masses is impossible in a non-broken SUSY.

3.3 Minimal supersymmetric Standard Model

SUSY can be defined in a variety of ways, for example the theory can have multiple generators and extra particles can be added. However, this thesis will focus on the minimal supersymmetric extension of the Standard Model (MSSM). The MSSM has four generators, one for each spinor degree of freedom. The supermultiplets of the MSSM can be seen in Tables 3.1 and 3.2 in a notation similar to Table 2.1 for the SM. Here we can see that one supermultiplet is made for each SM representation. The main change is that we now need two Higgs doublets. The extra Higgs doublet is required in order to insure anomaly cancellation. Now there are eight real degrees of freedom in the Higgs doublets and we still require three for the longitudinal components of the W- and Z-bosons. This results in five Higgs bosons, two charged and three neutral. Of these three neutral Higgs bosons one is CP-odd and two are CP-even. Of the new sfermions, the two neutral Higgsino, the neutral Wino and the Bino have the same quantum

Names		spin 0	spin 1/2	$SU(3)_C$, $SU(2)_L$, $U(1)_Y$
squarks, quarks	Q	$(\widetilde{u}_L \ \ \widetilde{d}_L)$	$(u_L \ \ d_L)$	($\mathbf{3}$, $\mathbf{2}$, $\frac{1}{6}$)
($\times 3$ families)	$\overline{u}$	$\widetilde{u}_R^*$	$u_R^\dagger$	($\overline{\mathbf{3}}$, $\mathbf{1}$, $-\frac{2}{3}$)
	$\overline{d}$	$\widetilde{d}_R^*$	$d_R^\dagger$	($\overline{\mathbf{3}}$, $\mathbf{1}$, $\frac{1}{3}$)
sleptons, leptons	L	$(\widetilde{\nu} \ \ \widetilde{e}_L)$	$(\nu \ \ e_L)$	($\mathbf{1}$, $\mathbf{2}$, $-\frac{1}{2}$)
($\times 3$ families)	$\overline{e}$	$\widetilde{e}_R^*$	$e_R^\dagger$	($\mathbf{1}$, $\mathbf{1}$, 1)
Higgs, higgsinos	H_u	$(H_u^+ \ \ H_u^0)$	$(\widetilde{H}_u^+ \ \ \widetilde{H}_u^0)$	($\mathbf{1}$, $\mathbf{2}$, $+\frac{1}{2}$)
	H_d	$(H_d^0 \ \ H_d^-)$	$(\widetilde{H}_d^0 \ \ \widetilde{H}_d^-)$	($\mathbf{1}$, $\mathbf{2}$, $-\frac{1}{2}$)

Table 3.1: Chiral supermultiplets in the MSSM, consisting of a left-handed Weyl-spinor and a complex scalar. [45]

Names	spin 1/2	spin 1	$SU(3)_C$, $SU(2)_L$, $U(1)_Y$
gluino, gluon	$\widetilde{g}$	g	($\mathbf{8}$, $\mathbf{1}$, 0)
winos, W bosons	$\widetilde{W}^\pm \ \ \widetilde{W}^0$	$W^\pm \ \ W^0$	($\mathbf{1}$, $\mathbf{3}$, 0)
bino, B boson	$\widetilde{B}^0$	B^0	($\mathbf{1}$, $\mathbf{1}$, 0)

Table 3.2: Gauge supermultiplets in the MSSM, consisting of a Majorana spinor and a gauge boson field. [45]

numbers. Therefore, these can mix into four neutralinos. In addition, the charged Winos and the charged Higgsinos also have the same quantum numbers, these mix to form two charginos of each charge.

We will break SUSY softly, this means we introduce all extra possible renormalizable terms as an extra Lagrangian: $\mathcal{L} = \mathcal{L}_{\text{SUSY}} + \mathcal{L}_{\text{soft}}$. If all possible soft SUSY breaking terms were introduced, the proton would become unstable. However we know the proton is stable (or at least has a very long lifetime). We could just set these terms to zero for no reason other than to prevent the proton decay, but typically it is preferred to have a reason to exclude these terms. Therefore we shall introduce a new conserved multiplicative quantum number called R-parity:

$$P_R = (-1)^{3(B-L)-2s}$$

where B is the baryon number, L is the lepton number and s is the spin. For all SM particles R-parity is $P_R = 1$. For their SUSY partners we shift the spin by $\pm 1/2$. This results in an R-parity $P_R = -1$ for all sparticles. Therefore, in order to conserve R-parity any vertex should have an even number of sparticles. This has two important consequences. First, sparticles are always produced in pairs at colliders. And secondly, the lightest supersymmetric particle (LSP) is stable as there is no lighter sparticle it can decay into. This new LSP is an interesting dark matter candidate if it is neutral and only weakly interacting.

SUSY itself does not add any new parameters, however since SUSY has to be broken new parameters will be added. There are 105 free parameters in the MSSM to be exact. 105 free parameters are far too many for a general experimental MSSM search. Therefore for the phenomenological prediction different assumptions are made. An example of an often used assumption is minimal Supergravity (mSUGRA). In mSUGRA all the parameters are run down from the GUT scale, the scale at which the couplings unite. This helps to reduce the amount
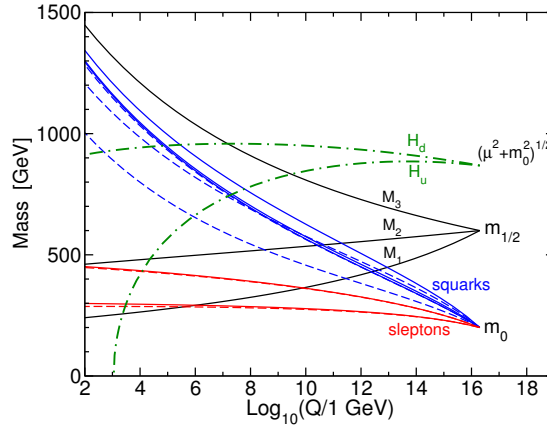
Figure 3.3: Renormalization group equations evolution of scalar and gaugino mass parameters in the MSSM with MSUGRA boundary conditions imposed at $Q_0 = 2 \times 10^{16}$ GeV. [45]

of parameters to four and a sign that are defined at the GUT scale. The four parameters are the mass of the scalars m_0, the mass of the gauginos $M_{1/2}$, the trilinear couplings A_0 and the ratio of the vacuum expectation values of the neutral components of the two Higgs doublets $\tan \beta$. The sign is the sign of the mass in the Higgs sector μ. The parameter μ itself and the bilinear couplings B can be determined by requiring that the electroweak symmetry breaking is implemented correctly at low energy scale.

As we assume mass unification at the GUT scale, the mass hierarchy of the sparticles is largely determined by the renormalization group equations. An example of a possible mass hierarchy can be seen in Figure 3.3. One important thing to note here is the mass parameter of one of the Higgs doublets automatically becomes negative allowing for electroweak symmetry breaking as it was explained in Section 2.1.

3.4 Experimental searches

No matter how elegant SUSY might be, in the end all that matters is which theory nature prefers. Therefore, we will need to either measure or exclude SUSY. In order to still reasonably solve the hierarchy problem the masses of the sparticles should not be higher than a couple of TeV. This is exactly the range in which the LHC can search for SUSY. The sparticles that have the largest production cross section are the colored sparticles (squarks and gluinos), because they interact through the strong interaction to the initial state partons. This can be seen more clearly in Figure 3.4.

Due to R-parity, we know that the sparticles should be produced in pairs at colliders. In addition, there is one stable LSP and the other sparticles are unstable. Therefore, when a squark or gluino is produced in a collision it will start a decay chain which ends with the LSP. This results in a signal in which one expects highly energetic jets (the colored SM particles from the decay chain) and missing energy (the LSP). However, this signal can become much harder to detect if, for example, the masses of the sparticles are closer together. This example would result in less energetic jets, making it harder to distinguish signal from background.

The current exclusion limits from the LHC for the squarks and gluinos lie around the $1 - 1.5$ TeV for mSUGRA depending on the parameters [52, 53]. For sleptons these limits are much lower at $100 - 300$ GeV and for gauginos $300 - 700$ GeV. However, these limits require different
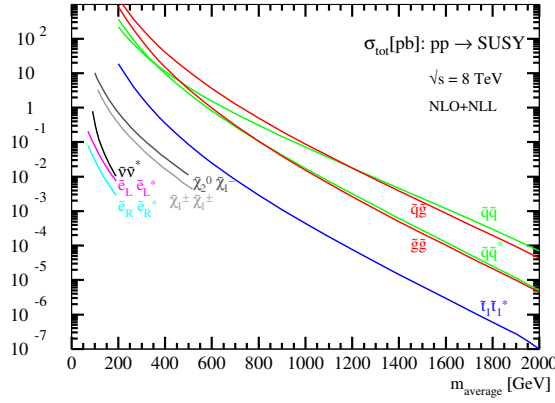
Figure 3.4: The production cross section for different sparticles at the LHC as a function of the average final state particle mass at NLO+NLL precision for squark and gluino production and NLO precision for the others. [54–60]

analyses if the model is changed. For example, if one removes the R-parity constraint the signal changes completely. You will no longer have a stable LSP, therefore missing energy will not be the key signal anymore. In this scenario the decay of the LSP also needs to be taken into account making the background harder to separate from the signal.

3.5 Theoretical status of squark and gluino production

As was stated before the dominant contributions to the SUSY production cross section are for the production of squarks and gluinos. This can also be seen in Figure 3.4. Therefore, we shall only focus on the theoretical status of these processes.

Squark and gluino production have been calculated up to NLO in fixed order computations for some time [56,57,61,62]. A significant contribution to these NLO computations comes from the region near absolute threshold. As stated before, this is the region where the initial state energy approaches the minimal final state energy: $\hat{s} \to 4m_{av}^2$ with m_{av} the average mass of the final state particles. There are two types of contributions that are dominant in this region. First there is the soft-gluon emission from both the initial and the final state. The second contribution is Coulomb corrections, originating from the exchange of a gluon between the two slow moving final state particles.

In order to improve these predictions resummation was used for the contributions near absolute threshold. The soft-gluon emission was calculated at next-to-leading logarithmic (NLL) accuracy [63–68]. Additionally Coulomb resummation was included using a Sommerfeld factor [64] and using the framework of effective field theories [69,70].

As the full NNLO computation is out of reach the approximate NNLO [71,72] has been computed by means of the next-to-next-to-leading logarithmic (NNLL) resummation. For squark-anti-squark production the soft-gluon resummation has been extended to NNLL level [73]. For gluino production the soft-gluon resummation has also been calculated up to NNLL level [74]. In the framework of soft-collinear effective theory (SCET) the stop-pair production cross section has been calculated at NNLL level [75]. Lastly, finite width effects have been studied for squark and gluino production in [76].

In Chapter 6 the focus for squark and gluino production will be laid on the increase in precision from NLL resummation to NNLL for all processes. This work is published in [77]. Similar work

has been done in the framework of SCET, where they additionally include Coulomb resummation [78, 79].

4 Soft Gluon Resummation

In this chapter the formalism of soft gluon resummation will be reviewed. First an intuitive way of computing the resummation formulas will be presented. Next, in Section 4.2, the more general equations for factorization for neutral particle production are shown. From this factorization we obtain resummation in Section 4.3. The differences needed order to include massive colored particles in the final state are displayed in Section 4.4. Finally, the methods used in the numerical codes are presented in Section 4.5.

4.1 The Leading Logarithmic terms

In order to provide an idea of how to compute the resummed formulas we will start with the cross section for a single emission. This will then be extended to multiple emissions. The computation will be done in both the soft and collinear limit in order to obtain the dominant logarithmic term often referred to as Leading Logarithmic (LL). This calculation is done using similar methods to those used in [80, 81].

4.1.1 Eikonal Feynman rules

In order to explore the infrared divergences we will start by introducing the eikonal approximation. It describes the emission of a soft gluon from a colored particle. As an example we will start by deriving the eikonal rule for the soft gluon emission from an initial state quark. This emission is in general described by the diagram:
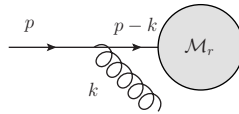
and the equation:

$$\mathcal{M}_e = \mathcal{M}_r \frac{i\left(\not{p} - \not{k} + m\right)}{(p-k)^2 - m^2 + i\epsilon} \left(-ig_s T^C_{ab}\gamma^\mu\right) u\left(p\right) \epsilon^*_\mu(k) \tag{4.1}$$

where $\mathcal{M}_r$ is the matrix element of the remaining process and we have included the mass m of the quark. If we use the anti-commutation relation for the gamma matrices $\{\gamma^\mu, \gamma^\nu\} = 2g^{\mu\nu}$:

$$\mathcal{M}_e = \mathcal{M}_r \left(-ig_s T^C\right) \frac{i\left\{\gamma^\mu\left(-\not{p} + \not{k} + m\right) + 2p^\mu - 2k^\mu\right\}}{-2p\cdot k + k^2 + i\epsilon} u\left(p\right) \epsilon^*_\mu(k) \tag{4.2}$$

If the relation $\not{p}u\left(p\right) = mu\left(p\right)$ is used the quark mass drops out. In addition we can approximate in the soft limit for the gluon momentum k. This implies that $k \to 0$ and $k^\mu \ll p^\mu$.

$$\mathcal{M}_e = \mathcal{M}_r u\left(p\right) g_s T^C_{ba} \frac{p^\mu}{-p\cdot k + i\epsilon} \epsilon^*_\mu(k) \tag{4.3}$$

This results in the eikonal rule for soft gluon emission from an initial state quark:

$$g_s T_{ba}^C \frac{p^\mu}{-p \cdot k + i\epsilon} \epsilon_\mu^*(k) \tag{4.4}$$

In general the eikonal rules are written as:

$$g_s T_j \frac{p_i^\mu}{p \cdot k - i\epsilon} \tag{4.5}$$

for incoming eikonal lines and

$$g_s T_j \frac{p_i^\mu}{p \cdot k + i\epsilon} \tag{4.6}$$

for outgoing eikonal lines. Here T_j is the color operator for different particles:

Outgoing quark/ incoming anti-quark: $T_j = T_{ab}^C$

Outgoing anti-quark/ incoming quark: $T_j = -T_{ba}^C$

gluon: $T_j = -if^{ABC}$

By means of these eikonal rules we can explore the infrared divergences. The cross section in the eikonal limit for massless initial state particles is proportional to:

$$\sigma_e \propto \sigma_b \frac{2p_1 \cdot p_2}{(p_1 \cdot k)(p_2 \cdot k)} = \sigma_b \frac{2p_1 \cdot p_2}{E_1 E_2 k_0^2 (1 - \cos^2\theta)} \tag{4.7}$$

with θ the angle between the emission and the initial state axis in the initial state center of mass frame, E_i indicates the initial state particle energy and k_0 indicates the emission energy. The contributions for emission from the same particle do not contribute as these are proportional to $p_i^2 = m_i^2 = 0$ and do not contribute for massless particles. Here we can see the soft divergence in the form of the k_0^{-2}. After phase space integration this results in a logarithmic divergence. The collinear divergence is for $\cos\theta \to \pm 1$, this is when the angle between the emission and one of the initial state partons is small.

If we extend the eikonal rules to multiple emissions from the same leg, we can see that they still factorize:

$$\frac{p^\mu}{p \cdot (k_1 + k_2)} \frac{p^\nu}{p \cdot k_2} + \frac{p^\mu}{p \cdot (k_1 + k_2)} \frac{p^\nu}{p \cdot k_1} = \frac{p^\mu p^\nu}{p \cdot (k_1 + k_2)} \left(\frac{1}{p \cdot k_2} + \frac{1}{p \cdot k_1} \right)$$

$$= \frac{p^\mu p^\nu}{(p \cdot k_1)(p \cdot k_2)} \tag{4.8}$$

with k_i the momentum of the ith emission.

4.1.2 Phase space factorization

Now that we have shown that the emission factorizes in the soft limit for an electroweak theory. As this process is Drell-Yan the only color operators originate from the emission, therefore this also factorizes. For QCD processes a color space will need to be chosen, this will be described in Section 4.4. The phase space only need to be looked at in order to show the factorization of the LL contribution. As before we will look at a single emission and extend this to multiple emissions.

For a single emission the phase space is described by

$$dPS_2 = \frac{d^3k_1}{(2\pi)^3 \, 2k_{1,0}} \frac{d^4Q}{(2\pi)^4} \, (2\pi)^4 \, \delta^4 \left(p_1 + p_2 - k_1 - Q\right) (2\pi) \, \delta \left((p_1 + p_2 - k_1)^2 - Q^2\right) \quad (4.9)$$

This is for the production of a neutral particle with invariant mass Q^2 from an initial state with momenta $p_{1,2}$. Examples of these types of processes are Drell-Yan or Higgs production. Integrating out the final state momentum Q results in:

$$
\begin{aligned}
dPS_2 &= \frac{d^3k_1}{(2\pi)^3 \, 2k_{1,0}} \, (2\pi) \, \delta \left((p_1 + p_2 - k_1)^2 - Q^2\right) \\[2mm]
&= \frac{d^3k_1}{(2\pi)^3 \, 2k_{1,0}} \, (2\pi) \, \delta \left(\hat{s} - 2k_1 \cdot (p_1 + p_2) - Q^2\right) \\[2mm]
&= \frac{d^3k_1}{(2\pi)^3 \, 2k_{1,0}} \frac{(2\pi)}{\hat{s}} \delta \left(x_1 - \hat{\tau}_Q\right) \quad (4.10)
\end{aligned}
$$

where we define the initial state invariant mass $\hat{s} = (p_1 + p_2)^2$, $x_1 = 1 - 2k_{1,0}/\sqrt{\hat{s}}$ and $\hat{\tau}_Q = Q^2/\hat{s}$.

If this is extended to multiple emissions this delta function becomes:

$$\delta \left(1 - \hat{\tau}_Q - \frac{2\left(k_{1,0} + \ldots k_{n,0}\right)}{\sqrt{\hat{s}}}\right) \approx \delta \left(x_1 \cdots x_n - \hat{\tau}_Q\right) \quad (4.11)$$

This expression does not factorize. However, there is a solution to this problem. The delta function contains a product of the terms we want factorized. If we transform this expression into Mellin space with respect to $\hat{\tau}_Q$ this does lead to a factorization for multiple emissions:

$$\int d\hat{\tau}_Q \, \hat{\tau}_Q^{N-1} \delta \left(x_1 \cdots x_n - \hat{\tau}_Q\right) = x_1^{N-1} \cdots x_n^{N-1} \quad (4.12)$$

where the Mellin transform is defined as

$$\tilde{f}(N) = \int_0^1 dx \, x^{N-1} f(x) \quad (4.13)$$

Alternatively we can look at the left hand side of Equation (4.11) and notice a sum of the terms that we desire to factorize. This can be resolved by transforming the expression into Laplace space with respect to $1 - \hat{\tau}_Q$:

$$\int d\hat{\tau}_Q \, e^{-\left(1-\hat{\tau}_Q\right)N} \delta \left(1 - \hat{\tau}_Q - \frac{2\left(k_{1,0} + \ldots k_{n,0}\right)}{\sqrt{\hat{s}}}\right) = e^{-(1-x_1)N} \cdots e^{-(1-x_n)N} \quad (4.14)$$

with the Laplace transform is defined as

$$\tilde{f}(N) = \int_0^1 dx \, e^{-(1-x)N} f(x) = \int_0^1 dz \, e^{-zN} f(x) \quad (4.15)$$

4.1.3 Computation of the virtual contribution

Now that we have shown the factorization of the matrix element and the phase space in Mellin space we can study the emission as a whole. In order to regularize the soft divergence we need to additionally include virtual contributions for eikonal gluon exchange between the initial state particles, which is given by the diagram:
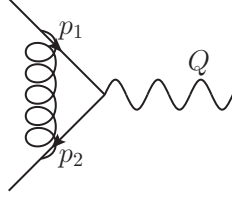
and the equation:

$$\sigma_V \propto \int \frac{d^4 k_1}{(2\pi)^4} \frac{2p_1 \cdot p_2}{E_1 E_2 \left(k_{1,0} - |\mathbf{k}_1| \cos\theta - i\epsilon\right)\left(k_{1,0} + |\mathbf{k}_1| \cos\theta + i\epsilon\right)} \frac{-i}{\left(k_{1,0}^2 - |\mathbf{k}_1|^2 + i\epsilon\right)} \quad (4.16)$$

with p_1 and p_2 the momenta of the two initial state particles and E_i their energies. For these virtual corrections the eikonal rules can also be used to obtain the soft contributions. Here the k_1 integral is a loop momentum integration. We can describe the $k_{1,0}$ integral one the basis of four poles in the complex plane:

$$\sigma_V \propto \int \frac{d^3 k_1}{(2\pi)^4} \frac{2p_1 \cdot p_2 \, dk_{1,0}}{E_1 E_2 \left(k_{1,0} - |\mathbf{k}_1| \cos\theta - i\epsilon\right)\left(k_{1,0} + |\mathbf{k}_1| \cos\theta + i\epsilon\right)}$$
$$\times \frac{-i}{\left(k_{1,0} - |\mathbf{k}_1| + i\epsilon\right)\left(k_{1,0} + |\mathbf{k}_1| - i\epsilon\right)} \quad (4.17)$$

In order to perform this integral we will close the contour in the lower half of the plane:

$$\sigma_V \propto \int \frac{d^3 k_1}{(2\pi)^3} \frac{-i2p_1 \cdot p_2}{E_1 E_2} \frac{-i2\pi}{2\pi}$$
$$\times \left[\frac{1}{2\left(|\mathbf{k}_1| - i\epsilon\right) |\mathbf{k}_1|^2 \left(1 - \cos^2\theta - i\epsilon\right)} + \frac{1}{2\left(|\mathbf{k}_1| \cos\theta - i\epsilon\right) |\mathbf{k}_1|^2 \left(1 - \cos^2\theta - i\epsilon\right)} \right] (4.18)$$

The second term only provides a phase that will not be discuss in greater detail here [81]. The Mellin transform of the delta function for the kinematics is the same as for Born. When this equation is combined with the real contribution we can use $k_{1,0}$ instead of $|\mathbf{k}_1|$ as the real emission is on-shell.

4.1.4 Combination of virtual and real emission

If we combine the eikonal cross section with the phase space integration in Mellin space this results in:

$$I = g_s^2 C_i \int \frac{d^3 k_1}{(2\pi)^3 \, 2k_{1,0}} \frac{2p_1 \cdot p_2}{E_1 E_2 k_{1,0}^2 \left(1 - \cos^2\theta\right)} \left[x_1^{N-1} - 1 \right] \quad (4.19)$$

where we have not included the factor $2\pi/\hat{s}$ as this is a part of the Born phase space in Mellin space. The -1 in the square brackets originates from the virtual contribution, this shows how the virtual contributions regulate the soft divergence of the real corrections. C_i represents the color factor of the emission and depends on the initial state particles ($C_q = C_F = 4/3$ and $C_g = C_A = 3$), this color factor is also a part of the virtual contribution.

Now that the integral for the real and virtual contributions have been formulated we can compute the emission integral:

$$I = 2\frac{\alpha_s C_i}{\pi} \int_0^{\sqrt{\hat{s}}/2} \frac{dk_{1,0}}{k_{1,0}} \int \frac{d\cos\theta}{(1 - \cos^2\theta)} \left[x_1^{N-1} - 1 \right] \tag{4.20}$$

where the integral over ϕ has been performed and simply returns a factor of 2π. Next we can use $x_1 = 1 - 2k_{1,0}/\sqrt{\hat{s}}$ to change the $k_{1,0}$ integral:

$$I = 2\frac{\alpha_s C_i}{\pi} \int_0^1 \frac{dx_1 \left[x_1^{N-1} - 1 \right]}{(1 - x_1)} \int_{-1}^1 \frac{d\cos\theta}{(1 - \cos^2\theta)} \tag{4.21}$$

From here we will use the collinear limit: $d\cos\theta \approx -d\theta^2/2$ and $1 - \cos^2\theta \approx \theta^2$, however we will need to take into account a factor of two for the collinear limit with respect to both initial state partons.

$$
\begin{aligned}
I &= 2\frac{\alpha_s C_i}{\pi} \int_0^1 \frac{dx_1 \left[x_1^{N-1} - 1 \right]}{(1 - x_1)} \int \frac{d\theta^2}{\theta^2} \\
&= 2\frac{\alpha_s C_i}{\pi} \int_0^1 \frac{dx_1 \left[x_1^{N-1} - 1 \right]}{(1 - x_1)} \int_{\mu_F^2}^{(1-x_1)^2 Q^2} \frac{dk_T^2}{k_T^2}
\end{aligned} \tag{4.22}
$$

with $k_T = (1 - x_1) Q$. The lower bound of the k_T^2 integral is the factorization scale μ_F, this is explained by the fact that the collinear emission from initial state particles is absorbed into the PDFs up to an energy defined by the factorization scale μ_F.

In addition to the emission the running coupling effects from α_s can also be considered. In order to take these effects into account the coupling is computed at a scale k_T, resulting in:

$$I = 2 \int_0^1 \frac{dx_1 \left[x_1^{N-1} - 1 \right]}{(1 - x_1)} \int_{\mu_F^2}^{(1-x_1)^2 Q^2} \frac{dk_T^2}{k_T^2} C_i \frac{\alpha_s \left(k_T^2 \right)}{\pi} \tag{4.23}$$

4.1.5 Exponentiation

Now that the emission has been computed and it factorizes for multiple emission we can finally resum these contributions.

$$\Delta_{i\bar{i}}^{LL} = \sum_{i=0}^{\infty} \frac{1}{n!} I^n = \exp\left\{ 2 \int_0^1 \frac{dx_1 \left[x_1^{N-1} - 1 \right]}{(1 - x_1)} \int_{\mu_F^2}^{(1-x_1)^2 Q^2} \frac{dk_T^2}{k_T^2} C_i \frac{\alpha_s \left(k_T^2 \right)}{\pi} \right\} \tag{4.24}$$

where the $1/n!$ originates from n same type final state particle, the emitted gluons.

These types of corrections can be generalized beyond LL by taking into account higher order color factors $A_i \left(\alpha_s \left(k_T^2 \right) \right) = A_i^{(1)} \alpha_s \left(k_T^2 \right) /\pi + A_i^{(2)} \left(\alpha_s \left(k_T^2 \right) /\pi \right)^2 + \ldots$:

$$\Delta_{i\bar{i}} = \exp\left\{ 2 \int_0^1 \frac{dx_1 \left[x_1^{N-1} - 1 \right]}{(1 - x_1)} \int_{\mu_F^2}^{(1-x_1)^2 Q^2} \frac{dk_T^2}{k_T^2} A_i \left(\alpha_s \left(k_T^2 \right) \right) \right\} \tag{4.25}$$

4.2 General factorization

In general the factorization of the infrared behavior of the cross section can be formulated in terms of different weights ω. The requirements on weight variables are [82]:

- Vanish in the soft limit.

- Infrared safe. This requires the weight to be symmetric in the final state momenta and $\omega_n (k_1, \ldots (1 - \alpha) \omega_{n-1}, \alpha \omega_{n-1}) = \omega_{n-1} (k_1, \ldots \omega_{n-1})$ with k_i the momenta of the final state particles.

- In the elastic limit the weight can be split into contributions from the jets and the soft functions that are additive and independent. $\omega = \omega_1 + \omega_2 + \omega_s$.

This requires a relation between a hadronic weight and the partonic weights that describe the different ways to approach the infrared limits. The final relation between the hadronic and partonic threshold variables will be defined as:

$$W = (1 - x_1) c_1 + (1 - x_2) c_2 + \omega \tag{4.26}$$

$$= \omega_1 c_1 + \omega_2 c_2 + \omega_s \tag{4.27}$$

with W the hadronic weight, x_i the fraction of the energy transmitted from the hadron to the parton i and ω the partonic weight. The variables c_i describe the way the soft limit is approached in the collinear limit, this will be described in greater detail in Section 7.5. The different weights that describe the different ways to approach infrared limits are labeled as ω_i for emission collinear to the initial particle i and ω_s for the soft limit. As an example we can look at the weight $1 - Q^2/\hat{s}$:

$$\frac{Q^2}{S} = x_1 x_2 \frac{Q^2}{\hat{s}}$$

$$W = 1 - \frac{Q^2}{S} = 1 - x_1 x_2 \frac{Q^2}{\hat{s}}$$

$$\approx 1 - x_1 + 1 - x_2 + 1 - \frac{Q^2}{\hat{s}}$$

$$= \omega_1 + \omega_2 + \omega_s \tag{4.28}$$

where the approximation is and expansion for $x_i \rightarrow 1$ and $Q^2 \rightarrow \hat{s}$. We will be looking at partonic cross sections and instead of PDFs, parton in parton functions will be used. This is why the $x_i \rightarrow 1$ limit can be used here.

The inclusive cross section for our set of hadronic kinematic variables, Π_n, for neutral particle production is given by [83]:

$$\frac{d\sigma_{AB \rightarrow c+X}}{d\Pi_n} = \sum_{i,j} \int dx_1 dx_2 \, f_{i/A} \left(x_1, \mu^2\right) f_{j/B} \left(x_2, \mu^2\right) \omega_{ij \rightarrow c+X} \left(\omega, \frac{\hat{\Pi}_n}{\mu^2}, \alpha_s \left(\mu^2\right)\right) \tag{4.29}$$

where $f_{i/A} \left(x, \mu^2\right)$ is the PDF for a parton i in a particle A and $\hat{\Pi}_n$ are the partonic kinematic variables for a $2 \rightarrow n$ process. The hadronic and partonic sets of kinematics depend on which weight is used, however for later sections within this chapter we will use Q^2 and the weight $1 - Q^2/\hat{s}$. However in Chapter 7 we will return to this with more general weights and the

different kinematics used for these. This equation is used to factorize the long range PDF effects from the short range hard process. Because the PDFs describe a parton in a hadron where the momentum of the parton is collinear to the hadron, collinear emission up to the factorization scale needs to be taken into account in the PDFs.

We will study this on the basis of the infrared-regulated, perturbative and factorized partonic cross section for neutral particle production, $i + j \to c + X$ [82]:

$$
\begin{aligned}
\frac{d\sigma_{ij \to c+X}}{d\hat{\Pi}_n} &= H_{ij}\left(\hat{\Pi}_n/\mu, n_i, \alpha_{\mathrm{s}}\left(\mu^2\right)\right) \int d\omega_1 d\omega_2 d\omega_s \delta\left(W - \omega_1 c_1 - \omega_2 c_2 - \omega_s\right) \\
&\quad \times \psi_{i/i}\left(\omega_1 \frac{Q}{\mu}, \frac{p_1 \cdot n_1}{\mu}, \alpha_{\mathrm{s}}\left(\mu^2\right), \epsilon\right) \psi_{j/j}\left(\omega_2 \frac{Q}{\mu}, \frac{p_2 \cdot n_2}{\mu}, \alpha_{\mathrm{s}}\left(\mu^2\right), \epsilon\right) \\
&\quad \times S\left(\frac{\omega_s Q}{\mu}, v_i, n_i, \alpha_{\mathrm{s}}\left(\mu^2\right)\right)
\end{aligned}
\tag{4.30}
$$

where ψ describes all collinear emission and are defined at fixed light-cone momentum instead of fixed energy, with ϵ the infrared regulator and n the gauge vector, S the soft emission and H describing the hard process. In this instance Q is replaced by another scale for different choices of the weight variable. Here we have not included the jet functions as there are no massless colored particles in the final state of the LO processes we are looking at. In order to describe the resummation we will apply the Laplace transformation:

$$
\tilde{\omega}_{ij}\left(N, \frac{\hat{\Pi}_n}{\mu^2}, \alpha_{\mathrm{s}}\left(\mu^2\right)\right) = \int_0^1 d\omega\, e^{-N\omega} \omega_{ij}\left(\omega, \frac{\hat{\Pi}_n}{\mu^2}, \alpha_{\mathrm{s}}\left(\mu^2\right)\right)
\tag{4.31}
$$

Alternatively Mellin space could be used if we approximate the weight relations (4.27) in a multiplicative manner, however the Mellin transform and the Laplace transform agree in the large N limit that we are interested in:

$$
\begin{aligned}
\int_0^1 d\omega\,(1-\omega)^{N-1} f\left(\omega\right) &= \int_0^1 d\omega\, e^{(N-1)\log(1-\omega)} f\left(\omega\right) \approx \int_0^1 d\omega\, e^{-(N-1)\omega} f\left(\omega\right) \\
&\approx \int_0^1 d\omega\, e^{-N\omega} f\left(\omega\right)
\end{aligned}
\tag{4.32}
$$

where we have performed an expansion for small ω and large N. For the invariant mass weight, $1 - Q^2/\hat{s}$, the multiplicative relation is exact, however this is not the case for other choices of the weight.

By comparing the Laplace transforms of Equations (4.29) and (4.30) for the partonic process $ij \to c + X$, we can find $\tilde{\omega}(N)$.

$$
\begin{aligned}
\int dW e^{-NW} \frac{d\sigma_{ij \to c+X}}{d\hat{\Pi}_n} &= \int dW e^{-NW} \int dx_1 dx_2\, f_{i/i}\left(x_1, \mu^2\right) f_{j/j}\left(x_2, \mu^2\right) \\
&\qquad \times \omega_{ij \to c+X}\left(\omega, \frac{\hat{\Pi}_n}{\mu^2}, \alpha_{\mathrm{s}}\left(\mu^2\right)\right) \\
&= \int d\omega\, dx_1 dx_2\, e^{-N(\omega + (1-x_1)c_1 + (1-x_2)c_2)} \\
&\qquad \times f_{i/i}\left(x_1, \mu^2\right) f_{j/j}\left(x_2, \mu^2\right) \omega_{ij \to c+X}\left(\omega, \frac{\hat{\Pi}_n}{\mu^2}, \alpha_{\mathrm{s}}\left(\mu^2\right)\right) \\
&= \tilde{f}_{i/i}\left(Nc_1, \mu^2\right) \tilde{f}_{j/j}\left(Nc_2, \mu^2\right) \tilde{\omega}_{ij \to c+X}\left(N, \frac{\hat{\Pi}_n}{\mu^2}, \alpha_{\mathrm{s}}\left(\mu^2\right)\right) \quad (4.33)
\end{aligned}
$$

The hadronic variables are now transformed into the partonic variables as we are studying a partonic process, if one defines the partonic variables using the initial state momenta before emitting particles through the parton in parton distribution functions $f_{i/i}$. On the other hand Equation (4.30) results in:

$$
\begin{aligned}
\int dW e^{-NW} \frac{d\sigma_{ij \to c+X}}{d\hat{\Pi}_3} &= H_{ij}\left(\hat{\Pi}_n/\mu, n_i, \alpha_{\mathrm{s}}\left(\mu^2\right)\right) \tilde{S}\left(\frac{Q}{\mu N}, v_i, n_i, \alpha_{\mathrm{s}}\left(\mu^2\right)\right) \\
&\qquad \times \tilde{\psi}_{i/i}\left(\frac{Q}{\mu N c_1}, \frac{p_1 \cdot n_1}{\mu}, \alpha_{\mathrm{s}}\left(\mu^2\right)\right) \tilde{\psi}_{j/j}\left(\frac{Q}{\mu N c_2}, \frac{p_2 \cdot n_2}{\mu}, \alpha_{\mathrm{s}}\left(\mu^2\right)\right) \quad (4.34)
\end{aligned}
$$

If we combine these two expressions this results in:

$$
\tilde{\omega}_{ij \to c+X}\left(N, \frac{\hat{\Pi}_n}{\mu^2}, \alpha_{\mathrm{s}}\left(\mu^2\right)\right) = H_{ij}\left(\hat{\Pi}_n\right) \frac{\tilde{\psi}_{i/i}\left(Nc_1\right) \tilde{\psi}_{j/j}\left(Nc_2\right)}{\tilde{f}_{i/i}\left(Nc_1\right) \tilde{f}_{j/j}\left(Nc_2\right)} \tilde{S}(N) \qquad (4.35)
$$

where we have suppressed most of the dependence of the different functions. Here we resum all infrared limit emission and subtract the emission that is included in the PDFs through use of the parton in parton distributions. In order to solve each of these equations, renormalization group equations will be used.

4.3 Resummation for Drell-Yan

Now that the factorization of the cross section has been established near threshold, we can look at how this allows us to obtain a resummed expression. Since resummation was first derived for Drell-Yan this is where we will start [84, 85]. The resummation for Drell-Yan will be explained on the basis of the method used in [82].

First we will look at the renormalization scale dependence of the different functions of the cross

section:

$$
\mu \frac{d}{d\mu} \log H = -\gamma_H \left(\alpha_s \right)
$$

$$
\mu \frac{d}{d\mu} \log \tilde{\psi}_i = -\gamma_{\psi_i} \left(\alpha_s \right) \tag{4.36}
$$

$$
\mu \frac{d}{d\mu} \log \tilde{S} = -\gamma_S \left(\alpha_s \right)
$$

where γ are the anomalous dimensions for each of the function and we represent $\psi_1 = \psi_{i/i}$ and $\psi_2 = \psi_{j/j}$. The factorized functions each depend explicitly and implicitly through means of α_s on the renormalization scale. The anomalous dimensions are assumed to be independent of the momenta N and the gauge vectors n. As the cross section is independent of the renormalization scale the sum of the different anomalous dimension adds up to 0:

$$
\mu \frac{d}{d\mu} \log \sigma = \gamma_H + \gamma_S + \gamma_{\psi_1} + \gamma_{\psi_2} = 0 \tag{4.37}
$$

This way the renormalization scale dependence of the partonic cross section cancels.

This leads to a scale dependence for the soft function:

$$
\tilde{S} \left(\frac{Q}{\mu N}, v_i, n, \alpha_s \left(\mu^2 \right) \right) = \tilde{S} \left(1, v_i, n_i, \alpha_s \left(\frac{Q^2}{N^2} \right) \right) \exp \left[\int_\mu^{Q/N} \frac{d\lambda}{\lambda} \gamma_S \left(\alpha_s \left(\lambda^2 \right) \right) \right] \tag{4.38}
$$

where we evolve the scale from Q/N to μ. Here the "natural" scale for the soft emission is Q/N and leads to a function $\tilde{S} \left(1, v_i, n, \alpha_s \left(\frac{Q^2}{N^2} \right) \right)$ which contains no logarithms. Equation 4.38 is able to resum all of the N-dependence of the soft function, because it only contains single logarithms of N.

For the initial state collinear function we can use a similar treatment:

$$
\tilde{\psi}_i \left(\frac{Q}{\mu N}, \frac{p_i \cdot n_i}{\mu}, \alpha_s \left(\mu^2 \right) \right) = \tilde{\psi}_i \left(1, \frac{\left(p_i \cdot n_i \right) N}{Q}, \alpha_s \left(\frac{Q^2}{N^2} \right) \right) \exp \left[\int_\mu^{Q/N} \frac{d\lambda}{\lambda} \gamma_{\psi_i} \left(\alpha_s \left(\lambda^2 \right) \right) \right] \tag{4.39}
$$

However for the collinear function there are two "natural" scales Q/N and $p_i \cdot n$. This is due to the fact that the collinear function includes double logarithms, i.e. contributions from both the soft and collinear region. Therefore it is not enough to only analyze the renormalization scale dependence, but we also need to study the gauge vector dependence.

As the cross section should also be independent of the choice of the gauge vectors n_1 and n_2, we also have the relation:

$$
0 = p_1 \cdot n_1 \frac{\partial}{\partial p_1 \cdot n_1} \left(\log \tilde{\psi}_1 + \log H + \log \tilde{S} \right) \tag{4.40}
$$

where we have left out $\tilde{\psi}_2$ because it does not depend on $p_1 \cdot n_1$. This allows us to write $\tilde{\psi}_1$ in terms of $\tilde{H}$ and $\tilde{S}$:

$$
p_1 \cdot n_1 \frac{\partial}{\partial p_1 \cdot n_1} \log \tilde{\psi}_1 \left(\frac{Q}{\mu N}, \frac{p_1 \cdot n_1}{\mu}, \alpha_s \left(\mu^2 \right) \right) = -p_1 \cdot n_1 \frac{\partial}{\partial p_1 \cdot n_1} \log H \left(\hat{\Pi}_3 / \mu, n_i, \alpha_s \left(\mu^2 \right) \right)
$$

$$
-p_1 \cdot n_1 \frac{\partial}{\partial p_1 \cdot n_1} \log \tilde{S} \left(\frac{Q}{\mu N}, v_i, n, \alpha_s \left(\mu^2 \right) \right)
$$

$$
= G \left(\frac{p_1 \cdot n_1}{\mu}, \alpha_s \left(\mu^2 \right) \right) + K \left(\frac{Q}{\mu N}, \alpha_s \left(\mu^2 \right) \right) \tag{4.41}
$$

using the definition for G and K:

$$G \equiv -p_1 \cdot n_1 \frac{\partial}{\partial p_1 \cdot n_1} \log H$$

$$K \equiv -p_1 \cdot n_1 \frac{\partial}{\partial p_1 \cdot n_1} \log \tilde{S} \tag{4.42}$$

As the anomalous dimension γ_{ψ_1} does not depend on $p_1 \cdot n_1$, $G + K$ is independent of the renormalization scale:

$$p_1 \cdot n_1 \frac{d}{dp_1 \cdot n_1} \gamma_{\psi_1} (\alpha_{\rm s}) = \mu \frac{d}{d\mu} \left[G \left(\frac{p_1 \cdot n_1}{\mu}, \alpha_{\rm s} (\mu^2) \right) + K \left(\frac{Q}{\mu N}, \alpha_{\rm s} (\mu^2) \right) \right] = 0 \tag{4.43}$$

again we can separate the variables

$$\mu \frac{d}{d\mu} K \left(\frac{Q}{\mu N}, \alpha_{\rm s} (\mu^2) \right) = -\gamma_K (\alpha_{\rm s} (\mu^2))$$

$$\mu \frac{d}{d\mu} G \left(\frac{p_1 \cdot n_1}{\mu}, \alpha_{\rm s} (\mu^2) \right) = \gamma_K (\alpha_{\rm s} (\mu^2)) \tag{4.44}$$

with γ_K a Sudakov anomalous dimension. This differential equation can be solved to result in:

$$K \left(\frac{Q}{\mu N}, \alpha_{\rm s} (\mu^2) \right) + G \left(\frac{p_1 \cdot n_1}{\mu}, \alpha_{\rm s} (\mu^2) \right) = K \left(1, \alpha_{\rm s} \left(\frac{Q^2}{N^2} \right) \right) + G \left(1, \alpha_{\rm s} \left((p_1 \cdot n_1)^2 \right) \right)$$

$$- \int_{Q/N}^{p_1 \cdot n_1} \frac{d\lambda}{\lambda} \gamma_K (\alpha_{\rm s} (\lambda^2)) \tag{4.45}$$

If the argument of $\alpha_{\rm s}$ in K is changed to $\alpha_{\rm s} \left((p_1 \cdot n_1)^2 \right)$, this results in

$$K \left(\frac{Q}{\mu N}, \alpha_{\rm s} (\mu^2) \right) + G \left(\frac{p_1 \cdot n_1}{\mu}, \alpha_{\rm s} (\mu^2) \right) = A' \left(\alpha_{\rm s} \left((p_1 \cdot n_1)^2 \right) \right) - \int_{Q/N}^{p_1 \cdot n_1} \frac{d\lambda}{\lambda} A (\alpha_{\rm s} (\lambda^2)) \tag{4.46}$$

where the functions A and A' are defined by

$$A (\alpha_{\rm s}) = \gamma_K (\alpha_{\rm s}) + \beta (g) \frac{\partial}{\partial g} K (1, \alpha_{\rm s}) \tag{4.47}$$

and

$$A' (\alpha_{\rm s}) = K (1, \alpha_{\rm s}) + G (1, \alpha_{\rm s}) \tag{4.48}$$

Making use of Equation (4.41) we can now describe the full N dependence of ψ_i:

$$\tilde{\psi}_i \left(1, \frac{(p_i \cdot n_i) N}{Q}, \alpha_{\rm s} \left(\frac{Q^2}{N^2} \right) \right) = \tilde{\psi}_i \left(1, 1, \alpha_{\rm s} \left(\frac{Q^2}{N^2} \right) \right) \tag{4.49}$$

$$\times \exp \left[- \int_{Q/N}^{p_i \cdot n_i} \frac{d\lambda}{\lambda} \left\{ \int_{Q/N}^{\lambda} \frac{d\xi}{\xi} A (\alpha_{\rm s} (\xi^2)) - A' (\alpha_{\rm s} (\lambda^2)) \right\} \right]$$

If this is combined with Equation (4.39) this results in:

$$\tilde{\psi}_i \left(\frac{Q}{\mu N}, \frac{(p_i \cdot n_i) N}{Q}, \alpha_{\rm s} \left(\frac{Q^2}{N^2} \right) \right) = \tilde{\psi}_i \left(1, 1, \alpha_{\rm s} \left(\frac{Q^2}{N^2} \right) \right) \exp \left[- \int_{Q/N}^{\mu} \frac{d\lambda}{\lambda} \gamma_{\psi_i} (\alpha_{\rm s} (\lambda^2)) \right] \tag{4.50}$$

$$\times \exp \left[- \int_{Q/N}^{p_i \cdot n_i} \frac{d\lambda}{\lambda} \left\{ \int_{Q/N}^{\lambda} \frac{d\xi}{\xi} A (\alpha_{\rm s} (\xi^2)) - A' (\alpha_{\rm s} (\lambda^2)) \right\} \right]$$

Finally Equations (4.38) and (4.50) can all be combined into Equation (4.34) resulting in the cross section:

$$
\begin{aligned}
\tilde{\sigma}\left(N\right) \;=\;& H\left(\hat{\Pi}_n/\mu, n_i, \alpha_s\left(\mu^2\right)\right) \tilde{\psi}_1\left(1, 1, \alpha_s\left(\frac{Q^2}{N^2}\right)\right) \tilde{\psi}_2\left(1, 1, \alpha_s\left(\frac{Q^2}{N^2}\right)\right) \tilde{S}\left(1, \alpha_s\left(\frac{Q^2}{N^2}\right)\right) \\
&\times \exp\left[-\int_{Q/N}^{\mu} \frac{d\lambda}{\lambda}\left\{\gamma_{\psi_1}\left(\alpha_s\left(\lambda^2\right)\right) + \gamma_{\psi_2}\left(\alpha_s\left(\lambda^2\right)\right) + \gamma_S\left(\alpha_s\left(\lambda^2\right)\right)\right\}\right] \\
&\times \exp\left[-\int_{Q/N}^{p_i \cdot n_i} \frac{d\lambda}{\lambda}\left\{\int_{Q/N}^{\lambda} \frac{d\xi}{\xi} 2A\left(\alpha_s\left(\xi^2\right)\right) - 2A'\left(\alpha_s\left(\lambda^2\right)\right)\right\}\right]
\end{aligned}
\tag{4.51}
$$

If we now set $p_i \cdot n_i$ and μ equal to Q this results in:

$$
\begin{aligned}
\tilde{\sigma}\left(N\right) \;=\;& H\left(\hat{\Pi}_n, \alpha_s\left(Q^2\right)\right) \tilde{\psi}_1\left(1, 1, \alpha_s\left(\frac{Q^2}{N^2}\right)\right) \tilde{\psi}_2\left(1, 1, \alpha_s\left(\frac{Q^2}{N^2}\right)\right) \tilde{S}\left(1, \alpha_s\left(\frac{Q^2}{N^2}\right)\right) \\
&\times \exp\left[-\int_{Q/N}^{Q} \frac{d\lambda}{\lambda}\left\{\int_{Q/N}^{\lambda} \frac{d\xi}{\xi} 2A\left(\alpha_s\left(\xi^2\right)\right) - 2B\left(\alpha_s\left(\lambda^2\right)\right)\right\}\right]
\end{aligned}
\tag{4.52}
$$

with

$$
B\left(\alpha_s\right) = A'\left(\alpha_s\right) - \frac{1}{2}\left(\gamma_S\left(\alpha_s\right) + \gamma_{\psi_1}\left(\alpha_s\right) + \gamma_{\psi_2}\left(\alpha_s\right)\right)
\tag{4.53}
$$

Alternative formulation

We can also make use of the dependence on the momentum transfer Q^2 to reformulate the Sudakov exponentiation in Equation (4.52). This method will only briefly be treated here, but a detailed explanation can be found in [82]. First we can use Equation (4.52) to show that the derivative can be written as

$$
Q^2 \frac{d}{dQ^2} \tilde{\sigma}\left(N, Q^2\right) = \tilde{W}\left(N, Q^2\right) \tilde{\sigma}\left(N, Q^2\right)
\tag{4.54}
$$

for a function $\tilde{W}$, where the Mellin transform is used to describe W:

$$
Q^2 \frac{d}{dQ^2} \sigma\left(z, Q^2\right) = \int_z^1 \frac{dz'}{z'} W\left(z', Q^2\right) \sigma\left(z/z', Q^2\right)
\tag{4.55}
$$

We normalize these functions such that

$$
\sigma\left(z, Q^2 = 0\right) = \delta\left(1 - z\right)
\tag{4.56}
$$

The physical idea behind this is that if there is no momentum transfer, there can also not be any additional radiation if the scattering is through an electroweak current, as for Drell-Yan.

The resulting solution with the boundary condition $\tilde{\sigma}\left(N, 0\right) = 1$ is

$$
\tilde{\sigma}\left(N, Q^2\right) = \exp\left[\int_0^{Q^2} \frac{d\xi}{\xi^2} \tilde{W}\left(N, \frac{\xi^2}{\mu^2}, \alpha_s\left(\mu^2\right), \epsilon\right)\right]
\tag{4.57}
$$

This equation can then be expanded and matched to the fixed order results of Drell-Yan. In this we can also already remove the parton in parton effects as was done in Equation (4.35). This

results in:

$$
\omega_{q\bar{q}\to B}^{\overline{\text{MS}}}\left(N,1,\alpha_{\text{s}}\left(Q^2\right)\right) = \exp\left[\int_0^1 dz \left(\frac{z^{N-1}-1}{1-z}\right)\left(1+z^2\right)\int_{(1-z)^2}^1 \frac{d\lambda}{\lambda}\left(-C_F\right)\frac{\alpha_{\text{s}}\left(\lambda Q^2\right)}{\pi}\right]
$$

$$
\times \exp\left[-\frac{\alpha_{\text{s}}\left(Q^2\right)}{2\pi}C_F\left(1-\frac{2\pi^2}{3}\right)\right] \tag{4.58}
$$

where $\mu = Q$ has been used. The terms of order $1/N$ will be neglected by approximating:

$$
\frac{1+z^2}{1-z} \overset{z\to 1}{\to} \frac{2}{1-z} \tag{4.59}
$$

This allows us to write the final equation as

$$
\omega_{q\bar{q}\to B}^{\overline{\text{MS}}}\left(N,1,\alpha_{\text{s}}\left(Q^2\right)\right) = R_{q\bar{q}}\left(\alpha_{\text{s}}\left(Q^2\right)\right) \tag{4.60}
$$

$$
\times \exp\left[-2\int_0^1 dz \frac{z^{N-1}-1}{1-z}\left\{\int_{(1-z)^2}^1 \frac{d\lambda}{\lambda}A\left(\alpha_{\text{s}}\left(\lambda Q^2\right)\right)+B\left(\alpha_{\text{s}}\left(Q^2\right)\right)\right\}\right]
$$

where the functions A and D can be expanded as

$$
A\left(\alpha_{\text{s}}\right) = \sum_{k=1}^\infty \left(\frac{\alpha_{\text{s}}}{\pi}\right)^k A^{(k)}
$$

$$
B\left(\alpha_{\text{s}}\right) = \sum_{k=1}^\infty \left(\frac{\alpha_{\text{s}}}{\pi}\right)^k B^{(k)}
$$

and we have absorbed the N independent terms in an overall factor $R_{q\bar{q}}$. For Drell-Yan $A^{(1)} = C_F$ and in the $\overline{\text{MS}}$ factorization scheme $B^{(1)} = 0$. We can see that this result agrees with the result that was derived in the previous section, Equation (4.25) with $\mu_F = Q$. At NLL we include the coefficient $A_i^{(2)} = C_i\left(C_A\left(\frac{67}{18}-\frac{\pi^2}{6}\right)-\frac{5}{9}n_l\right)/2$ in general [86]. For NNLL in resummation we need additional contributions leading to the exponent:

$$
\Delta_{i\bar{i}}(N) = \exp\left[2\int_0^1 dz \frac{z^{N-1}-1}{1-z}\left\{\int_1^{(1-z)^2} \frac{d\lambda}{\lambda}A\left(\alpha_{\text{s}}\left(\lambda Q^2\right)\right)+D\left(\alpha_{\text{s}}\left((1-z)^2 Q^2\right)\right)\right\}\right] \tag{4.61}
$$

where we need to take into account $A^{(i)}$ for $i = 1, 2, 3$ and $D^{(1)}$.

We have now been including all contributions, both soft and collinear, into the exponential. Earlier we separated contributions into soft-wide angle S and collinear ψ/f in the factorization. The form of S given for $\mu = Q$ is

$$
\tilde{S}\left(N,Q^2,\alpha_{\text{s}}\left(Q^2\right)\right) = \tilde{S}\left(1,\alpha_{\text{s}}\left(\frac{Q^2}{N^2}\right)\right)\Delta_{S_{i\bar{i}}}\left(N,Q^2,\alpha_{\text{s}}\left(Q^2\right)\right) \tag{4.62}
$$

$$
= \tilde{S}\left(1,\alpha_{\text{s}}\left(\frac{Q^2}{N^2}\right)\right)\exp\left[\int_0^1 dz \frac{z^{N-1}-1}{1-z}\Gamma_{S_{i\bar{i}}}\left(\alpha_{\text{s}}\left((1-z)^2 Q^2\right)\right)\right]
$$

where we have defined the soft anomalous dimension for neutral particle production as

$$
\Gamma_{S_{i\bar{i}}}\left(\alpha_{\text{s}}\right) = \sum_{k=1}^\infty \left(\frac{\alpha_{\text{s}}}{\pi}\right)^k \Gamma_{S_{i\bar{i}}}^{(k)} \tag{4.63}
$$

with the one-loop soft anomalous dimension given by

$$\Gamma_{S_{i\bar{i}}}^{(1)} = C_i \left(1 - \log \left(2 \frac{(v_i \cdot n)^2}{|n|^2} \right) - i\pi \right) \tag{4.64}$$

with $v_i = p_i \sqrt{2/\hat{s}}$ a dimensionless version of the momentum. The calculation of this contribution is done through residue of the UV divergent contribution of a gluon exchange between the two initial state partons. The computation of the soft anomalous dimension will be explored in greater detail in Section 7.3. After removing this soft-wide angle contribution from the collinear contribution, this results in:

$$\frac{\tilde{\psi}_{i/i}(N) \, \tilde{\psi}_{\bar{i}/\bar{i}}(N)}{\tilde{f}_{i/i}(N) \, \tilde{f}_{\bar{i}/\bar{i}}(N)} = \frac{\exp\left[2 \int_0^1 dz \frac{z^{N-1}-1}{1-z} \left\{ \int_1^{(1-z)^2} \frac{d\lambda}{\lambda} A\left(\alpha_{\mathrm{s}}\left(\lambda Q^2\right)\right) \right\} \right]}{\Delta_{S_{i\bar{i}}}\left(N, Q^2, \alpha_{\mathrm{s}}\left(Q^2\right)\right)} \tag{4.65}$$

4.4 Resummation for massive colored particle production

As we are also interested in colored final states and specifically two massive colored particles, the resummation needs to be computed for massive colored final states. Gluon emission from massive particles does not contain any collinear divergences, as the mass regulates this divergence. Therefore, we do not need to take into account final state jet functions, describing the collinear emission from final state particles. For the description of the final state jet functions [87] can be consulted. In this section we will follow [88–90].

First the factorization theorem, presented in Equation (4.35), needs to be modified to include final state emission. The main difference is that the soft function is dependent on the color structure of the hard process from which the soft gluon is emitted:

$$\tilde{\omega}_{ij\to kl+X}\left(N, \frac{\hat{\Pi}_n}{\mu^2}, \alpha_{\mathrm{s}}\left(\mu^2\right)\right) = \frac{\tilde{\psi}_{i/i}\left(Nc_1, \frac{Q}{\mu}, \alpha_{\mathrm{s}}\left(\mu^2\right), \epsilon\right) \tilde{\psi}_{j/j}\left(Nc_2, \frac{Q}{\mu}, \alpha_{\mathrm{s}}\left(\mu^2\right), \epsilon\right)}{\tilde{f}_{i/i}\left(Nc_1, \frac{Q}{\mu}, \alpha_{\mathrm{s}}\left(\mu^2\right), \epsilon\right) \tilde{f}_{j/j}\left(Nc_2, \frac{Q}{\mu}, \alpha_{\mathrm{s}}\left(\mu^2\right), \epsilon\right)}$$

$$\times \sum_{I,J} H_{ij\to kl,IJ}\left(\hat{\Pi}_n, \alpha_{\mathrm{s}}\left(\mu^2\right)\right) \tilde{S}_{ij\to kl,JI}\left(\frac{Q}{\mu N}, \alpha_{\mathrm{s}}\left(\mu^2\right)\right) \tag{4.66}$$

Because the collinear emission and the parton in parton distributions decouple from the soft gluon emission, the collinear emission is proportional to the unit matrix in color space and only depends on the color structure of the initial partons. The infrared divergences from the collinear emission $\tilde{\psi}$ cancel against the infrared divergences from the parton in parton distributions $\tilde{f}$, so the resulting cross section function $\tilde{\omega}$ is infrared finite. The hard function is defined as:

$$H_{ij\to kl,IJ}\left(\hat{\Pi}_n, \alpha_{\mathrm{s}}\left(\mu^2\right)\right) = h_{ij\to kl,I}\left(\hat{\Pi}_n, \alpha_{\mathrm{s}}\left(\mu^2\right)\right) h_{ij\to kl,J}^*\left(\hat{\Pi}_n, \alpha_{\mathrm{s}}\left(\mu^2\right)\right) \tag{4.67}$$

with h_I the matrix element projected onto a color basis c_I. With the LO soft function given by:

$$\tilde{S}_{ij\to kl,JI}^{(0)} = \mathrm{tr}\left(c_J^\dagger c_I\right) \tag{4.68}$$

this color basis can be chosen in any way, however it will be convenient to choose the s-channel basis as the soft anomalous dimension matrix will diagonalize in the the absolute threshold for this color basis. The practical computations for finding the color basis will be presented in Section 7.2.1 and we will make use of them in Section 7.3.2.

As before we will be making using of renormalization group equations in order to compute the resummation exponentials. The independence on the renormalization scale of the cross section results in the requirement on the product of the soft and hard function:

$$\mu\frac{d}{d\mu}\log\left[H_{ij\to kl,IJ}\tilde{S}_{ij\to kl,JI}\right] = \gamma_{\psi_i} + \gamma_{\psi_j} \tag{4.69}$$

Therefore the ultraviolet divergences from the soft function have to be compensated by similar terms in the hard function. The soft and hard function are renormalized multiplicatively:

$$H^{\text{bare}}_{ij\to kl,IJ} = Z_i^{-1}Z_j^{-1}(Z_{ij\to kl})^{-1}_{IK}H_{ij\to kl,KL}\left(Z^{\dagger}_{ij\to kl}\right)^{-1}_{LJ} \tag{4.70}$$

$$\tilde{S}^{\text{bare}}_{ij\to kl,JI} = \left(Z^{\dagger}_{ij\to kl}\right)_{JK}\tilde{S}_{ij\to kl,KL}(Z_{ij\to kl})_{LI} \tag{4.71}$$

where H^{bare} and $\tilde{S}^{\text{bare}}$ are the unrenormalized quantities, $Z_{i,j}$ are the renormalization constants of the incoming fields to the hard process and $Z_{ij\to kl}$ is the renormalization matrix for the soft function. The $Z_{ij\to kl}$ matrix is defined to include the outgoing field renormalizations. From Equation (4.71) we can now derive the evolution equation for the soft function

$$\mu\frac{d}{d\mu}\tilde{S}_{ij\to kl,JI} = -\Gamma^{\dagger}_{ij\to kl,JK}\tilde{S}_{ij\to kl,KI} - \tilde{S}_{ij\to kl,JK}\Gamma_{ij\to kl,KI} \tag{4.72}$$

with $\Gamma_{ij\to kl}$ the soft anomalous dimension matrix. The soft anomalous dimension matrix is computed on the basis of the residue of the renormalization of matrix element at one loop by using dimensional regularization in $d = 4 - \epsilon$ dimensions:

$$\Gamma_{ij\to kl,IJ}(\alpha_{\text{s}}) = -\alpha_{\text{s}}\frac{\partial}{\partial\alpha_{\text{s}}}\text{Res}_{\epsilon\to 0}(Z_{ij\to kl})_{IJ}(\alpha_{\text{s}},\epsilon) \tag{4.73}$$

The computation of the soft anomalous dimension matrix will be presented in Section 7.3 by means of the process $pp \to t\bar{t}H$.

The general solution for Equation (4.72) making use of the path-ordered exponentials is

$$\tilde{S}_{ij\to kl,JI}\left(\frac{Q}{\mu N},\alpha_{\text{s}}(\mu^2)\right) = \bar{\text{P}}\exp\left[\int_{\mu}^{Q/N}\frac{dq}{q}\Gamma^{\dagger}_{ij\to kl}(\alpha_{\text{s}}(q^2))\right]\tilde{S}_{ij\to kl,JI}\left(1,\alpha_{\text{s}}\left(\frac{Q^2}{N^2}\right)\right)$$

$$\times\text{P}\exp\left[\int_{\mu}^{Q/N}\frac{dq}{q}\Gamma_{ij\to kl}(\alpha_{\text{s}}(q^2))\right] \tag{4.74}$$

where P and $\bar{\text{P}}$ denote the path-ordering and reverse path-ordering in the variable q respectively. The path-ordered exponential orders $\Gamma_{ij\to kl}(\alpha_{\text{s}}(\mu^2))$ to the far right and $\Gamma_{ij\to kl}(\alpha_{\text{s}}(Q^2/N^2))$ to the far left. Reverse path-ordering orders it in the opposite way. If the soft anomalous dimension matrix is diagonal the path ordering is not needed and the soft function becomes:

$$\tilde{S}_{ij\to kl,JI}\left(\frac{Q}{\mu N},\alpha_{\text{s}}(\mu^2)\right) = \tilde{S}_{ij\to kl,JI}\left(1,\alpha_{\text{s}}\left(\frac{Q^2}{N^2}\right)\right)$$

$$\times\exp\left[\int_{\mu}^{Q/N}\frac{dq}{q}\{\lambda_J^*(\alpha_{\text{s}}(q^2)) + \lambda_I(\alpha_{\text{s}}(q^2))\}\right] \tag{4.75}$$

At the NLL accuracy the one loop soft anomalous dimension is needed and $\tilde{S}_{ij\to kl,JI}(1,\alpha_{\text{s}}(Q^2/N^2))$ is given by the LO soft function $\tilde{S}^{(0)}_{ij\to kl,JI}$. The diagonal form for the soft anomalous dimension can either be achieved by a diagonalization procedure which will be presented in Section 7.3.6 or

by choosing the appropriate color basis. For the absolute threshold we will use a color basis that will diagonalize the soft anomalous dimension matrix. For absolute threshold this will result in the soft function:

$$\tilde{S}_{ij \to kl,JI} \left(\frac{Q}{\mu N}, \alpha_{\mathrm{s}} \left(\mu^2 \right) \right) \quad = \quad \tilde{S}^{(0)}_{ij \to kl,JI} \exp \left[\int_{\mu}^{Q/N} \frac{dq}{q} \frac{\alpha_{\mathrm{s}} \left(q^2 \right)}{\pi} D^{(1)}_{ij \to kl,I} \right] \qquad (4.76)$$

with

$$D^{(1)}_{ij \to kl,I} = \lim_{\beta \to 0} \frac{\pi}{\alpha_{\mathrm{s}}} 2\mathcal{R}e \left(\Gamma^{(1)}_{ij \to kl,II} \right) \qquad (4.77)$$

The computation of the soft anomalous dimension matrix will be done for the example of $pp \to t\bar{t}H$ in Section 7.3.

Alternatively the exponential can be formulated as:

$$\tilde{S}_{ij \to kl,JI} \left(\frac{Q}{\mu N}, \alpha_{\mathrm{s}} \left(\mu^2 \right) \right) = \tilde{S}^{(0)}_{ij \to kl,JI} \exp \left[\int_0^1 dz \frac{z^{N-1} - 1}{1 - z} \frac{\alpha_{\mathrm{s}} \left((1 - z)^2 Q^2 \right)}{\pi} D^{(1)}_{ij \to kl,I} \right] (4.78)$$

If we split the resummation up into the Drell-Yan contribution, as in Equation (4.61), and the soft-wide angle final state particle contribution we will need to subtract the Drell-Yan soft-wide angle term from the soft anomalous dimension:

$$\bar{\Gamma}^{(1)}_{ij \to kl,IJ} = \Gamma^{(1)}_{ij \to kl,IJ} - \frac{\alpha_{\mathrm{s}}}{2\pi} \sum_{p=\{i,j\}} C_p \left(1 - \log \left(2 \frac{(v_i \cdot n)^2}{|n|^2} \right) - i\pi \right) \delta_{IJ} \qquad (4.79)$$

This can only be done if $c_1 = c_2 = 1$. If this is not the case the collinear and soft contributions need to be kept separately in different exponentials with rescaled N. If this separation is performed we obtain two exponentials that depend on the initial state color factors and the soft-wide angle emission which depends on the color factor for the color basis.

4.5 Numerical treatment

Now that the resummation equations have all been derived we can look at the methods that will be used in the practical applications of the next three chapters. The final hadronic cross section including the resummation effects for $c_1 = c_2 = 1$ is:

$$\Sigma^{(\mathrm{res})}_{h_1 h_2 \to kl} = \sum_{i,j} \sum_I \int_{C_T} \frac{dN}{2\pi i} \tau^{-N} \tilde{f}_{i/h_1} \left(N + 1, \mu_F^2 \right) \tilde{f}_{j/h_2} \left(N + 1, \mu_F^2 \right) \hat{\Sigma}^{(0)}_{ij \to kl} \left(N, \mu_R^2 \right)$$

$$\times C_{ij \to kl,I} \left(N \right) \Delta_i \left(N + 1, \mu_R^2, \mu_F^2 \right) \Delta_j \left(N + 1, \mu_R^2, \mu_F^2 \right) \Delta_{ij \to kl,I} \left(N + 1, \mu_R^2 \right) (4.80)$$

where Σ is the cross section, σ, for absolute threshold resummation and the differential cross section with respect to the final state invariant mass Q^2, $d\sigma/dQ^2$, for invariant mass resummation. The inverse Mellin transform variable is given by $\tau = W^2/S$ with W^2 the relevant scale for the resummation (M^2 or Q^2) and S the invariant mass squared of the hadronic initial state. For a clarification on the source of the $N + 1$ in the resummation exponentials [64] can be consulted. The factor $C_{ij \to kl,I}$ is the matching coefficient which takes into account NLO effects of non-logarithmic origin. The definitions of the resummation exponentials are:

$$\Delta_i \left(N, \mu_R^2, \mu_F^2 \right) = \exp \left[g_1 \left(b_0 \alpha_{\mathrm{s}} \log N \right) \log N + g_2 \left(b_0 \alpha_{\mathrm{s}} \log N \right) + g_3 \left(b_0 \alpha_{\mathrm{s}} \log N \right) \alpha_{\mathrm{s}} + \ldots \right] \quad (4.81)$$

and

$$\Delta_{ij\rightarrow kl,I}\left(N+1,\mu_R^2\right) = \exp\left[h_2\left(b_0\alpha_s\log N\right) + h_3\left(b_0\alpha_s\log N\right)\alpha_s + \ldots\right] \tag{4.82}$$

up to the NNLL order. At LL g_1 is included, at NLL g_2 and h_2 are included and at NNLL g_3 and h_3 are included, these functions can be found in [64, 73, 91]. Finally the PDFs in Mellin space are given by:

$$\tilde{f}_{i/h_1}\left(N,\mu_F^2\right) = \int_0^1 dx\, x^{N-1} f_{i/h_1}\left(x,\mu_F^2\right) \tag{4.83}$$

For the contour C_T we use the prescription defined in [92]. For this we will parametrize the Mellin moment as:

$$N = C_{MP} + y e^{\pm i\phi} \tag{4.84}$$

with C_{MP} a real shift that places the integration contour to the right of all singularities except the Landau pole $N_L = \exp\left[1/\left(2\alpha_s b_0\right)\right]$ and ϕ an angle that places the end point of the integration bound with negative real values to allow for a suppression from τ^{-N}. Only one of the branches needs to be integrated over and the other can be taken into account due to the fact that $\hat{\Sigma}_{ij\rightarrow kl}^{\mathrm{res.}}\left(N^*,\mu_R^2,\mu_F^2\right) = \hat{\Sigma}_{ij\rightarrow kl}^{\mathrm{res.*}}\left(N,\mu_R^2,\mu_F^2\right)$. The final result can then be found by multiplying the real part by 2.

In practice we want to preserve the full fixed order result and only use resummation for higher order corrections. Therefore, we will match the resummed results to the fixed order results:

$$\begin{aligned}
\Sigma_{h_1h_2\rightarrow kl}^{(\mathrm{f.o.+r.o.})} &= \Sigma_{h_1h_2\rightarrow kl}^{\mathrm{f.o.}}\left(\tau,\mu_R^2,\mu_F^2\right) \\
&+ \sum_{i,j}\sum_I \int_{C_T}\frac{dN}{2\pi i}\tau^{-N}\tilde{f}_{i/h_1}\left(N+1,\mu_F^2\right)\tilde{f}_{j/h_2}\left(N+1,\mu_F^2\right) \\
&\times \left\{\hat{\Sigma}_{ij\rightarrow kl}^{\mathrm{r.o.}}\left(N,\mu_R^2,\mu_F^2\right) - \hat{\Sigma}_{ij\rightarrow kl}^{\mathrm{r.o.}}\left(N,\mu_R^2,\mu_F^2\right)|_{\mathrm{f.o.}}\right\}
\end{aligned} \tag{4.85}$$

where f.o. indicates the order of the fixed order computation, r.o. is the order of the resummation and $\hat{\Sigma}_{ij\rightarrow kl}^{\mathrm{r.o.}}|_{\mathrm{f.o.}}$ is the expansion of the resummation in α_s up to the order of the fixed order computation.

When $\tau/\left(x_1 x_2\right)$ is close to 1 the suppression for large values of $|N|$ is lost. Therefore as a final practical consideration we will look at improving numerical stability in the large $|N|$ limit. There are two methods to do this through means of the treatment of the PDFs. For one method we use PDFs in Mellin space and the other is by using the derivative of the PDFs.

Mellin space parton distribution functions   For the Mellin space PDFs we can make use of the `PEGASUS` [93] code. In this code the parametrization used in the PDFs are implemented in Mellin space instead. For example for MSTW [94] the x space parametrization at an initial scale is given by:

$$x f_i\left(x,\mu_{F,0}^2\right) = \sum_l A_l x^{\gamma_l}\left(1-x\right)^{\delta_l} \tag{4.86}$$

In Mellin space this is given by the Euler beta function

$$\tilde{f}_{i/h_1}\left(N,\mu_F^2\right) = \sum_l A_l \beta\left(N+\gamma_l-1,1+\delta_l\right) \tag{4.87}$$

From these initial scale conditions the PDFs can be evolved to other scales in Mellin space. For a more detailed explanation [93] can be read. The disadvantage of this method is that it requires a specific parametrization to be used for the PDFs, which does not work for all PDFs, for example NNPDFs [95].

Derivative method Alternatively we can obtain extra suppression in the large N limit by rewriting the cross section. We will start with the cross section equation of the form:

$$\Sigma^{(\text{res})}_{h_1 h_2 \to kl} = \sum_{i,j} \int_\tau^1 \frac{dz}{z} \left(\frac{\tau}{z}\right) \int_{\tau/z}^1 \frac{dx}{x} f_{i/h_1}\left(x, \mu_F^2\right) f_{j/h_2}\left(\frac{\tau}{xz}, \mu_F^2\right) \hat{\Sigma}^{\text{res}}_{ij \to kl}\left(z, \mu_R^2, \mu_F^2\right) \quad (4.88)$$

with the resummed cross section given by:

$$\hat{\Sigma}^{\text{res}}_{ij \to kl}\left(z, \mu_R^2, \mu_F^2\right) = \frac{1}{2\pi i} \int_{C_T} dN\, z^{-N} \hat{\Sigma}^{\text{res}}_{ij \to kl}\left(N, \mu_R^2, \mu_F^2\right) \quad (4.89)$$

where the resummation is performed in Mellin space. We can perform the method introduced in [96], in order to introduce a N^{-2} suppression to the cross section:

$$\Sigma^{(\text{res})}_{h_1 h_2 \to kl} = \int_{C_T} \frac{dN}{2\pi i} \tau^{-N} \sum_{i,j} \left[N \tilde{f}_{i/h_1}\left(N+1, \mu_F^2\right)\right] \left[N \tilde{f}_{j/h_2}\left(N+1, \mu_F^2\right)\right]$$

$$\times \frac{\hat{\Sigma}^{\text{res}}_{ij \to kl}\left(N, \mu_R^2\right)}{N^2} \quad (4.90)$$

This results in the inverse Mellin transform

$$\Sigma^{(\text{res})}_{h_1 h_2 \to kl} = \sum_{i,j} \int_\tau^1 \frac{dz}{z} \left(\frac{\tau}{z}\right) \int_{\tau/z}^1 \frac{dx}{x} \mathcal{F}_{i/h_1}\left(x, \mu_F^2\right) \mathcal{F}_{j/h_2}\left(\frac{\tau}{xz}, \mu_F^2\right) \hat{S}^{\text{res}}_{ij \to kl}\left(z, \mu_R^2, \mu_F^2\right) \quad (4.91)$$

with

$$\hat{S}^{\text{res}}_{ij \to kl}\left(z, \mu_R^2, \mu_F^2\right) = \frac{1}{2\pi i} \int_{C_T} dN\, z^{-N} \frac{\hat{\Sigma}^{\text{res}}_{ij \to kl}\left(N, \mu_R^2, \mu_F^2\right)}{N^2} \quad (4.92)$$

and the function $\mathcal{F}_{i/h_1}$ the inverse Mellin transform of $N \tilde{f}_{i/h_1}$ which can be rewritten by partial integration

$$N \tilde{f}_{i/h_1}\left(N+1, \mu_F^2\right) = \int_0^1 dx\, N x^N f_{i/h_1}\left(x, \mu_F^2\right) = \int_0^1 dx\, x f_{i/h_1}\left(x, \mu_F^2\right) \frac{d}{dx} x^N$$

$$= \int_0^1 dx\, x^N \left[-\frac{d}{dx} x f_{i/h_1}\left(x, \mu_F^2\right)\right] \quad (4.93)$$

where we make use of the fact that the parton distribution vanishes at $x = 1$ and the cross section vanishes for $x \to 0$. Therefore we can express $\mathcal{F}_{i/h_1}$ in terms of the derivative with respect to x:

$$\mathcal{F}_{i/h_1}\left(x, \mu_F^2\right) = -\frac{d}{dx} x f_{i/h_1}\left(x, \mu_F^2\right) \quad (4.94)$$

This method can be used to create a stronger suppression than N^{-2} by taking a higher order derivative. The disadvantage of this method is that it is more numerically intensive, however it can be used for any type of PDF.

5 Soft Gluon Resummation for Gluon-Induced Higgs Strahlung

In this chapter the threshold resummation techniques from Chapter 4 will be applied to the gluon-induced Higgs Strahlung process. The resummation will be done through the use of two different approaches to the threshold limit. This research was published in [97]. First the motivation for applying the resummation to this process will be discussed. In Section 5.1 the different definitions of threshold will be discussed. The LO cross section in Mellin space will be derived in Section 5.2. The final process dependent ingredient for the resummation, the matching coefficient, will be presented in Section 5.3. Finally, the numerical results will be presented and discussed in Section 5.4. The results of the combination with the rest of the $pp \to HZ$ results is presented in Section 5.5.

The improvements from the NLO QCD corrections to the $gg \to HZ$ cross section are shown in Table 5.1. Here it can be seen that, though the scale dependence improves, it still results in a significant uncertainty $(20 - 30\%)$. In order to improve the precision of the results, threshold resummation can be considered. The major reason to use threshold resummation is that it was very successful for the similar loop-induced process $gg \to H$ [91, 98, 99]. Due to the similarities between the processes one could argue that the same type of improvements can be expected. It may look like threshold resummation would not provide a large contribution to the corrections, due to the fact that the HZ final state is far from hadronic absolute threshold. However, the gluons in the initial state have a strong contribution from the small x region, where the gluon only has a small fraction of the proton momentum. Therefore, due to the initial state gluons there can be large contributions from the partonic threshold region.

5.1 Threshold definitions

As was stated in Section 2.2 a reason to study soft gluon resummation for $gg \to HZ$ is the similarity to $gg \to H$ and the success the resummation had for this process. For $gg \to H$ there is a unique definition of threshold, because there is only one final state particle that is produced on-shell. This single definition of threshold is when the initial state center of mass energy approaches the Higgs mass $(\sqrt{\hat{s}} \to m_H)$. However, for our process there are two final state particles. This allows the approach of threshold to be defined in multiple ways. In general within the formulas our threshold is defined for $\sqrt{\hat{s}} \to W$ with W our threshold parameter.

Invariant mass threshold approach

The first threshold approach definition we will be exploring is invariant mass threshold. Here threshold is defined as when the center of mass energy of the initial state approaches the invariant mass of the final state $(\hat{s} \to Q^2)$. In order to access the final state variable Q^2 we need to use the differential cross section with respect to Q^2. At LO this threshold is always exactly satisfied and

$\sqrt{s}$ [TeV]	m_H[GeV]	$\sigma_{gg}^{\mathrm{LO}}$[fb]	$\sigma_{gg}^{\mathrm{NLO}}$[fb]
8	115	$19.8^{+61\%}_{-34\%}$	$39.3^{+32\%}_{-24\%}$
8	120	$18.7^{+61\%}_{-34\%}$	$37.2^{+32\%}_{-24\%}$
8	125	$17.7^{+61\%}_{-34\%}$	$35.1^{+32\%}_{-24\%}$
8	130	$16.7^{+61\%}_{-34\%}$	$33.1^{+32\%}_{-24\%}$
14	115	$79.1^{+51\%}_{-31\%}$	$152^{+27\%}_{-21\%}$
14	120	$75.1^{+51\%}_{-31\%}$	$144^{+27\%}_{-21\%}$
14	125	$71.1^{+51\%}_{-31\%}$	$136^{+27\%}_{-21\%}$
14	130	$67.2^{+51\%}_{-31\%}$	$129^{+27\%}_{-21\%}$

Table 5.1: Cross section for HZ production through gluon fusion for LHC energies and for masses near the mass of the discovered Higgs boson. The scale uncertainty is given in percent and is computed by rescaling $\mu_R = \mu_F$ by factors 3 and 1/3 relative to $\mu_0 = \sqrt{(p_H + p_Z)^2}$. [32]

the process can only move away from threshold by emitting extra particles. For this approach of threshold we will use the hadronic threshold parameter $\tau = \tau_Q = Q^2/s$ and the partonic threshold parameter as $\hat{\tau} = \tau/(x_1 x_2) = Q^2/\hat{s}$. From here on out we will refer to invariant mass threshold approach as Q-approach.

In the Q-approach the logarithmic terms that are resummed take the form of:

$$\alpha_{\mathrm{s}}^m \left(\frac{\log^n (1 - \hat{\tau}_Q)}{1 - \hat{\tau}_Q} \right)_+, \quad m \leq 2n - 1 \tag{5.1}$$

where the plus distribution is used to cancel the divergence at $x = x_0 \in [0, 1]$ and is defined by means of an integration:

$$\int_0^1 dx \, (f(x))_+ = \int_0^1 dx \, (f(x) - f(x_0)) \tag{5.2}$$

The advantage of this approach for resummation is that one can still access the invariant mass variable. This invariant mass variable is the natural scale for the Drell-Yan production used for the lower order terms in the $q\bar{q} \to HZ$ process. In addition one could argue that the only scale the gluon emission from the initial state can know about is the invariant mass of the final state particles and not their actual masses. The mass of the final state particles will only enter in the integration limits of Q^2.

Absolute threshold approach

The alternative threshold approach is the absolute threshold approach. In this case threshold is defined as when the center of mass of the initial state approaches the sum of the masses of the final state ($\sqrt{\hat{s}} \to M = m_H + m_Z$). This allows us to define the hadronic and partonic threshold parameters as $\tau = \tau_Q = M^2/s$ and $\hat{\tau} = \tau/(x_1 x_2) = M^2/\hat{s}$ respectively. Absolute threshold approach will be referred to as M-approach.

The logarithmic terms of the M-approach take the form:

$$\alpha_{\mathrm{s}}^{m} \log^{n} \left(1 - \hat{\tau}_M\right), \quad m \leq 2n \tag{5.3}$$

In order to see the differences between the resummed logarithms we can calculate what happens if we integrate out the logarithmic terms of the Q-approach:

$$\int_{\hat{\tau}_M}^{1} d\hat{\tau}_Q \left(\frac{\log^n \left(1 - \hat{\tau}_Q\right)}{1 - \hat{\tau}_Q}\right)_{+} \hat{\sigma}\left(\hat{\tau}_Q\right)$$

$$= \int_{0}^{1} d\hat{\tau}_Q \frac{\log^n \left(1 - \hat{\tau}_Q\right)}{1 - \hat{\tau}_Q} \left(\hat{\sigma}\left(\hat{\tau}_Q\right) - \hat{\sigma}\left(1\right)\right) - \int_{0}^{\hat{\tau}_M} d\hat{\tau}_Q \frac{\log^n \left(1 - \hat{\tau}_Q\right)}{1 - \hat{\tau}_Q} \hat{\sigma}\left(\hat{\tau}_Q\right)$$

$$= \int_{\hat{\tau}_M}^{1} d\hat{\tau}_Q \frac{\log^n \left(1 - \hat{\tau}_Q\right)}{1 - \hat{\tau}_Q} \left(\hat{\sigma}\left(\hat{\tau}_Q\right) - \hat{\sigma}\left(1\right)\right) - \int_{0}^{\hat{\tau}_M} d\hat{\tau}_Q \frac{\log^n \left(1 - \hat{\tau}_Q\right)}{1 - \hat{\tau}_Q} \hat{\sigma}\left(1\right)$$

$$= \int_{\hat{\tau}_M}^{1} d\hat{\tau}_Q \frac{\log^n \left(1 - \hat{\tau}_Q\right)}{1 - \hat{\tau}_Q} \left(\hat{\sigma}\left(\hat{\tau}_Q\right) - \hat{\sigma}\left(1\right)\right) + \frac{\log^{n+1} \left(1 - \hat{\tau}_M\right)}{n + 1} \hat{\sigma}\left(1\right) \tag{5.4}$$

where $\hat{\sigma}$ is a function that is similar to the partonic cross section without the delta function in $\hat{\tau}_Q$, but with $\hat{s}$ replaced by $\hat{s} \rightarrow Q^2 = \hat{s}\hat{\tau}_Q$. The last term in the final expression can be recognized as the resummed logarithms of the M-approach. The extra integral on the left of the final expression is a lower order logarithmic effect with respect to the M-approach term. These lower order terms are also resummed in the Q-approach.

5.2 Leading order cross section

The first process dependent ingredient to the resummation is the LO cross section in Mellin space. This needs to be treated separately for Q- and M-approaches.

Invariant mass threshold approach

As stated before, for the LO the invariant mass of the final state particles is equal to the initial state center of mass energy squared. This leads to a differential cross section proportional to a delta function:

$$\frac{d\hat{\sigma}_{gg \rightarrow HZ}^{\mathrm{LO}}}{dQ^2} = \hat{\sigma}_{gg \rightarrow HZ}^{\mathrm{LO}}\left(\hat{s}\right) \delta\left(\hat{s} - Q^2\right) \tag{5.5}$$

Next this cross section needs to be transformed into Mellin space:

$$\frac{d\tilde{\hat{\sigma}}_{gg \rightarrow HZ}^{\mathrm{LO}}}{dQ^2} = \int_{0}^{1} d\hat{\tau}_Q \, \hat{\tau}_Q^{N-1} \hat{\sigma}_{gg \rightarrow HZ}^{\mathrm{LO}}\left(\hat{s}\right) \delta\left(\hat{s} - Q^2\right) = \frac{\hat{\sigma}_{gg \rightarrow HZ}^{\mathrm{LO}}\left(\hat{s} = Q^2\right)}{Q^2} \tag{5.6}$$

Absolute threshold approach

The treatment of the Mellin space LO for the M-approach is slightly more difficult than for the Q-approach. There is no delta function for the threshold parameter. For absolute threshold the threshold is a limit of LO and not a requirement at LO. This makes sure it is not possible to

exactly resolve this integral analytically. There are two ways to approach this problem. One solution is to do the integration numerically. This method could work, but it is not the solution we opted for. The reason for this was the longer numerical computation time and possibility for numerical instabilities.

The second solution is to use an approximation. The most logical approximation to use here is the heavy top mass limit, which is also used for the NLO computation [32]. In the heavy top mass limit the LO cross section becomes:

$$\lim_{m_t \to \infty} \hat{\sigma}^{\mathrm{LO}}_{gg \to HZ}(\hat{s}) \equiv \hat{\sigma}^{\mathrm{LO}}_{\infty}(\hat{s}) = \kappa \frac{\lambda^{3/2}(\hat{s},\, m_H^2,\, m_Z^2)}{m_Z^4 \hat{s}^2} \tag{5.7}$$

with

$$\lambda(x,\, y,\, z) = x^2 + y^2 + z^2 - 2xy - 2yz - 2zx \tag{5.8}$$

and

$$\kappa = \frac{1}{\pi}\left(\frac{\alpha \alpha_{\mathrm{s}}}{64 c_W^2 s_W^2}\right)^2$$

incorporates all the coupling constants.

If one tries to Mellin transform the heavy top mass limit of the LO cross section one would run into a problem. For $\hat{s} \to \infty$ this cross section diverges, therefore we cannot transform this cross section into Mellin space. It is logical that we experience problems in this limit, because the heavy top mass limit cannot be an appropriate approximation if we approach large partonic energies. However, as this is a resummation near threshold we can approximate the heavy top mass limit of the LO cross section near absolute threshold.

$$\hat{\sigma}^{\mathrm{LO}}_{\infty}(\hat{s}) \overset{\hat{s} \to M^2}{\to} \hat{\sigma}^{\mathrm{LO}}_{\infty,\mathrm{thr.}}(\hat{s}) = \kappa \frac{8 m_H^{3/2}}{m_Z^{5/2}(m_H + m_Z)}(1 - \hat{\tau}_M)^{3/2} \tag{5.9}$$

where the higher order terms in $(1 - \hat{\tau}_M)$ have been dropped. For this cross section there is a stronger suppression near threshold than the usual $(1 - \hat{\tau}_M)^{1/2}$ from the phase space integration. The additional factor of $(1 - \hat{\tau}_M)$ originates from the matrix element squared. In the threshold limit the Z and Higgs bosons are produced at rest, therefore they have no orbital angular momentum. The total angular momentum is thus given by the spin of the Z-boson ($j = 1$). This configuration of initial and final states is forbidden by the Landau-Yang theorem, so the matrix element must vanish at absolute threshold. Using the absolute threshold limit for the LO in the resummation is a reasonable assumption because the resummed logarithms are dominant in that region.

Equation (5.9) can be transformed in Mellin space, resulting in:

$$
\begin{aligned}
\tilde{\sigma}^{\mathrm{LO}}_{\infty,\mathrm{thr.}}(N) &= \int_0^1 d\hat{\tau}_M\, \hat{\tau}_M^{N-1} \kappa \frac{8 m_H^{3/2}}{m_Z^{5/2}(m_H + m_Z)}(1 - \hat{\tau}_M)^{3/2} \\[2mm]
&= \kappa \frac{6\sqrt{\pi} m_H^{3/2}}{m_Z^{5/2}(m_H + m_Z)} \frac{\Gamma(N)}{\Gamma(N + 5/2)}
\end{aligned} \tag{5.10}
$$

with the Euler's Gamma function (Γ) obeying $z\Gamma(z) = \Gamma(z + 1)$ and $\Gamma(1) = 1$.

In order to improve the prediction using this approximation, we will rescale the final result by the ratio of the hadronic cross sections $\sigma^{\mathrm{LO}}/\sigma^{\mathrm{LO}}_{\infty,\mathrm{thr.}}$. This approximation method works quite well and through tests for the Q-approach the difference has been confirmed to be below the percent level for the matched cross section.

5.3 Matching coefficient

The final process dependent ingredient needed for a full NLL calculation is the matching coefficient. The calculation of the matching coefficient requires a full analytical expression of the NLO computation. This NLO result needs to be Mellin transformed, divided by the Mellin transform of the LO cross section and expanded near threshold (large N). Finally from this expression we can extract the constant terms in N. The remaining terms, that diverge for large values of N, will be the same as the expansion of the resummation exponential. This prescription requires a significant amount of work, however this can be simplified using a trick.

In order to gain a better understanding of this trick the basics of dipole subtraction [100] need to be explained. A NLO calculation can be split up into the virtual correction originating from the loop calculation, the real correction originating from the emission of a gluon or quark and the collinear counter term originating from the PDFs. Each of these contributions can contain infrared divergences and should be formulated in $d = 4 - 2\epsilon$ dimensions. These infrared divergences cancel when all contributions are taken into account. The dipole subtraction method uses an auxiliary term, which encapsulates all the singular behavior. This extra term can be subtracted from the real correction and added to the virtual correction in order to make both terms infrared finite.

In this way the full NLO correction can be written as:

$$
\begin{aligned}
\Sigma^{\mathrm{NLO}} &= \int_3 d\Sigma^{\mathrm{R}} + \int_2 d\Sigma^{\mathrm{V}} + \int_2 d\Sigma^{\mathrm{C}} \\
&= \int_3 \left[d\Sigma^{\mathrm{R}}|_{\epsilon=0} - d\Sigma^{\mathrm{A}}|_{\epsilon=0} \right] + \int_2 \left[d\Sigma^{\mathrm{V}} + d\Sigma^{\mathrm{A}} + d\Sigma^{\mathrm{C}} \right]_{\epsilon=0} \quad (5.11)
\end{aligned}
$$

here Σ can either be the cross section (in the case of M-approach) or the differential cross section (in the case of Q-approach). The label R marks the real corrections with the three particle phase space, V marks the virtual corrections with the two particle phase space and C marks the collinear counter term. In the second step we use the dipole subtraction method in order to remove the infrared divergences from the two and three particle phase space separately. This introduces the auxiliary term marked by A. The trick allows us to argue that the three particle phase space term here is suppressed with respect to the two particle phase space in the threshold limit. This argument has to be treated separately for the two different threshold approaches.

The two particle phase space integral that will contribute to the matching coefficient is given by:

$$
\begin{aligned}
\int_2 \left[d\hat{\sigma}^{\mathrm{V}} + d\hat{\sigma}^{\mathrm{A}} + d\hat{\sigma}^{\mathrm{C}} \right]_{\epsilon=0} &= \hat{\sigma}^{\mathrm{virt.}} + \int_{\hat{\tau}_M}^1 d\hat{\tau}_Q \left[\mathbf{P}^{gg}\left(\hat{\tau}_Q\right) + \mathbf{K}^{gg}\left(\hat{\tau}_Q\right) \right] \hat{\sigma}^{\mathrm{LO}}\left(\hat{s} \to \hat{\tau}_Q \hat{s} = Q^2\right) \\
&= \hat{\sigma}^{\mathrm{virt.}} + \int_{M^2}^{\hat{s}} dQ^2 \frac{\hat{\tau}_Q}{Q^2} \left[\mathbf{P}^{gg}\left(\hat{\tau}_Q\right) + \mathbf{K}^{gg}\left(\hat{\tau}_Q\right) \right] \hat{\sigma}^{\mathrm{LO}}\left(Q^2\right) \quad (5.12)
\end{aligned}
$$

using the $\mathbf{P}^{gg}$ and $\mathbf{K}^{gg}$ from [100] and $\sigma^{\mathrm{virt.}}$, the virtual corrections with the $1/\epsilon$ divergences already removed, taken from [32].

Invariant mass threshold approach

For the Q-approach the type of terms we need to take into account for the matching coefficient are terms proportional to $\delta\left(1 - \hat{\tau}_Q\right)$. In addition the expansion in $\hat{\tau}_Q$ will also contain the

logarithmic terms that are resummed, which lead to additional constant terms when Mellin transformed. Any other terms after the Mellin transform will only result in suppressed terms in the large N limit compared to LO, which we are not interested in. All the kinematic divergences are removed from the real emission by subtracting the auxiliary term, $\hat{\sigma}^{\mathrm{A}}$. As we are only interested in terms that contain a divergence for the $\hat{\tau}_Q \to 1$ limit, this means the three particle phase space only contains terms that are not included in the matching coefficient.

Therefore we are allowed to describe the matching coefficient by means of the differential of Equation (5.12) with respect to Q^2:

$$
\frac{d}{dQ^2} \int_2 \left[d\hat{\sigma}^{\mathrm{V}} + d\hat{\sigma}^{\mathrm{A}} + d\hat{\sigma}^{\mathrm{C}} \right]_{\epsilon=0} = \frac{d\hat{\sigma}^{\mathrm{virt.}}}{dQ^2} + \frac{\hat{\tau}_Q}{Q^2} \left[\mathbf{P}^{gg} \left(\hat{\tau}_Q \right) + \mathbf{K}^{gg} \left(\hat{\tau}_Q \right) \right] \hat{\sigma}^{\mathrm{LO}} \left(Q^2 \right)
$$

$$
= \hat{\sigma}^{\mathrm{virt.}} \delta \left(\hat{s} - Q^2 \right) + \frac{\hat{\sigma}^{\mathrm{LO}} \left(Q^2 \right)}{Q^2} \hat{\tau}_Q \left[\mathbf{P}^{gg} \left(\hat{\tau}_Q \right) + \mathbf{K}^{gg} \left(\hat{\tau}_Q \right) \right] \quad (5.13)
$$

Finally we need to perform the Mellin transform with respect to $\hat{\tau}_Q$ and to divide by the Mellin space LO cross section $(\hat{\sigma}^{\mathrm{LO}} \left(Q^2 \right) / Q^2)$:

$$
\frac{\alpha_{\mathrm{s}}}{\pi} \mathcal{C}_{Q^2}^{(1)} = \frac{\sigma^{virt.}}{\hat{\sigma}^{\mathrm{LO}}} + \left\{ \int_0^1 d\hat{\tau}_Q \, \hat{\tau}_Q^N \left[\mathbf{P}^{gg} \left(\hat{\tau}_Q \right) + \mathbf{K}^{gg} \left(\hat{\tau}_Q \right) \right] \right\}_{N-const.} \quad (5.14)
$$

where $N-const.$ indicates the constant terms in N of the expansion for the integral. This integral is given by:

$$
\int_0^1 d\hat{\tau}_Q \, \hat{\tau}_Q^N \left[\mathbf{P}^{gg} \left(\hat{\tau}_Q \right) + \mathbf{K}^{gg} \left(\hat{\tau}_Q \right) \right]
$$

$$
= \frac{\alpha_{\mathrm{s}}}{\pi} \int_0^1 d\hat{\tau}_Q \, \hat{\tau}_Q^N \left[2C_A \left\{ 2 \left(\frac{\log \left(1 - \hat{\tau}_Q \right)}{1 - \hat{\tau}_Q} \right)_+ - \left(\frac{1}{1 - \hat{\tau}_Q} \right)_+ \log \left(\frac{\mu_F^2}{Q^2} \hat{\tau}_Q \right) \right. \right.
$$

$$
\left. - \left(\frac{1 - \hat{\tau}_Q}{\hat{\tau}_Q} - 1 + \hat{\tau}_Q \left(1 - \hat{\tau}_Q \right) \right) \log \left(\frac{\mu_F^2}{\left(1 - \hat{\tau}_Q \right)^2 Q^2} \hat{\tau}_Q \right) - \delta \left(1 - \hat{\tau}_Q \right) \frac{\pi^2}{6} \right\}
$$

$$
\left. - \delta \left(1 - \hat{\tau}_Q \right) \left\{ \left(\frac{11}{6} C_A - \frac{2}{3} T_R n_l \right) \log \left(\frac{\mu_F^2}{Q^2} \right) + \left(\frac{50}{9} - \frac{2\pi^2}{3} \right) C_A - \frac{16}{9} T_R n_l \right\} \right]
$$

$$
\approx \frac{\alpha_{\mathrm{s}}}{\pi} \left[2C_A \left\{ \left(\log \left(N \right) + \gamma_E \right)^2 + \frac{\pi^2}{6} + \left(\log \left(N \right) + \gamma_E \right) \log \left(\frac{\mu_F^2}{Q^2} \right) - \frac{\pi^2}{6} \right\} \right.
$$

$$
\left. - \left\{ \left(\frac{11}{6} C_A - \frac{2}{3} T_R n_l \right) \log \left(\frac{\mu_F^2}{Q^2} \right) + \left(\frac{50}{9} - \frac{2\pi^2}{3} \right) C_A - \frac{16}{9} T_R n_l \right\} \right] \quad (5.15)
$$

with n_l the number of light quark flavors, $T_R = 1/2$, $C_A = 3$ in the number of colors and γ_E is Euler's constant. The logarithmic terms in this expression are the NLO expansion of the resummation factor and the remaining constant terms are part of the matching coefficient:

$$
\mathcal{C}_{Q^2}^{(1)} = \frac{\pi}{\alpha_{\mathrm{s}}} \frac{\hat{\sigma}^{\mathrm{virt.}}}{\hat{\sigma}^{\mathrm{LO}}} + \left[\left\{ \frac{2}{3} T_R n_l - \left(\frac{11}{6} - 2\gamma_E \right) C_A \right\} \log \left(\frac{\mu_F^2}{Q^2} \right) \right.
$$

$$
\left. - \left(\frac{50}{9} - \frac{2\pi^2}{3} - 2\gamma_E^2 \right) C_A + \frac{16}{9} T_R n_l \right] \quad (5.16)
$$

Absolute threshold approach

Next the same calculation can be repeated for the M-approach and it will provide a very similar result. The terms we want to take into account for the matching coefficient of the M-approach are proportional to at least $(1 - \hat{\tau}_M)^{3/2}$. As stated for the Q-approach, the three particle integrand does not contain any kinematic divergences in $\hat{\tau}_Q$. This means the $\hat{\tau}_Q$ integral will always provide an extra $(1 - \hat{\tau}_M)$ suppression in addition to the $(1 - \hat{\tau}_M)^{3/2}$ from Born. This suppression allows the three particle integral to be neglected in comparison to the two particle integral. This suppression was confirmed numerically by computing the three particle integral divided by Born in the absolute threshold limit. Now we can calculate the contribution to the matching coefficient through:

$$\int_2 \left[d\hat{\sigma}^{\mathrm{V}} + d\hat{\sigma}^{\mathrm{A}} + d\hat{\sigma}^{\mathrm{C}} \right]_{\epsilon=0} = \hat{\sigma}^{\mathrm{virt.}} + \int_{\hat{\tau}_M}^1 d\hat{\tau}_Q \left[\mathbf{P}^{gg}(\hat{\tau}_Q) + \mathbf{K}^{gg}(\hat{\tau}_Q) \right] \hat{\sigma}^{\mathrm{LO}}(\hat{\tau}_Q \hat{s}) \quad (5.17)$$

In order to approach this we will treat the virtual corrections term and the $\hat{\tau}_Q$ integral separately. First we will treat the integral:

$$\int_0^1 d\hat{\tau}_M \int_{\hat{\tau}_M}^1 d\hat{\tau}_Q \left[\mathbf{P}^{gg}(\hat{\tau}_Q) + \mathbf{K}^{gg}(\hat{\tau}_Q) \right] \hat{\tau}_M^{N-1} \hat{\sigma}^{\mathrm{LO}}(\hat{\tau}_Q \hat{s})$$

$$= \int_0^1 d\hat{\tau}_Q \int_0^{\hat{\tau}_Q} d\hat{\tau}_M \left[\mathbf{P}^{gg}(\hat{\tau}_Q) + \mathbf{K}^{gg}(\hat{\tau}_Q) \right] \hat{\tau}_M^{N-1} \hat{\sigma}^{\mathrm{LO}}(\hat{\tau}_Q \hat{s})$$

$$= \int_0^1 d\hat{\tau}_Q \int_0^1 dx \left[\mathbf{P}^{gg}(\hat{\tau}_Q) + \mathbf{K}^{gg}(\hat{\tau}_Q) \right] x^{N-1} \hat{\tau}_Q^N \hat{\sigma}^{\mathrm{LO}}(M^2/x)$$

$$= \int_0^1 d\hat{\tau}_Q \hat{\tau}_Q^N \left[\mathbf{P}^{gg}(\hat{\tau}_Q) + \mathbf{K}^{gg}(\hat{\tau}_Q) \right] \tilde{\sigma}^{\mathrm{LO}}(N) \quad (5.18)$$

here we used $x = \hat{\tau}_M/\hat{\tau}_Q$. From this final equation we can recognize the same Mellin transform as in the Q-approach, which is given in Equation (5.15). The only difference is that this expression is approximated near absolute threshold, therefore the Q^2 in the scale dependent logarithmic terms becomes M^2. In addition $\tilde{\sigma}^{\mathrm{LO}}(N)$ is also approximated in the same way as for the leading order resulting in $\tilde{\sigma}^{\mathrm{LO}}_{\infty,\mathrm{thr.}}(N)$.

The next term to treat is the virtual correction. The virtual corrections can be split into two parts, one part proportional to LO and the other part called the "reducible" contribution:

$$\hat{\sigma}^{\mathrm{virt.}} = \frac{\alpha_s}{\pi} \left(\frac{164}{9} + \frac{23}{6} \log\left(\frac{\mu_R^2}{\hat{s}} \right) \right) \hat{\sigma}^{\mathrm{LO}}(\hat{s}) + \hat{\sigma}^{(\mathrm{virt,red})} \quad (5.19)$$

The part proportional to LO can be dealt with in the same way as LO, however the "reducible" part needs to be approximated near threshold as well.

$$\hat{\sigma}^{(\mathrm{virt., red.})} \overset{\hat{s} \to M^2}{\longrightarrow} \hat{\sigma}^{(\mathrm{virt,red})}_{\mathrm{thr.}} = -\frac{2}{9} \frac{\alpha_s}{\pi} \hat{\sigma}^{\mathrm{LO}}_{\infty,\mathrm{thr.}}(\hat{s}) \left[2 + \frac{m_H}{m_Z} + \frac{3m_Z + m_H}{2m_H} \log\left(\frac{m_H}{m_Z} \right) \right] \quad (5.20)$$

The approximation was shown in [97]. This approximation allows us to perform the Mellin transform in the same way as for the LO cross section.

Combining all components provides us with the matching coefficient:

$$\mathcal{C}^{(1)}_{M^2} = \left\{ \frac{2}{3} T_R n_l - \left(\frac{11}{6} - 2\gamma_E \right) C_A \right\} \log\left(\frac{\mu_F^2}{M^2} \right) - \left(\frac{50}{9} - \frac{2\pi^2}{3} - 2\gamma_E^2 \right) C_A + \frac{16}{9} T_R n_l$$

$$+ \frac{164}{9} + \frac{23}{6} \log\left(\frac{\mu_R^2}{M^2} \right) - \frac{2}{9} \left[2 + \frac{m_H}{m_Z} + \frac{3m_Z + m_H}{2m_H} \log\left(\frac{m_H}{m_Z} \right) \right] \quad (5.21)$$
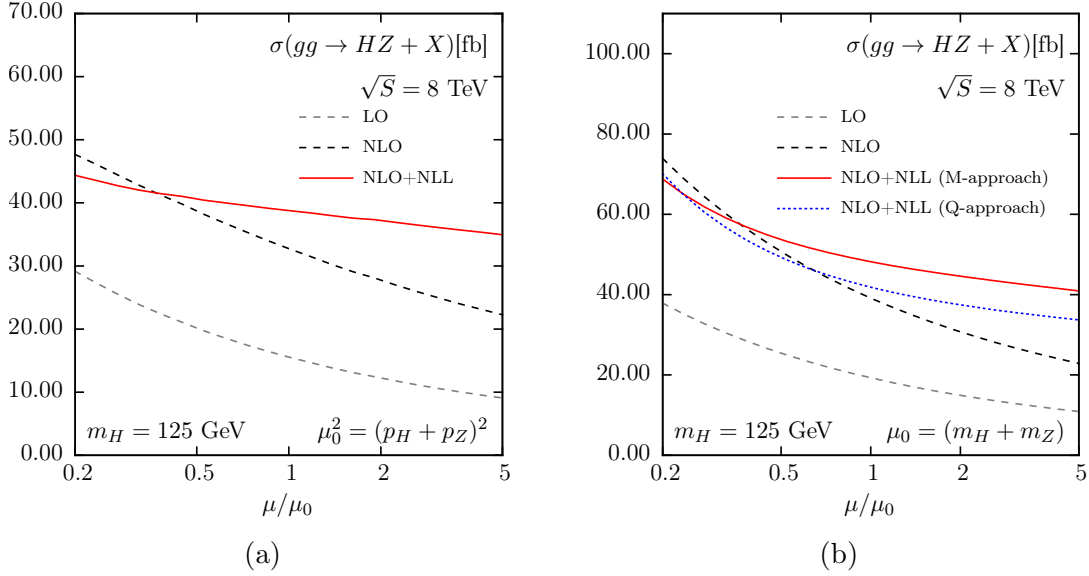
Figure 5.1: The scale dependence of the total inclusive cross section for gluon induced HZ production for $\sqrt{s} = 8$ TeV at LO (lower gray dashed), NLO (upper black dashed) and NLO+NLL (red solid). (a) For the Q-approach with the central scale $\mu_0^2 = Q^2$, (b) for the M-approach with the central scale $\mu_0^2 = M^2$. In addition (b) shows the Q-approach with the central scale choice $\mu_0^2 = M^2$ for comparison (blue dotted).

5.4 Numerical Results

Now that all the necessary ingredients for the resummation have been calculated, the numerical results of this resummation can be presented. First we will investigate the NLO+NLL cross section. This means that the NLL resummation is matched to the NLO result from [32] in the same manner as in Equation (4.85). After this the stability of these higher order corrections will be studied on the basis of NNLL resummation.

The central scale, μ_0, that will be chosen depends on the resummation approach that is investigated. For the fixed order computations the invariant mass of the final state Z- and Higgs bosons is usually chosen as the central scale. For the Q-approach we will choose this scale. However, for the M-approach there is no access to this variable. For the M-approach instead we will use a central scale $\mu_0 = M = m_H + m_Z$. This is the more natural scale for the absolute threshold resummation and the only scale we have access to.

The next choice is the use of PDF set. As the $gg \to HZ$ process enters for the first time at order α_s^2, it can be considered LO. From the point of view of the DGLAP and renormalization equations this means it should use LO PDFs. The NLO+NLL computation would then use NLO PDFs. This is the viewpoint taken for the NLO computations in [32]. For our computation we will take a different viewpoint. The LO $gg \to HZ$ computation enters the total $pp \to HZ$ result at the NNLO order. Therefore the computation should be done using NNLO PDFs in order to combine it into a total $pp \to HZ$ cross section. This would imply that we should use N³LO PDFs for the NLO+NLL computation, however as these do not exist yet we used a NNLO PDF set, more specifically the MSTW2008NNLO set [94]. Finally we use $m_t = 172.5$ GeV for the on-shell top mass and $m_b = 4.75$ GeV for the on-shell bottom mass.

In Figure 5.1 the results for NLO+NLL resummation for the total inclusive cross section can be seen for the center of mass energy of 8 TeV, for the Q-approach (a) and the M-approach (b).
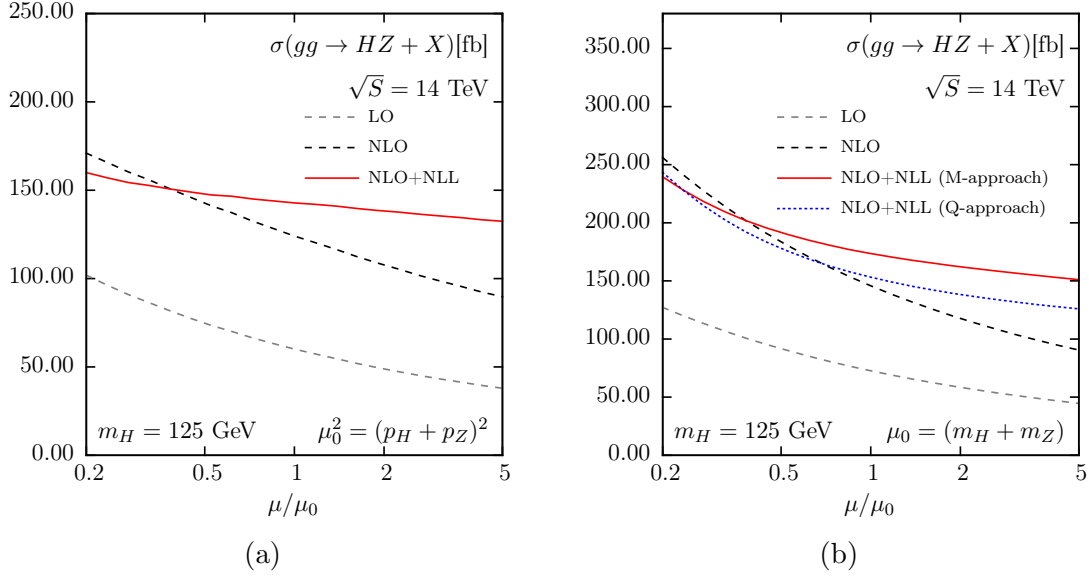
Figure 5.2: The scale dependence of the total inclusive cross section for gluon induced HZ production for $\sqrt{s} = 14$ TeV at LO (lower gray dashed), NLO (upper black dashed) and NLO+NLL (red solid). (a) For the Q-approach with the central scale $\mu_0^2 = Q^2$, (b) for the M-approach with the central scale $\mu_0^2 = M^2$. In addition (b) shows the Q-approach with the central scale choice $\mu_0^2 = M^2$ for comparison (blue dotted).

The unphysical scales are varied simultaneously, $\mu = \mu_F = \mu_R$, from $\mu_0/5$ to $5\mu_0$. In addition the LO and NLO cross sections are given for comparison. Here it can be seen that the scale dependence decreases through the inclusion of NLL resummation for both approaches. The scale dependence for the more "natural" central scale choice, $\mu_0^2 = Q^2$, is significantly smaller. The main cause for this is the larger scale dependence of the NLO cross section. For comparison the NLO+NLL result for Q-approach is also given for the central scale $\mu_0 = M$. It can also be noted that the Q-approach has a larger scale dependence than the M-approach for the central scale $\mu_0 = M$. This can be accounted to the fact that the typical scale logarithms are of the type $\log\left(W^2/\mu^2\right)$. These logarithms can become significantly larger for $W^2 = Q^2$ than for $W = M$. Also due to the fact that the absolute threshold region is emphasized in comparison to the situations with large invariant masses through the choice $\mu_0 = M$, the effect of the M-approach resummation has a greater enhancement with respect to Q-approach resummation. However, the comparison is still reassuring as the two results are similar.

Figure 5.2 displays the same results for 14 TeV collisions. The increase in cross section and the overall scale dependent behavior is the same as for 8 TeV collisions and has the same effects as were discussed above.

As the invariant mass is the more suitable scale for our process and the results that were presented above, we will consider the Q-approach with $\mu_0^2 = Q^2$ the definitive result. We will from now on only use the Q-approach for this process and base our final numerical predictions on the results obtained through the Q-approach.

Next, in order to check the stability of our predictions with respect to higher order corrections, we can study an increase in the resummation precision. This will be done through means of the process independent exponential factor Δ_g, which was described in Equation (4.81). For this factor we can increase the precision from NLL to NNLL without any new computations. We will not include NNLO contributions to the hard matching coefficient as the NNLO computations
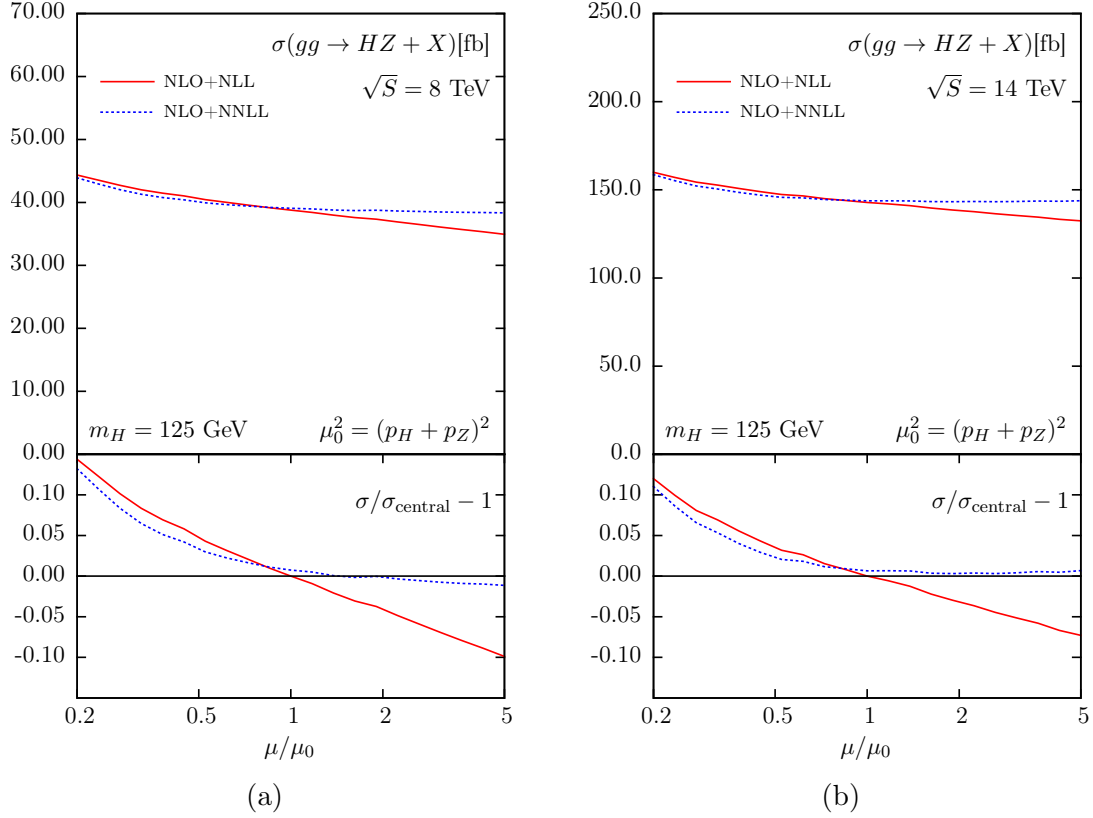
Figure 5.3: The scale dependence of the total inclusive cross section for gluon induced HZ production at (a) $\sqrt{s} = 8$ TeV and (b) $\sqrt{s} = 14$ TeV for NLO+NLL (red solid) and NLO+NNLL (blue dotted) both in the Q-approach. The upper plot shows the absolute values, whereas the lower plot shows the relative deviation from $\sigma_{\text{central}} \equiv \sigma_{gg \to HZ}\left(\mu^2 = Q^2\right)$, with $\mu = \mu_R = \mu_F$ is equal to the renormalization and factorization scales.

for $gg \to HZ$ have not been done at this time. These results will not be considered final as this is not a full NNLL computation.

A choice that can still be made is whether to match the NNLL resummation to NLO or an approximation of the NNLO cross section. The approximation of the NNLO cross section is a near threshold approximation of the cross section. This approximate cross section originates from the expansion of the resummation and transforming it back into x-space. Therefore, there is no new information added through this matching and the differences between NLO+NNLL and NNLO$_{\text{approx.}}$+NNLL are all of lower order in the threshold limit. For this check of the possible size of higher order corrections we will match to NLO.

In Figure 5.3 the results of the comparison between the NLO+NLL and NLO+NNLL in the Q-approach can be seen. In the upper half the cross sections can be seen in the same manner as the NLO+NLL results were presented in Figures 5.1 and 5.2. In the lower half of Figure 5.3 the relative deviation from the chosen central value is shown. The central value is the chosen value that will be used for the combination with the rest of the $pp \to HZ$ results. This central value is chosen as NLO+NLL in the Q-approach with the scales set to the central scale $\mu_F^2 = \mu_R^2 = Q^2$. From Figure 5.3 we can see that the scale dependence of the NLO+NNLL is slightly smaller than that of the NLO+NLL. This is expected as we include some of the higher order terms in the perturbative expansion. Important is to also note that the scale dependence of the NLO+NNLL is fully encapsulated by the NLO+NLL scale dependence. This implies that

$\sqrt{s}$	m_H	$\sigma_{gg \to HZ}$			
[TeV]	[GeV]	NLO		NLO+NLL	
		[pb]	[%]	[pb]	[%]
8.00	125.0	0.0328	$^{+30}_{-23}$	0.0389	$^{+8.1}_{-6.5}$
8.00	125.5	0.0325	$^{+30}_{-23}$	0.0386	$^{+8.1}_{-6.5}$
8.00	126.0	0.0324	$^{+30}_{-23}$	0.0384	$^{+8.2}_{-6.6}$
13.0	125.0	0.1057	$^{+26}_{-21}$	0.1220	$^{+7.0}_{-5.2}$
13.0	125.5	0.1049	$^{+26}_{-20}$	0.1211	$^{+7.3}_{-5.2}$
13.0	126.0	0.1044	$^{+26}_{-21}$	0.1205	$^{+6.7}_{-5.5}$
13.5	125.0	0.1149	$^{+26}_{-20}$	0.1325	$^{+7.1}_{-5.2}$
13.5	125.5	0.1141	$^{+26}_{-20}$	0.1316	$^{+7.2}_{-5.0}$
13.5	126.0	0.1135	$^{+26}_{-20}$	0.1308	$^{+7.1}_{-5.0}$
14.0	125.0	0.1243	$^{+26}_{-20}$	0.1431	$^{+7.1}_{-4.9}$
14.0	125.5	0.1237	$^{+26}_{-20}$	0.1424	$^{+7.3}_{-5.0}$
14.0	126.0	0.1228	$^{+26}_{-20}$	0.1414	$^{+7.3}_{-4.9}$

Table 5.2: The $gg \to HZ$ contribution to the total inclusive HZ production cross section for various center-of-mass energies $\sqrt{s}$ and Higgs masses m_H. The third and fourth column displays the NLO result, while the fifth and sixth column shows the NLO+NLL prediction (based on the Q-approach). The uncertainties (column 4 and 6) are due to scale variation over $\mu \epsilon \, [1/3, 3] \, Q$.

our more conservative theoretical uncertainty estimate from the NLO+NLL fully includes the uncertainty estimate from NLO+NNLL. Despite all of this NLO+NNLL should still only be used as an indicator of possible higher order effects as $\mathcal{O}\left(1/N\right)$ and α_s^3 contributions can still result in sizable corrections.

5.5 Total inclusive $pp \to HZ$ production cross section

In this section the NLO+NLL results for $gg \to HZ$ will finally be combined with the NNLO non-$gg \to HZ$ results in order to see the impact our resummation has to the total $pp \to HZ$ cross section. These results will be presented for twelve benchmark points using four different hadronic center of mass energies and three different values for the Higgs boson mass. These points are used at by the experimentalists at the LHC through the LHC-HXSWG [14–16].

First the results for the $gg \to HZ$ channel will be presented. As stated before, this will be calculated using the Q-approach with the scales set to the pair invariant mass of the final state $\mu_F^2 = \mu_R^2 = Q^2$. The scale uncertainty will be calculated by varying the renormalization and factorization scale simultaneously in the interval $[1/3, 3] \, Q$. In Table 5.2 these results are shown with, for comparison, the NLO results included. The result that stands out the most is the strong reduction in scale uncertainty, which is reduced by a factor of 3 to 4 by including the NLL resummation. The correction to the cross section from the resummation is about a 18% increase for $\sqrt{s} = 8$ TeV and a 15% increase for $\sqrt{s} = 13$ to 14 TeV.

In order to combine these results into a total inclusive $pp \to HZ$ cross section the non-$gg \to HZ$ results were provided by vh@nnlo [101]. The central values of the $gg \to HZ$ and non-$gg \to HZ$

$\sqrt{s}$	m_H	$\sigma_{pp \to HZ}$			
[TeV]	[GeV]	incl. gg @ NLO		incl. gg @ NLO+NLL	
		[pb]	[%]	[pb]	[%]
8.00	125.0	0.4157	$+3.1$ -2.8	0.4217	$+1.5$ -1.5
8.00	125.5	0.4104	$+3.1$ -2.8	0.4165	$+1.5$ -1.5
8.00	126.0	0.4054	$+3.2$ -2.8	0.4114	$+1.5$ -1.6
13.0	125.0	0.8696	$+3.8$ -3.8	0.8859	$+1.6$ -2.0
13.0	125.5	0.8594	$+3.8$ -3.8	0.8757	$+1.7$ -1.9
13.0	126.0	0.8501	$+3.8$ -3.9	0.8663	$+1.6$ -2.1
13.5	125.0	0.9190	$+3.9$ -3.8	0.9366	$+1.6$ -2.0
13.5	125.5	0.9085	$+3.8$ -3.8	0.9259	$+1.6$ -2.0
13.5	126.0	0.8988	$+3.8$ -3.9	0.9162	$+1.5$ -2.0
14.0	125.0	0.9690	$+4.0$ -3.9	0.9878	$+1.7$ -2.0
14.0	125.5	0.9574	$+4.0$ -3.9	0.9761	$+1.7$ -2.0
14.0	126.0	0.9465	$+4.1$ -3.9	0.9652	$+1.7$ -2.0

Table 5.3: The full $pp \to HZ$ inclusive cross section for various center-of-mass energies $\sqrt{s}$ and Higgs masses m_H. The third and fourth columns include the NLO result for the $gg \to HZ$ contribution, while the fifth and sixth columns include the NLO+NLL prediction for the $gg \to HZ$ contribution (based on the Q-approach). The uncertainties (column 4 and 6) are due to scale variation over $\mu \epsilon [1/3, 3] Q$ with $\mu_F = \mu_R$ for the $gg \to HZ$ contribution and the renormalization and factorization scale varied independently for the other contributions.

components are added in order to produce the central $pp \to HZ$ result. The scale uncertainty of the non-$gg \to HZ$ component is determined by varying the renormalization and factorization scale independently in the interval $[1/3, 3] Q$. The final results of this project can be seen in Table 5.3. For comparison the results with $gg \to HZ$ computed at NLO (gg@NLO results) are also included. The gg@NLO results coincide with the currently used results from the LHC-HXSWG. The scale uncertainty reduction is still approximately a factor 2 for $pp \to HZ$. This shows that a large contribution to the scale uncertainty of $pp \to HZ$ originates in $gg \to HZ$. Another indicator to this fact is that the $pp \to HZ$ at NNLO has a significantly larger scale uncertainty than $pp \to HW$ ($0.705 \pm 1.0\%$ pb for $\sqrt{S} = 8$ TeV and $m_H = 125$ GeV), which does not have the gluon initial state without extra real emission. The inclusion of the NLL resummation for $gg \to HZ$ brings the combined $pp \to HZ$ scale uncertainty closer to the $pp \to HW$ uncertainty. The corrections to the cross section are approximately 1.5% for 8 TeV and 2% for 13 to 14 TeV.

6 Soft-Gluon Resummation for Squark and Gluino Production

In this chapter we will use more techniques from Chapter 4 in order to calculate the cross sections for squark and gluino production at NNLL accuracy. For this computation final state emission effects also need to be taken into account and Coulomb effects will also be included. In Section 6.1 the previously computed results at NLL accuracy will be discussed including all the process dependent results that go into such a computation. The included contributions for the increase in accuracy to the NNLL accuracy will be described in Section 6.2. Finally, the numerical results for the NNLL computation of squark and gluino production will be presented in Section 7.4.3.

6.1 NLL resummation

In order to treat the final state emission in resummation, we need to decompose the LO cross section into different color channels. Any choice of the color basis is valid, however some make the calculations easier. The basis that simplifies the computation for the absolute threshold resummation is the s-channel color basis. In this basis the soft anomalous dimension matrix needed for the final state emission diagonalizes in the absolute threshold limit. This basis must be calculated for every initial and final state combination. An example of this is the squark anti-squark production with the quark anti-quark initial state. For this combination the color representation of the initial and final state are the same: $\mathbf{3} \otimes \bar{\mathbf{3}} = \mathbf{1} \oplus \mathbf{8}$. The LO cross sections in this color basis and the calculation of this basis can be found in [63–65]. Also in Chapter 7 this computation will be done in greater detail for $pp \to t\bar{t}H$.

Next we need to transform the LO cross section into Mellin space. Unlike for $gg \to HZ$, we will use the exact LO cross section and analytically transform it to Mellin space. This computation and its results can be found in [77].

The same color basis as for LO is used for the soft anomalous dimension in order to calculate $D^{(1)}_{ij \to kl, I}$ from Equation (4.77), for the partonic process $ij \to kl$ and color channel I. In the absolute threshold resummation this results in $D^{(1)}_{ij \to kl, I} = -C_I$, where C_I is the quadratic casimir invariant for the representation of the color channel I. The full computation of the soft anomalous dimension matrix will be explained in greater detail in Chapter 7. The results of the soft anomalous dimension matrix can be found in [63–65].

The NLL resummation results will not be the focus of this chapter as they are not the focus of this research. For greater detail on these computations and results [63–67] can be read.

6.2 Precision increase to NNLL resummation

In order to improve the predictions from NLL, certain new ingredients need to be calculated. They can all be described in one matching coefficient:

$$
\begin{aligned}
C_{ij \to kl,I}(N) &= \mathcal{C}^{\mathrm{Coul}}_{ij \to kl,I} \mathcal{C}_{ij \to kl,I} \\
&= \left(1 + \frac{\alpha_{\mathrm{s}}}{\pi} \mathcal{C}^{\mathrm{Coul},(1)}_{ij \to kl,I}(N) + \left(\frac{\alpha_{\mathrm{s}}}{\pi}\right)^2 \mathcal{C}^{\mathrm{Coul},(2)}_{ij \to kl,I}(N) + \dots\right) \\
&\quad \times \left(1 + \frac{\alpha_{\mathrm{s}}}{\pi} \mathcal{C}^{(1)}_{ij \to kl,I} + \left(\frac{\alpha_{\mathrm{s}}}{\pi}\right)^2 \mathcal{C}^{(2)}_{ij \to kl,I} + \dots\right)
\end{aligned}
\tag{6.1}
$$

at NNLL this will be described by

$$
\begin{aligned}
C^{\mathrm{NNLL}}_{ij \to kl,I}(N) &= 1 + \frac{\alpha_{\mathrm{s}}}{\pi}\left(\mathcal{C}^{\mathrm{Coul},(1)}_{ij \to kl,I}(N) + \mathcal{C}^{(1)}_{ij \to kl,I}\right) \\
&\quad + \left(\frac{\alpha_{\mathrm{s}}}{\pi}\right)^2 \left(\mathcal{C}^{\mathrm{Coul},(2)}_{ij \to kl,I}(N) + \mathcal{C}^{(2)}_{ij \to kl,I} + \mathcal{C}^{(1)}_{ij \to kl,I}\mathcal{C}^{\mathrm{Coul},(1)}_{ij \to kl,I}(N)\right)
\end{aligned}
\tag{6.2}
$$

Here the matching coefficient has been split up into a Coulomb coefficient ($\mathcal{C}^{\mathrm{Coul}}_{ij \to kl,I}$) and a hard matching coefficient ($\mathcal{C}_{ij \to kl,I}$). The Coulomb has been shown to factorize from the soft gluon emission [69, 102]. This matching coefficient is one of the process dependent parts of Equation (4.80).

6.2.1 Hard matching coefficient

The first ingredient that needs to be calculated is the one-loop hard matching coefficient, $\mathcal{C}^{(1)}_{ij \to kl,I}$. The hard matching coefficients are calculated in a way that is similar to the method presented in Chapter 5. However, as we now also have colored particles in the final state, the dipole contributions are more complicated. This computation was presented in [68, 73] and was calculated using the final state dipoles from [103].

The second order hard matching coefficient will be set to zero, $\mathcal{C}^{(2)}_{ij \to kl,I} = 0$, as the NNLO calculation has not been completed at this time.

6.2.2 Coulomb corrections

As was mentioned in Chapter 1 other than the logarithmic terms originating from soft-gluon emission, there are also the Coulomb contributions that are enhanced at the absolute threshold. The Coulomb corrections originate from the exchange of a gluon between two slowly moving final state particles. For $gg \to HZ$ we did not need to include such contributions as the only colored particles are the initial state gluons and these are not slow moving. However, for squark and gluino production we have colored particles in the final state. They are slow moving near absolute threshold and can therefore have sizable Coulomb corrections.

For the calculation of the Coulomb corrections we will be following [104]. We will perform the computation for the top anti-top system, however the procedure would be very similar for squarks and gluinos. As the Coulomb corrections are of the type $\alpha_{\mathrm{s}}/\beta$ with $\beta = \sqrt{1 - 4m^2_{av}/\hat{s}}$, we are interested in the region where $\beta = \mathcal{O}(\alpha_{\mathrm{s}})$. Using the optical theorem we can calculate the
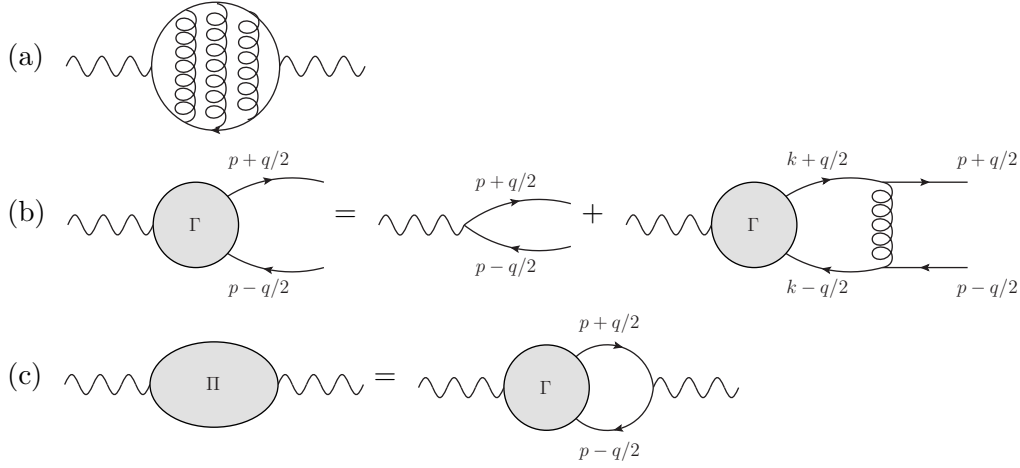
Figure 6.1: (a) Type of diagrams for Coulomb corrections, these are ladder diagrams containing any number of uncrossed gluons. (b) The equation for the vertex correction Γ^μ in the ladder approximation. (c) The equation for the self energy contribution of the top quark Π_t in the ladder approximation.

Coulomb corrections through use of the diagram shown in Figure 6.1 (a). This is equivalent to the contributions to the photon self energy from a top quark loop, Π. The dominant contributions in the non-relativistic limit to this self energy involve the exchange of multiple uncrossed gluons, this can be seen in Figure 6.1. We can describe this in an iterative equation by means of Π_t and vertex Γ^μ:

$$i\left(g^{\mu\nu}q^2 - q^\mu q^\nu\right)\Pi_t\left(q^2\right) = -e^2\int\frac{d^4p}{(2\pi)^4}\text{tr}\left[S_F\left(p+q/2\right)T^a\Gamma^\mu\left(p,q\right)S_F\left(p-q/2\right)T^a\gamma^\nu\right] \quad (6.3)$$

where S_F is the fermion propagator. As we are interested in the dominant contributions in the non-relativistic limit this propagator can be approximated near threshold. In order to do this we will set $q = (2m_t + E, \mathbf{0})$, making E the binding energy of the $t\bar{t}$ system and $E = \mathcal{O}\left(\beta^2\right)$. All three-momenta are treated as being of the order β. Using these assumptions we can approximate the fermion propagator as:

$$S_F\left(p\pm q/2\right) = \frac{i\left(\not{p}\pm\not{q}/2 + m_t\right)}{\left(p\pm q/2\right)^2 - m_t^2 + i\Gamma_t m_t} \rightarrow \frac{i2m_t\left(1\pm\gamma^0\right)/2}{2m_t\left(E/2\pm p^0 - |\mathbf{p}|^2/(2m_t) + i\Gamma_t/2\right)} \quad (6.4)$$

For the non-relativistic expansion we will ignore the momentum dependence of Γ_t.

In order to write the equation for Γ^μ we will also need to look at the gluon propagator in the non-relativistic limit. We will use the instantaneous Coulomb part of the gluon propagator:

$$G_{\text{Coul.}}^{\mu\nu}\left(k\right) = \delta_0^\mu\delta_0^\nu\frac{1}{|\mathbf{k}|^2} \quad (6.5)$$

On the basis of these approximate equations we can formulate an iterative equation for Γ^μ:

$$\Gamma^\mu\left(p,q\right) = \gamma^\mu + \int\frac{d^4k}{(2\pi)^4}\left[\frac{1+\gamma^0}{2}\Gamma^\mu\left(k,q\right)\frac{1-\gamma^0}{2}\right]$$

$$\times\frac{\tilde{V}\left(\mathbf{p}-\mathbf{k}\right)}{\left(E/2+k^0-|\mathbf{k}|^2/(2m_t)+i\Gamma_t/2\right)\left(E/2-k^0-|\mathbf{k}|^2/(2m_t)+i\Gamma_t/2\right)} \quad (6.6)$$

where the potential $\tilde{\mathbf{V}}\left(\mathbf{p}-\mathbf{k}\right)$ is defined as

$$\tilde{V}\left(\mathbf{p}-\mathbf{k}\right) = -\frac{4}{3}\frac{4\pi\alpha_{\mathrm{s}}}{\left|\mathbf{p}-\mathbf{k}\right|^{2}} \tag{6.7}$$

As the function $\Gamma^{\mu}\left(p,q\right)$ does not depend on p^{0}, we can perform the k^{0} integration. In addition we will simplify the Dirac structure by defining:

$$\frac{1+\gamma^{0}}{2}\Gamma^{\mu}\frac{1-\gamma^{0}}{2} \equiv \frac{1+\gamma^{0}}{2}\gamma^{\mu}\frac{1-\gamma^{0}}{2}\tilde{\Gamma} \tag{6.8}$$

Using these simplifications we obtain:

$$\tilde{\Gamma}\left(\mathbf{p},E\right) = 1 + \int\frac{d^{3}k}{\left(2\pi\right)^{3}}\tilde{V}\left(\mathbf{p}-\mathbf{k}\right)\frac{\tilde{\Gamma}\left(\mathbf{k},E\right)}{E+i\Gamma_{t}-\left|\mathbf{k}\right|^{2}/m_{t}} \tag{6.9}$$

From here we can see if we define

$$\tilde{G}\left(\mathbf{k},E+i\Gamma_{t}\right) = -\frac{\tilde{\Gamma}\left(\mathbf{k},E\right)}{E+i\Gamma_{t}-\left|\mathbf{k}\right|^{2}/m_{t}} \tag{6.10}$$

and transform into coordinate space we obtain the Schrödinger equation:

$$\left[H-\left(E+i\Gamma_{t}\right)\right]G\left(\mathbf{r},E+i\Gamma_{t}\right) = \delta^{3}\left(\mathbf{r}\right) \tag{6.11}$$

with the Hamiltonian

$$H = -\frac{1}{m_{t}}\nabla^{2}+V\left(\mathbf{r}\right) \tag{6.12}$$

Here we can recognize the function $G\left(\mathbf{r},E\right)$ as the Schrödinger Green's function $G\left(\mathbf{r},\mathbf{r}',E\right)$ evaluated at $\mathbf{r}'=0$.

If we now return to our calculation of the expression $\Pi_{t}\left(E\right)$ in the non-relativistic limit we obtain:

$$\begin{aligned}\Pi_{t}\left(E\right) &=& \frac{2}{3}\frac{e^{2}}{m_{t}^{2}}\int\frac{d^{3}p}{\left(2\pi\right)^{3}}\frac{\tilde{\Gamma}\left(\mathbf{k},E\right)}{E+i\Gamma_{t}-\left|\mathbf{k}\right|^{2}/m_{t}}\\ &=& -\frac{2}{3}\frac{e^{2}}{m_{t}^{2}}G\left(\mathbf{r}=0,\mathbf{r}'=0,E+i\Gamma_{t}\right)\end{aligned} \tag{6.13}$$

Finally we use the optical theorem

$$2\mathcal{I}m\left[\mathcal{M}\left(a\rightarrow a\right)\right] = \sum_{f}C_{f}\int d\Pi_{f}\left|\mathcal{M}\left(a\rightarrow f\right)\right|^{2} \tag{6.14}$$

with f all possible final states and C_{f} a combinatorial factor for identical particles in the final state f. Here we can focus of the final state for $t\bar{t}$. This results in a cross section:

$$\sigma\left(e^{+}e^{-}\rightarrow t\bar{t}\right) = \frac{8\pi^{2}\alpha^{2}}{3m_{t}^{2}}\mathcal{I}m\left[G\left(\mathbf{r}=0,\mathbf{r}'=0,E+i\Gamma_{t}\right)\right] \tag{6.15}$$

Therefore it is possible to calculate the Coulomb corrections through means of the Schrödinger Green's function. For higher order corrections in the Coulomb resummation the potential needs to include terms of higher orders in α_{s}. In this work we will expand the Coulomb resummation

up to order α_s^2 in order to be able to analytically perform the Mellin transform. For this we will need the potential up to NLO in α_s [105]:

$$V(\mathbf{r}) = \kappa_{ij \to kl, I} \frac{\alpha_s}{|\mathbf{r}|} \left\{ 1 + \frac{\alpha_s}{4\pi} \left[8\pi b_0 \left(\log \left(\mu |\mathbf{r}| \right) + \gamma_E \right) + 2a_1 \right] \right\} \tag{6.16}$$

with $a_1 = (31 C_A - 20 T_R n_l) / 9$ and the QCD running coupling $b_0 = (11 C_A - 4 T_R n_l) / (12\pi)$. The process dependence lies in the color factor $\kappa_{ij \to kl, I} = T_k T_l = (C_I - C_k - C_l) / 2$ and if it is positive this results in a repulsive potential whereas if it is negative the potential is attractive. Using this potential the Green's function is obtained:

$$G(E + i\Gamma_{av}) = i \frac{v m_{red}^2}{\pi} - \kappa_{ij \to kl, I} \frac{\alpha_s}{\pi} m_{red}^2 \left[g_{\text{LO}} + \frac{\alpha_s}{4\pi} g_{\text{NLO}} + \ldots \right] \tag{6.17}$$

with

$$g_{\text{LO}} = L - \psi^{(0)}$$

$$g_{\text{NLO}} = 4\pi b_0 \left[L^2 - 2L \left(\psi^{(0)} - \kappa \psi^{(1)} \right) + \kappa \psi^{(2)} + \left(\psi^0 \right)^2 - 3\psi^{(1)} - 2\kappa \psi^{(0)} \psi^{(1)} \right.$$

$$\left. 4 \, _4F_3 \left(1, 1, 1, 1; 2, 2, 1 - \kappa; 1 \right) \right] + a_1 \left[L - \psi^{(0)} + \kappa \psi^{(0)} \right] \tag{6.18}$$

with $a_1 = (31 C_A - 20 T_f n_l) / 9$ and

$$\kappa = -i \kappa_{ij \to kl, I} \frac{\alpha_s}{2v}, \quad v = \sqrt{\frac{E + i\Gamma_{av}}{2m_{red}}}, \quad L = \log \frac{i\mu}{4 m_{red} v} \tag{6.19}$$

The n-th derivative $\psi^{(n)} = \psi^{(n)} (1 - \kappa)$ of the digamma function $\psi(z) = \gamma_E + (d/dz) \log \Gamma(z)$ is evaluated at $(1 - \kappa)$. The reduced mass is given by $m_{red} = m_k m_l / (m_k + m_l)$ and v is the non-relativistic velocity.

One-loop Coulomb coefficient

Expanding the imaginary part of the Coulomb Green's function up to $\mathcal{O}(\alpha_s)$ results in the one-loop Coulomb correction:

$$\sigma_{ij \to kl, I}^{\text{Coul},(1)} = -\frac{\alpha_s \pi}{2} \sqrt{\frac{2 m_{red}}{m_{av}}} \frac{1}{\beta} \kappa_{ij \to kl, I} \sigma_{ij \to kl}^{(0)} \tag{6.20}$$

In order to take these contributions into account we will take the one-loop Coulomb correction and Mellin transform it. This calculation can be found in [77]. The sign of the one-loop Coulomb contribution is determined by the sign of $\kappa_{ij \to kl, I}$.

Two-loop Coulomb coefficient

For the two-loop Coulomb correction we will expand the imaginary part of the Green's function up to order α_s^2. This results in:

$$\sigma_{ij \to kl, I}^{\text{Coul},(2)} = \sigma_{ij \to kl}^{(0)} \frac{\alpha_s^2}{(4\pi)^2} \left\{ \frac{4\pi^4 \left(\kappa_{ij \to kl, I} \right)^2}{3\beta^2} \frac{2 m_{red}}{m_{av}} \right.$$

$$\left. + \frac{\pi^2 \kappa_{ij \to kl, I}}{\beta} \sqrt{\frac{2 m_{red}}{m_{av}}} \left[8\pi b_0 \left(2 \log \left(\frac{2 m_{av}}{\mu} \right) + \log \left(\beta^2 \right) + \log \left(\frac{2 m_{red}}{m_{av}} \right) \right) - 2a_1 \right] \right\} \tag{6.21}$$

This result agrees with [106]. In this case we will not transform the Coulomb correction exactly. Instead we will approximate the LO contribution for the s-wave contribution (proportional to β). When the Coulomb correction is Mellin transformed and divided by the Mellin transform of LO, this results in:

$$\frac{\alpha_s^2}{(4\pi)^2} \left\{ \frac{8}{3} \left(\kappa_{ij\to kl,I}\right)^2 \pi^4 N \frac{2m_{red}}{m_{av}} + \kappa_{ij\to kl,I}\pi^2 \sqrt{\frac{N}{\pi}} \sqrt{\frac{2m_{red}}{m_{av}}} \left[-16\pi b_0 \left(\log\left(N\right) + \gamma_E\right)\right.\right.$$

$$\left. -4a_1 + 32\pi b_0 \log\left(2\right) - 16\pi b_0 \log\left(\frac{\mu^2}{m_{av}^2}\right) + 16\pi b_0 \log\left(\frac{2m_{red}}{m_{av}}\right)\right]$$

$$\left. +\frac{4}{3}\left(\kappa_{ij\to kl,I}\right)^2 \pi^4 \frac{2m_{red}}{m_{av}}\right\} \tag{6.22}$$

Finally we also include extra terms of non-Coulombic origin $\kappa_{ij\to kl,I}\left[C_A - 2\kappa_{ij\to kl,I}\left(1 + v_{spin}\right)\right]\log\beta$ from [106] with v_{spin} a spin dependent variable and can be found in [78]. This provides the final result:

$$\frac{\alpha_s^2 \mathcal{C}^{coul,(2)}}{\pi^2} = \frac{\alpha_s^2}{(4\pi)^2} \left\{ \frac{8}{3} \left(\kappa_{ij\to kl,I}\right)^2 \pi^4 N \frac{2m_{red}}{m_{av}} + \kappa_{ij\to kl,I}\pi^2 \sqrt{\frac{N}{\pi}} \sqrt{\frac{2m_{red}}{m_{av}}} \left[-16\pi b_0 \left(\log\left(N\right) + \gamma_E\right)\right.\right.$$

$$\left. -4a_1 + 32\pi b_0 \log\left(2\right) - 16\pi b_0 \log\left(\frac{\mu^2}{m_{av}^2}\right) + 16\pi b_0 \log\left(\frac{2m_{red}}{m_{av}}\right)\right]$$

$$\left. +16\pi^2 \kappa_{ij\to kl,I} \left(C_A - 2\kappa_{ij\to kl,I}\left(1 + v_{spin}\right)\right) \left(1 - \log\left(2\right) - \frac{1}{2}\log\left(N\right) - \frac{1}{2}\gamma_E\right)\right.$$

$$\left. +\frac{4}{3}\left(\kappa_{ij\to kl,I}\right)^2 \pi^4 \frac{2m_{red}}{m_{av}}\right\} \tag{6.23}$$

This result is a reasonable approximation for all channels with the LO contributions in the s-wave and the two-loop Coulomb is not used for the p-wave contributions.

6.3 Numerical results

Now that all the different elements have been calculated we can look at the numerical results. We will sum over all flavors and chiralities ($\tilde{q}_L$ and $\tilde{q}_R$) of the final state squarks with the exception of the top squarks, due to the large mixing effects and the mass splitting in the stop sector [107]. We assume all the squark types that are summed over to be mass degenerate.

For the different parameters we will choose the renormalization and factorization scale equal $\mu = \mu_F = \mu_R$ with a central scale of m_{av} and a top mass of $m_t = 173.07$ GeV [108] is used. The chosen PDFs are the MSTW2008 set [94]. For the NNLL calculation and the approximated NNLO results we will use the NNLO PDF sets with $\alpha_s\left(M_Z\right) = 0.117$ by default. In the NLO and NLL computations we will use the NLO PDF sets with $\alpha_s\left(M_Z\right) = 0.120$. In order to treat the PDFs for the resummation in the standard x-space formulation we will use the method introduced in [96]. Alternatively, when needed, we will use the program `PEGASUS` [93] in order to derive the PDFs in Mellin space based on the MSTW parametrization at the initial factorization scale [94].

Our results will be given for an LHC center-of-mass energy of 8 TeV and at various levels of theoretical accuracy:

- The NLO cross sections [56], denoted as σ^{NLO}.

- The NLL cross section matched to the NLO results, based on calculations presented in [63–65]. They are denoted as $\sigma^{\text{NLO+NLL}}$.

- The approximated NNLO cross sections, calculated by adding the near-threshold approximations of the NNLO corrections in β-space [106] to the NLO cross section. They are denoted as $\sigma^{\text{NNLO}_{\text{Approx}}}$.

- The NNLL matched cross sections $\sigma^{\text{NNLL matched}}$. The NNLL cross section matched to NNLO$_{\text{Approx}}$ is used for the s-wave channels. The contributions from the β^2-suppressed p-wave channels are taken into account at NLO+NLL accuracy. Both the s-wave and the p-wave have been computed using the MSTW 2008 NNLO PDFs. If the NLO PDFs are used instead for the suppressed p-wave contributions, this leads to a negligible difference in the full result.

All the computations have been completed using two independent codes. The only exception to this the NLO results, which were generated by the public code `PROSPINO`.

In Figures 6.2 and 6.3 and in Table 6.1 the production cross section results for the four different squark and gluino pair production processes and the total cross section for all four processes are presented including the theoretical uncertainties on the cross section. The latter include the scale uncertainty, computed by varying the factorization and renormalization scales simultaneously between $m_{av}/2 \leq \mu \leq 2m_{av}$, and the 68% C.L. PDF and α_{s} uncertainties from MSTW2008 PDFs. The scale uncertainty is added linearly to the combined PDF and α_{s} uncertainties which are added in quadrature to each other. For comparison we show the NLO+NLL uncertainties in Figures 6.2 and 6.3. Here it can be seen that the scale uncertainties decrease for most processes when going from NLO+NLL precision to NNLL matched precision. The only exception to this is gluino-pair production. The scale dependence will be discussed in greater detail when discussing Figure 6.6. The dominant contribution to the NNLL matched uncertainties are the PDF and α_{s} uncertainties. These uncertainties are larger for the NNLL matched cross section than for the NLO+NLL cross section. The main driving force behind this increase in uncertainty is the increase in the α_{s} uncertainty when switching from NLO to NNLO PDFs. Table 6.1 provides an overview of the different cross sections and uncertainties for the different processes.

Next we can study the relative corrections the NNLL resummation provides with respect to the NLO cross section. In order to accomplish this we will define a K-factor as

$$K_X = \frac{\sigma^X}{\sigma^{\text{NLO}}} \tag{6.24}$$

where X indicates the precision that is currently looked at. The mass dependence of the four squark and gluino pair production processes for equal squark and gluino masses can be seen in Figure 6.4. In this figure we can see the relative corrections increasing for larger masses. This is to be expected, because the larger masses will bring the process closer to absolute threshold making the threshold enhanced terms more important. The largest corrections are for gluino-pair production, this is to be expected due to the larger color factors of the gluinos than for the squarks.

Relative to the other processes the $\tilde{q}\tilde{q}$ production process does not have as strong an increase for larger masses in the K-factor for the NNLL matched cross section. This behavior arises due to two different effects. The first effect is caused by the one-loop Coulomb corrections. The one-loop Coulomb correction for the sextet color structure is negative, leading to a decrease
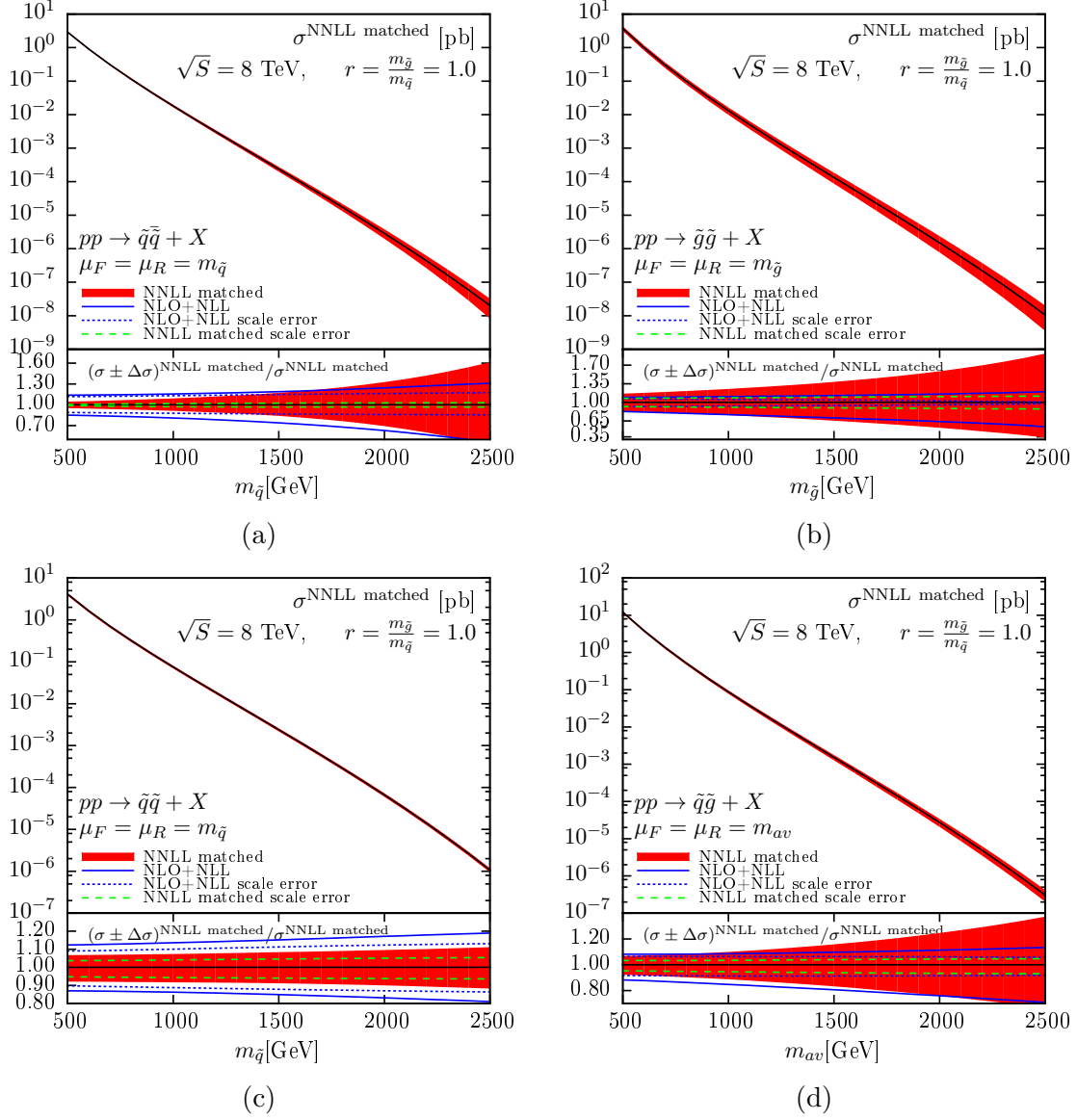
(a)

(b)

(c)

(d)

Figure 6.2: The NNLL matched cross section for the four processes of pair production of squarks and gluinos, including the theoretical uncertainty band for the NNLO approximation. The uncertainty band includes the 68% C.L. PDF and α_s uncertainties, added quadratically, and the scale uncertainty varied in the range $m_{av}/2 \leq \mu \leq 2m_{av}$, added linearly to the combined PDF and α_s uncertainty. The energy is that of the LHC at 8 TeV. The squark and gluino masses have been taken equal and the common renormalization and factorization scale has been set equal to the average mass of the two particles produced. For comparison, we also show the scale and total uncertainty of the NLO+NLL prediction.

process	m[GeV]	$\sigma^{\text{NNLL matched}}$[pb]	Scale Error	PDF Error	α_{s} Error	Total Error
$\tilde{q}\bar{\tilde{q}}$	500	2.90	$+0.37\%$ -1.2%	$+2.6\%$ -2.3%	$+3.2\%$ -2.8%	$+4.5\%$ -4.8%
$\tilde{q}\bar{\tilde{q}}$	1000	1.80×10^{-2}	$+1.7\%$ -2.8%	$+6.0\%$ -5.3%	$+4.5\%$ -2.9%	$+9.2\%$ -8.8%
$\tilde{q}\bar{\tilde{q}}$	1500	2.37×10^{-4}	$+2.4\%$ -3.3%	$+11\%$ -12%	$+9.6\%$ -5.2%	$+17\%$ -16%
$\tilde{q}\bar{\tilde{q}}$	2000	2.86×10^{-6}	$+2.7\%$ -3.3%	$+20\%$ -25%	$+22\%$ -12%	$+33\%$ -31%
$\tilde{q}\bar{\tilde{q}}$	2500	2.01×10^{-8}	$+3.0\%$ -3.3%	$+37\%$ -50%	$+45\%$ -24%	$+61\%$ -59%
$\tilde{g}\tilde{g}$	500	3.72	-8.1% $+7.6\%$	$+6.7\%$ -6.8%	$+5.5\%$ -4.3%	$+16\%$ -16%
$\tilde{g}\tilde{g}$	1000	1.30×10^{-2}	-9.3% $+8.6\%$	$+12\%$ -13%	$+11\%$ -7.3%	$+25\%$ -24%
$\tilde{g}\tilde{g}$	1500	1.33×10^{-4}	-10% $+9.7\%$	$+20\%$ -21%	$+21\%$ -12%	$+38\%$ -35%
$\tilde{g}\tilde{g}$	2000	1.49×10^{-6}	-12% $+11\%$	$+31\%$ -31%	$+36\%$ -19%	$+59\%$ -48%
$\tilde{g}\tilde{g}$	2500	1.05×10^{-8}	-12% $+12\%$	$+49\%$ -45%	$+64\%$ -30%	$+92\%$ -66%
$\tilde{q}\tilde{q}$	500	4.13	$+3.7\%$ -5.2%	$+2.6\%$ -2.0%	$+1.7\%$ -1.7%	$+6.8\%$ -7.9%
$\tilde{q}\tilde{q}$	1000	7.51×10^{-2}	$+4.1\%$ -5.7%	$+3.3\%$ -2.5%	$+0.41\%$ -0.50%	$+7.4\%$ -8.3%
$\tilde{q}\tilde{q}$	1500	2.39×10^{-3}	$+4.6\%$ -6.0%	$+3.7\%$ -2.8%	-0.60% $+0.48\%$	$+8.4\%$ -8.9%
$\tilde{q}\tilde{q}$	2000	6.66×10^{-5}	$+5.0\%$ -6.2%	$+4.3\%$ -3.5%	-1.5% $+1.5\%$	$+9.6\%$ -10%
$\tilde{q}\tilde{q}$	2500	1.07×10^{-6}	$+5.4\%$ -6.4%	$+5.2\%$ -4.7%	-2.5% $+2.5\%$	$+11\%$ -12%
$\tilde{q}\tilde{g}$	500	12.1	-4.7% $+3.2\%$	$+2.3\%$ -2.1%	$+2.7\%$ -2.3%	$+6.7\%$ -7.8%
$\tilde{q}\tilde{g}$	1000	8.74×10^{-2}	-5.4% $+3.4\%$	$+4.9\%$ -5.0%	$+4.4\%$ -3.1%	$+10\%$ -11%
$\tilde{q}\tilde{g}$	1500	1.52×10^{-3}	-6.1% $+3.9\%$	$+8.6\%$ -9.3%	$+8.2\%$ -5.1%	$+16\%$ -17%
$\tilde{q}\tilde{g}$	2000	2.72×10^{-5}	-6.7% $+4.4\%$	$+14\%$ -15%	$+15\%$ -8.7%	$+25\%$ -24%
$\tilde{q}\tilde{g}$	2500	3.05×10^{-7}	-7.0% $+4.7\%$	$+21\%$ -22%	$+24\%$ -14%	$+37\%$ -33%
inclusive	500	22.9	$+2.2\%$ -3.0%	$+1.7\%$ -1.6%	$+1.8\%$ -1.5%	$+4.7\%$ -5.2%
inclusive	1000	1.94×10^{-1}	$+2.3\%$ -3.4%	$+2.7\%$ -2.7%	$+2.2\%$ -1.5%	$+5.8\%$ -6.4%
inclusive	1500	4.29×10^{-3}	$+2.9\%$ -4.0%	$+3.8\%$ -3.8%	$+3.0\%$ -1.9%	$+7.8\%$ -8.2%
inclusive	2000	9.81×10^{-5}	$+3.6\%$ -4.6%	$+4.9\%$ -4.9%	$+4.3\%$ -2.7%	$+10\%$ -10%
inclusive	2500	1.40×10^{-6}	$+4.2\%$ -5.1%	$+6.2\%$ -6.1%	$+5.7\%$ -3.6%	$+13\%$ -12%

Table 6.1: The NNLL matched cross section prediction for different SUSY-QCD processes at the LHC with $\sqrt{S} = 8$ TeV. The scale, PDF, α_{s} and total uncertainty are shown separately. The MSTW 2008 NNLO PDFs [94] have been adopted, the squark and gluino masses have been taken equal and the common renormalization and factorization scale has been set equal to the squark/gluino mass.
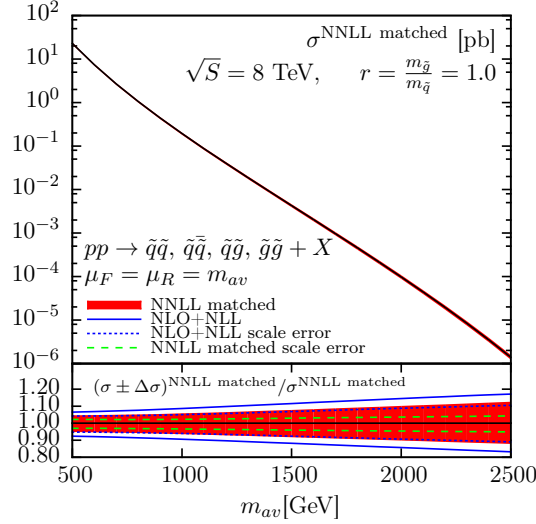
Figure 6.3: The NNLL matched cross section for the sum of the four processes of pair pro-
duction of squarks and gluinos, including the theoretical uncertainty band for the
NNLO approximation. The uncertainty band includes the 68% C.L. PDF and α_{s}
uncertainties, added quadratically, and the scale uncertainty varied in the range
$m_{av}/2 \leq \mu \leq 2m_{av}$, added linearly to the combined PDF and α_{s} uncertainty. The
energy is that of the LHC at 8 TeV. The squark and gluino masses have been taken
equal and the common renormalization and factorization scale has been set equal to
the average mass of the two particles produced. For comparison, we also show the
scale and total uncertainty of the NLO+NLL prediction.

in the cross section, whereas the anti-triplet has a positive Coulomb contribution leading to
an increase. The importance of the negative sextet contribution is enhanced for larger squark
masses due to the relative size of the color channels in the LO contributions with increasing mass.
The sextet color channel becomes dominant at high masses, whereas the anti-triplet is dominant
for low masses. A comparison can most easily be made with $\tilde{q}\tilde{g}$ production as it also has one
initial state configuration at LO. In this example the 15-plet color channel contribution to LO,
which has a negative Coulomb contribution, is not dominant when compared to the other color
channels. In addition the Coulomb corrections have a smaller overall contribution compared to
the logarithms for $\tilde{q}\tilde{g}$ when compared to $\tilde{q}\tilde{q}$. The second effect is due to the difference in behavior
for the NNLO PDFs and the NLO PDFs for the valence quarks and gluons. The ratio of the
NNLO PDFs to NLO PDFs increases for increasing values of x for gluons, whereas it decreases
for quarks. This leads to an enhancement for all processes with gluons in the initial state for
the NNLL and NNLO corrections with respect to the NLO+NLL that grows with increasing
masses for the final state particles. For the processes with quarks in the initial state this leads
to a suppression of these corrections for large masses. The $\tilde{q}\tilde{q}$-production process is the only
process that takes place at LO exclusively in the qq channel.

In Figure 6.5 we show the mass dependence of the K-factor for different ratios (r) of the squark
and gluino masses. The differences in the corrections for the various mass ratios can be largely ex-
plained by the r-dependence of the matching coefficients $\mathcal{C}^{\mathrm{NNLL}}_{ij\rightarrow kl,I}$, composed of the hard matching
coefficients [68] and the Coulomb contributions. The two-loop Coulomb coefficient only depends
on r for $\tilde{q}\tilde{g}$-production, resulting in an additional r-dependence for the K_{NNLL}-factor for this
production process.

Finally we will discuss the scale dependence for the different processes. This result can be seen
in Figure 6.6. For this analysis the squark and gluino masses are taken to be equal to 1.2 TeV.
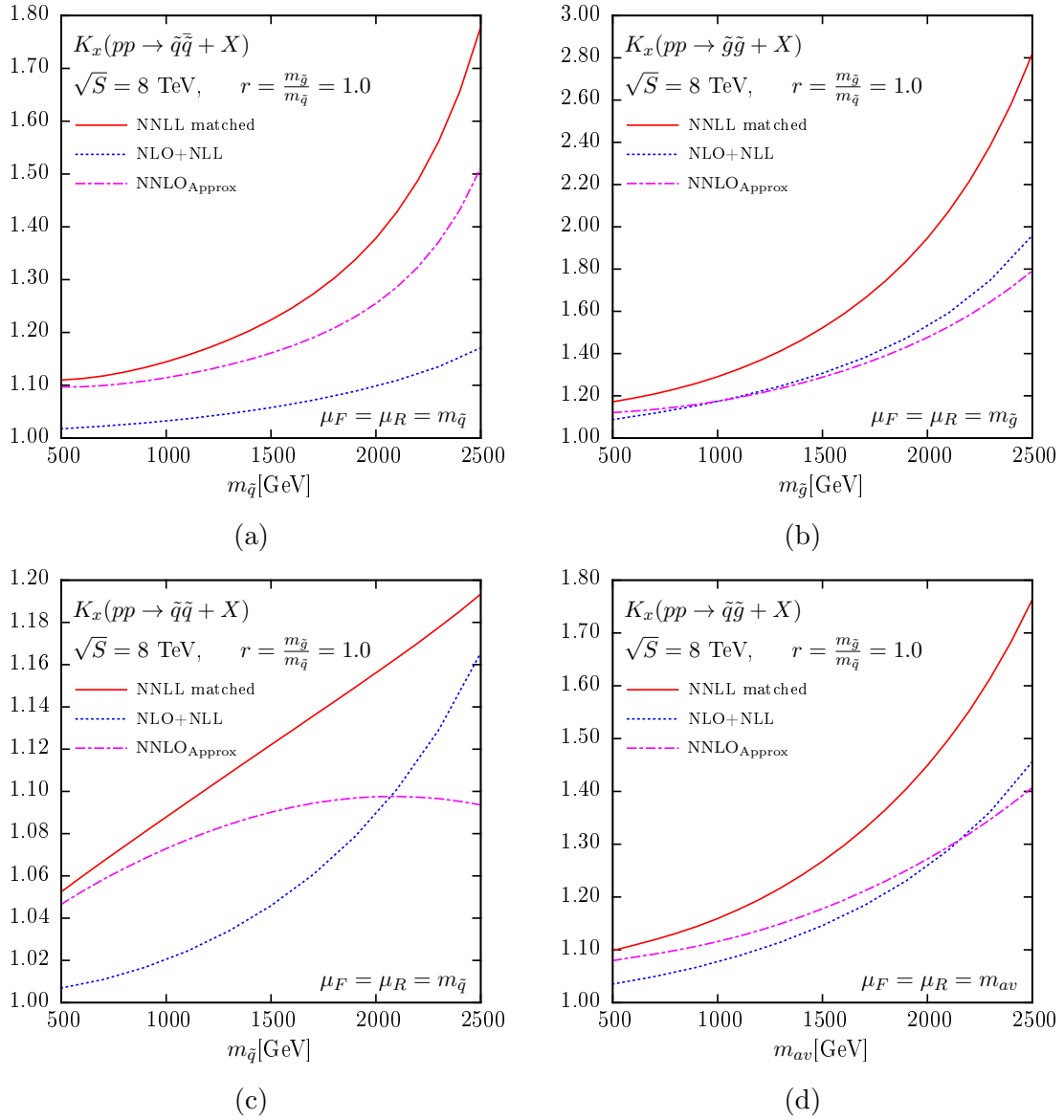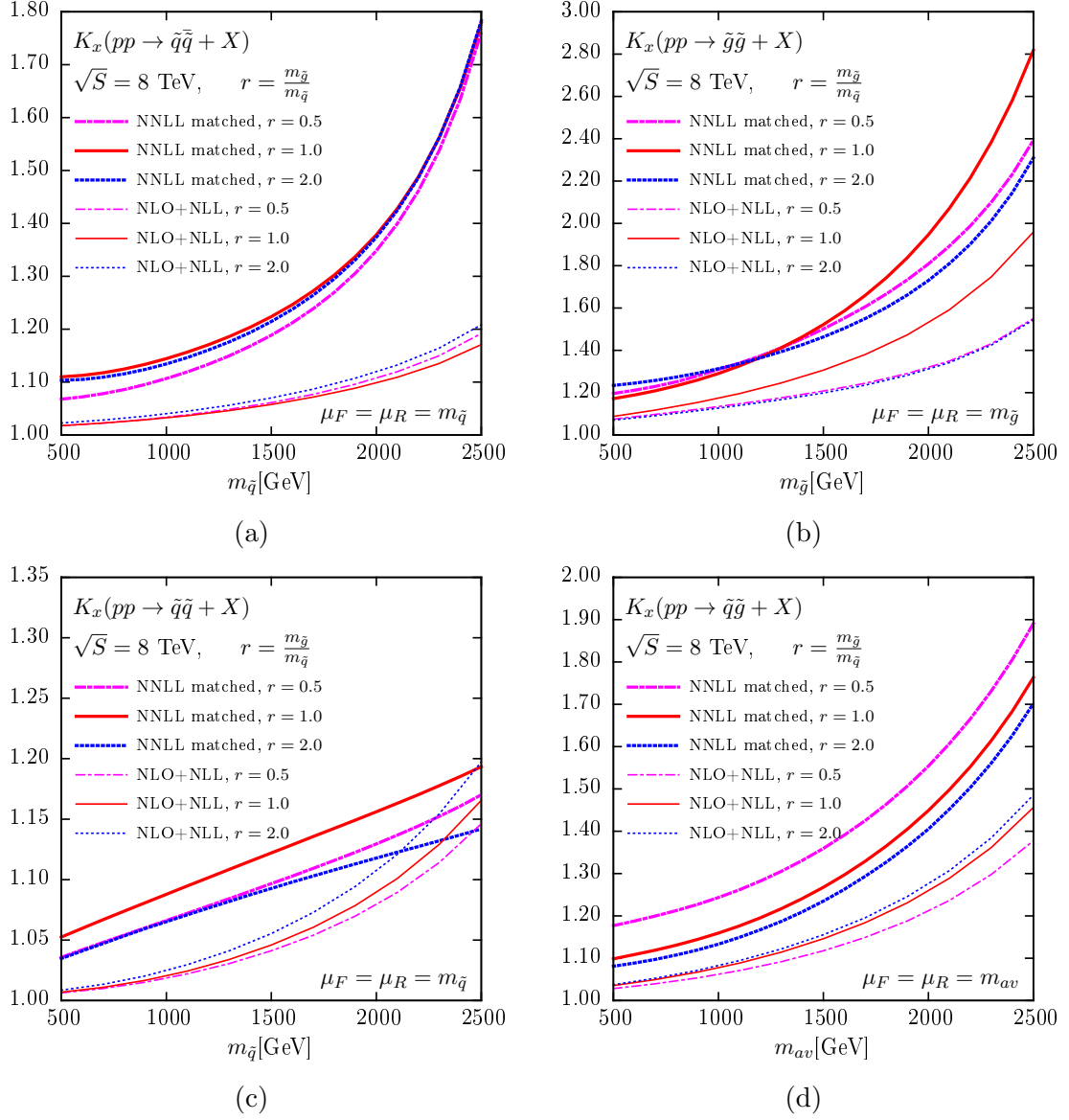
Figure 6.4: The K_X-factor for the NNLL matched, NLO+NLL and NNLO$_{\text{Approx}}$ predictions for different SUSY-QCD processes at the LHC with $\sqrt{S} = 8$ TeV. The squark and gluino masses have been taken equal and the common renormalization and factorization scale has been set equal to the average mass of the two particles produced.

(a)

(b)

(c)

(d)

Figure 6.5: The K_X-factor for the NNLL matched and NLO+NLL predictions for different values of $r = m_{\tilde{g}}/m_{\tilde{q}} = 0.5, 1, 2$ for the four pair-production processes of squarks and gluinos at the LHC with $\sqrt{S} = 8$ TeV. The common renormalization and factorization scale has been set equal to the average mass of the two particles produced.

The scale is varied around the central scale $\mu_0 = m_{\tilde{q}} = m_{\tilde{g}}$ from $\mu = \mu_0/5$ to $\mu = 5\mu_0$. It can be observed that the scale dependence decreases when the NNLL matched corrections are included for all processes except gluino-pair production.

In order to study the cause of the increased scale dependence for gluino-pair production we will study the scale dependence of several levels between NLO+NLL and NNLL matched. In Figure 6.7 (a) we present, in addition to NNLL matched, the scale dependence for gluino-pair production of NLO+NLL with $\mathcal{C}^{(1)}$, where the exponential is taken at the NLL order but in addition the one loop hard matching coefficient, $\mathcal{C}^{(1)}_{ij \to kl,I}$, is included while all Coulomb corrections are excluded. In addition, the NLO+NLL with $\mathcal{C}^{(1)} \& \mathcal{C}^{\text{Coul},(1)}$ result is presented, for this the one loop Coulomb corrections, $\mathcal{C}^{\text{Coul},(1)}_{ij \to kl,I}$, are included in addition to the hard coefficient. Finally the NNLO$_{\text{Approx.}}$+NNLL (w/o $\mathcal{C}^{\text{Coul},(1,2)}$) is shown, here the exponential is is computed at NNLL order, but the one and two loop Coulomb corrections are not included, while the one loop hard matching coefficient is still included. From Figure 6.7 (a) we can see that the increase in scale dependence in the low scale region is a result of the inclusion of the one loop Coulomb corrections. The effect of the one loop Coulomb corrections is decreased for the NNLL exponential compared to the NLL exponential.

To better understand the source of this we show the scale dependence for the the ratio of NLL with $\mathcal{C}^{(1)} \& \mathcal{C}^{\text{Coul},(1)}$ over NLL with $\mathcal{C}^{(1)}$ split up in the different components for the different color channels. This is shown for the resummed contribution in Figure 6.8 (a) and for the expansion up to NLO order in Figure 6.8 (b). From this it can be seen that the low scale behavior of the resummation is not largely altered by the inclusion of the one-loop Coulomb corrections, but the expansion is influenced in the low scale region by the Coulomb corrections. The behavior shown by the **27** color channel is slightly different due to the repulsive nature of the Coulomb corrections in this color channel. This results in a factor below one that decreases with decreasing scale, which is a mirrored behavior with respect to the other color channels. The cause for the behavior for the expansion is that the term added to the expansion is proportional to $\tilde{\sigma}_{\text{LO}} \mathcal{C}^{\text{Coul},(1)}$, where the LO increases rapidly for small scales due to the α_{s} and PDF scale dependence. For the resummation the additional term is $\tilde{\sigma}_{NLL+\mathcal{C}^{(1)}} \mathcal{C}^{\text{Coul},(1)}$, which has very little scale dependence, as can be seen in Figure 6.7 (a). In addition the dominant color channel for NLL with $\mathcal{C}^{(1)}$, **27**, decreases in importance due to the negative Coulomb contribution for this channel. These effects combine to result in the change in scale dependence in the low scale region when including the one-loop Coulomb corrections.

In addition for large scales there is a contribution from higher order logarithms. These logarithms are most dominant for $gg \to \tilde{g}\tilde{g}$ due to the large color factors in the process. This effect can be seen clearly when looking at Figure 6.7 (b), which shows the scale dependence of the NNLL resummation, the NNLL expanded to NNLO order as well as the NNLO$_{\text{Approx.}}$ and NNLL matched. Here it can be seen that the low scale behavior of the resummed and expanded contributions are the same, this means the low scale behavior of the NNLL matched is dominated by the NNLO$_{\text{Approx.}}$. For large scales the higher logarithmic terms become dominant for the resummed contribution and are responsible for the large scale dependence of the NNLL matched.

These observations were confirmed to also apply for larger masses of the gluinos ($m_{\tilde{g}} = 2.5$ TeV).
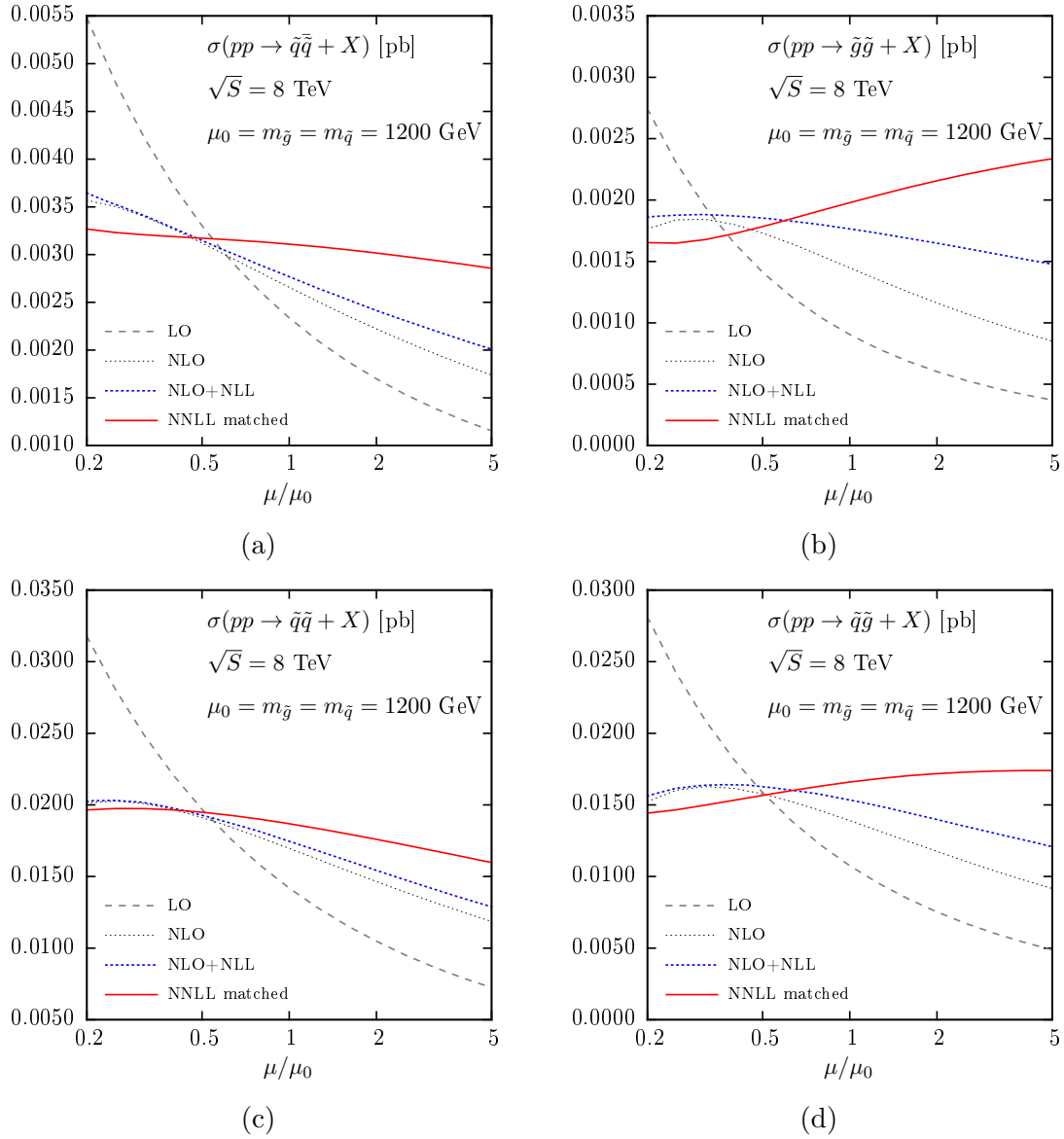
Figure 6.6: Scale dependence of the LO, NLO, NLO+NLL and NNLL matched cross sections for the four different SUSY-QCD processes at the LHC with $\sqrt{S} = 8$ TeV. The squark and gluino masses have been taken equal to 1.2 TeV.
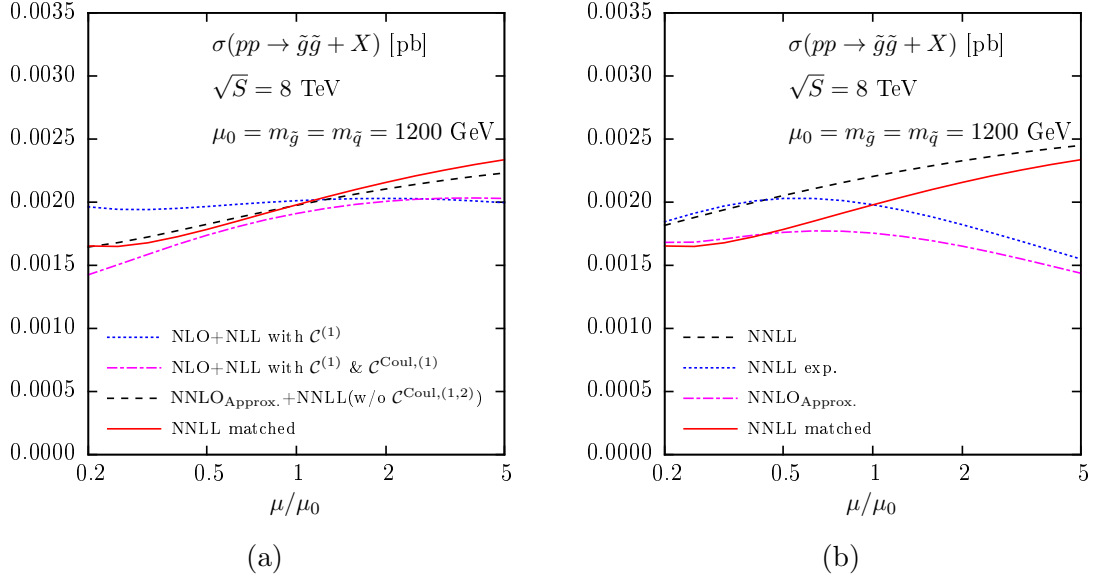
Figure 6.7: Scale dependence of different parts of the gluino pair production cross section: intermediate levels of accuracy (a), and a split-up of the cross section into resummed and expanded parts for NNLL matched, compared to the full NNLL matched result as well as NNLO$_{\text{Approx.}}$ (b).
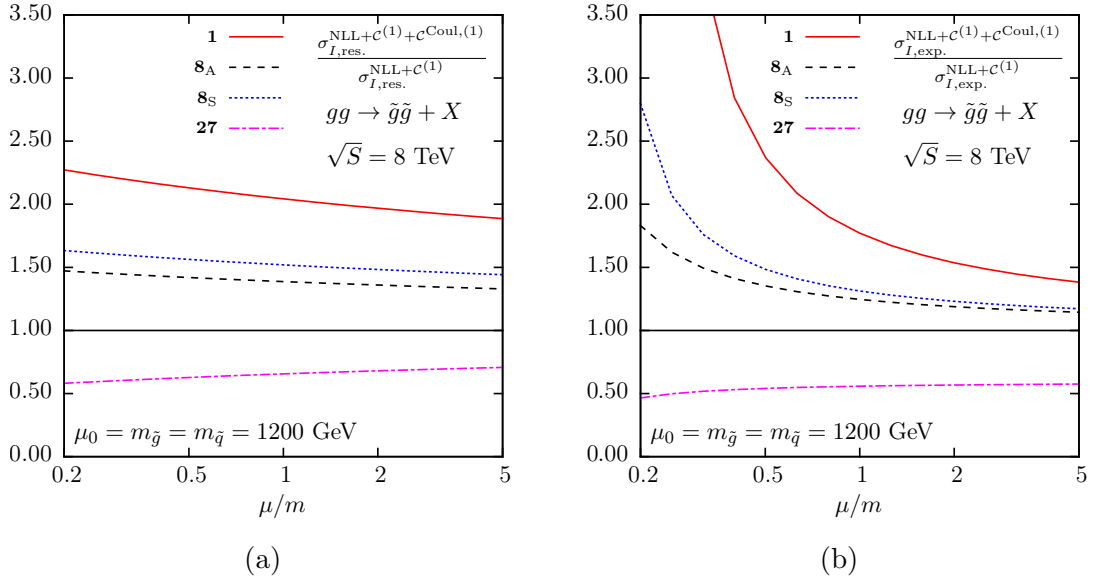

Figure 6.8: Ratio of the cross sections for NLL with $\mathcal{C}^{(1)}$ & $\mathcal{C}^{\text{Coul},(1)}$ over NLL with $\mathcal{C}^{(1)}$ when varying the scale with $m = 1200$ GeV for the resummed part (a) and the expanded part (b).

7 Resummation Techniques Applied to $t\bar{t}H$

This chapter will explore the application of resummation techniques to final states containing more than two particles. The resummation formulas have already been shown to work for and arbitrary number of partons [109–111], however so far no calculations have been performed in the traditional, Mellin space, resummation framework for $2 \to 3$ scattering at Born level. As an example the resummation techniques will be applied to the process of Higgs emission of a top anti-top pair. The main difference between a two final state particle process and a three final state particle process is the kinematics. Therefore, these will be treated first in Section 7.1. As there are colored final state particles, the soft anomalous dimension matrix will need to be calculated in a specific color basis. This computation is explored in Section 7.3. Next for the NLL computation we will include the hard matching coefficient. With all these ingredients the absolute threshold resummation at NLL order can be applied and these results are presented in Section 7.4. Finally we will explore the possibility of defining threshold in different ways. These different definitions will allow for differential distributions to be explored.

7.1 Kinematics

We study the $2 \to 3$ process on the basis of the example $i\,(1) + j\,(2) \to t\,(3) + \bar{t}(4) + H\,(5) + X(k)$, where the numbers indicate the momenta labels used. The hadronic momenta will be labeled with A and B, where $p_1 = x_1 p_A$ and $p_2 = x_2 p_B$ with x_i the fractions of energy of the hadrons the partons carry.

The definitions of the partonic invariant variables we will use are:

$$
\begin{aligned}
\hat{s} &= (p_1 + p_2)^2 \\
s_{kl} &= (p_k + p_l)^2 \\
t_{ik} &= (p_i - p_k)^2 \\
\tilde{t}_{ik} &= t_{ik} - p_k^2
\end{aligned}
\tag{7.1}
$$

where k and l are used to indicate final state particles and i is used to indicate an initial state particle.

The hadronic variables we will use are:

$$
\begin{aligned}
S &= (p_A + p_B)^2 \\
Q_{kl}^2 &= (p_k + p_l)^2 \\
T_{Ik} &= (p_I - p_k)^2 \\
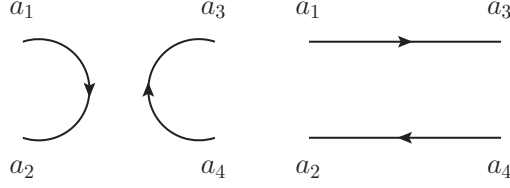\tilde{T}_{Ik} &= T_{Ik} - p_k^2
\end{aligned}
\tag{7.2}
$$

Figure 7.1: An illustrative representation of a color basis for $q\bar{q} \to Q\bar{Q}X$.

For the default phase space integration we will use the same variables as in [37]. This kinematic configuration describes the phase space through the intermediate state $t\bar{t}$ with invariant mass s_{34}. This results in the phase space variables s_{34}, the polar angle of the fifth particle in the initial state center-of-mass frame (θ_5^{CM}) and the solid angle of the third particle in the rest frame of particles 3 and 4 using the direction of flight of the $t\bar{t}$ intermediate state in the initial state center-of-mass frame as the z-axis, Ω_3^*.

7.2 Born cross section

7.2.1 Color basis

In order to calculate the resummation including final state emission, a color basis will need to be specified first. There are multiple possible bases that can be used, however in practice it is most useful to define a basis that results in a diagonal form for the threshold limit of the soft anomalous dimension. This color basis can be found by using the method used in [102] and coincides with the s-channel color basis. For this color basis we require the basis to be orthogonal and to be an eigenvector of the quadratic Casimir operator. The first condition leads to the requirement:

$$tr\left(c_I^\dagger c_J\right) = A_I \delta_{IJ} \tag{7.3}$$

for the color basis c_I with A_I an arbitrary normalization factor that can depend on the element of the color basis. Here repeated indices are not summed over. The second condition is described by:

$$(T_1 + T_2)^2 c_I = C_I c_I \tag{7.4}$$

with T_i the color operator from a gluon emission from particle i and C_I the quadratic Casimir invariant. When writing this condition out explicitly including indices this results in:

$$\left((T_1)_{a_1 b_1}^C \delta_{a_2 b_2} + (T_2)_{a_2 b_2}^C \delta_{a_1 b_1}\right) \left((T_1)_{b_1 d_1}^C \delta_{b_2 d_2} + (T_2)_{b_2 d_2}^C \delta_{b_1 d_1}\right) \delta_{a_3 d_3} \delta_{a_4 d_4} (c_I)_{d_1 d_2 d_3 d_4}$$
$$= C_I (c_I)_{a_1 a_2 a_3 a_4} \tag{7.5}$$

Through the general connection of color indices we can see that a complete set of the color basis, for example for $q(1)\,\bar{q}(2) \to Q(3)\,\bar{Q}(4)$, is:

$$\delta_{a_2 a_1} \delta_{a_3 a_4}, \quad \delta_{a_2 a_4} \delta_{a_3 a_1} \tag{7.6}$$

This can be seen on the basis of the diagrams seen in Figure 7.1. Here the indices are taken against the color flow resulting in the basis given in Equation 7.6.

Using the two conditions we find the result for $q\bar{q} \to Q\bar{Q}B$ (up to normalization factors):

$$c_I = \begin{pmatrix} \delta_{a_2 a_1} \delta_{a_3 a_4} \\ T^D_{a_2 a_1} T^D_{a_3 a_4} \end{pmatrix} \tag{7.7}$$

$$c_I^\dagger = \begin{pmatrix} \delta_{a_1 a_2} \delta_{a_4 a_3} \\ T^D_{a_1 a_2} T^D_{a_4 a_3} \end{pmatrix} \tag{7.8}$$

with the index a_i related to external particle i. For $gg \to Q\bar{Q}B$ the procedure for the computation of the color basis results in:

$$c_I = \begin{pmatrix} \delta^{A_1 A_2} \delta_{a_3 a_4} \\ T^D_{a_3 a_4} d^{D A_1 A_2} \\ i T^D_{a_3 a_4} f^{D A_1 A_2} \end{pmatrix} \tag{7.9}$$

$$c_I^\dagger = \begin{pmatrix} \delta^{A_2 A_1} \delta_{a_4 a_3} \\ T^D_{a_4 a_3} d^{D A_2 A_1} \\ i T^D_{a_4 a_3} f^{D A_2 A_1} \end{pmatrix} \tag{7.10}$$

For these computations the color package [112] for `FORM` [113] was used.

We can compute the Born matrix element squared in these color bases by:

$$M^{(0)}_{IJ} = h^{(0)}_I h^{(0)*}_K S^{(0)}_{KJ} \equiv H^{(0)}_{IK} S^{(0)}_{KJ} \tag{7.11}$$

with $S^{(0)}_{IJ} = tr\left(c_I^\dagger c_J\right)$. Where the Born matrix element can be calculated in this basis by:

$$h^{(0)}_I = \left(S^{(0)}_{IK}\right)^{-1} tr\left(c_K^\dagger \mathcal{A}\right) \tag{7.12}$$

$$h^{(0)*}_J = tr\left(\mathcal{A}^\dagger c_K\right) \left(S^{(0)}_{KJ}\right)^{-1} \tag{7.13}$$

with $\mathcal{A}$ the matrix element.

7.2.2 Matrix element in color space

The different types of diagrams that contribute are shown in Figure 7.2. For each of these diagrams the Higgs boson can be emitted from any top quark. The matrix elements of the different types of diagrams each have their own color operators.

For the quark initial there is only one type of color structure given by the s-channel. We can extract the color operator out of the matrix element:

$$\mathcal{A}^{q\bar{q} \to t\bar{t}H}_{a_1 a_2 a_3 a_4} = T^C_{a_2 a_1} T^C_{a_3 a_4} \mathcal{M}_{q\bar{q} \to t\bar{t}H} \tag{7.14}$$

With this we can project the matrix element into color space

$$h^{q\bar{q} \to t\bar{t}H(0)}_I = \left(S^{(0)}_{IK}\right)^{-1} tr\left(c_K^\dagger \mathcal{A}\right) = \left(S^{(0)}_{IK}\right)^{-1} \begin{pmatrix} 0 \\ \frac{C_A C_F}{2} \mathcal{M} \end{pmatrix} = \begin{pmatrix} 0 \\ \mathcal{M}_{q\bar{q} \to t\bar{t}H} \end{pmatrix} \tag{7.15}$$

The resulting matrix element squared matrix is

$$H_{IJ}^{q\bar{q}\to t\bar{t}H,(0)} = \begin{pmatrix} 0 & 0 \\ 0 & |\mathcal{M}|^2 \end{pmatrix} \tag{7.16}$$

and

$$S_{IJ}^{q\bar{q}\to t\bar{t}H,(0)} = \begin{pmatrix} C_A^2 & 0 \\ 0 & \frac{C_A C_F}{2} \end{pmatrix} \tag{7.17}$$

The gluon initial state has three different types of diagrams: s-channel (b) which will be indicated by $\mathcal{A}_1$, t-channel (c) indicated by $\mathcal{A}_2$ and u-channel (d) indicated by $\mathcal{A}_3$. Again the color operator will be extracted from the matrix element

$$\mathcal{A}_{a_1 a_2 a_3 a_4}^{gg\to t\bar{t}H,(1)} = T_{a_3 c}^{A_1} T_{ca_4}^{A_2} \mathcal{M}_{gg\to t\bar{t}H}^{(1)} \tag{7.18}$$

$$\mathcal{A}_{a_1 a_2 a_3 a_4}^{gg\to t\bar{t}H,(2)} = T_{a_3 c}^{A_2} T_{ca_4}^{A_1} \mathcal{M}_{gg\to t\bar{t}H}^{(2)} \tag{7.19}$$

$$\mathcal{A}_{a_1 a_2 a_3 a_4}^{gg\to t\bar{t}H,(3)} = i f^{A_1 A_2 C} T_{a_3 a_4}^{C} \mathcal{M}_{gg\to t\bar{t}H}^{(3)} \tag{7.20}$$

Projecting the matrix element into color space results in

$$h_I^{(0)} = \left(S_{IK}^{(0)}\right)^{-1} tr\left(c_K^\dagger \mathcal{A}\right) = \left(S_{IK}^{(0)}\right)^{-1} \begin{pmatrix} C_F C_A \left(\mathcal{M}_{gg\to t\bar{t}H}^{(2)} + \mathcal{M}_{gg\to t\bar{t}H}^{(3)}\right) \\ C_F \frac{(C_A^2-4)}{2} \left(\mathcal{M}_{gg\to t\bar{t}H}^{(2)} + \mathcal{M}_{gg\to t\bar{t}H}^{(3)}\right) \\ C_F \frac{C_A^2}{2} \left(2\mathcal{M}_{gg\to t\bar{t}H}^{(1)} + \mathcal{M}_{gg\to t\bar{t}H}^{(2)} - \mathcal{M}_{gg\to t\bar{t}H}^{(3)}\right) \end{pmatrix}$$

$$= \begin{pmatrix} \frac{1}{2C_A} \left(\mathcal{M}_{gg\to t\bar{t}H}^{(2)} + \mathcal{M}_{gg\to t\bar{t}H}^{(3)}\right) \\ \frac{1}{2} \left(\mathcal{M}_{gg\to t\bar{t}H}^{(2)} + \mathcal{M}_{gg\to t\bar{t}H}^{(3)}\right) \\ \frac{1}{2} \left(2\mathcal{M}_{gg\to t\bar{t}H}^{(1)} + \mathcal{M}_{gg\to t\bar{t}H}^{(2)} - \mathcal{M}_{gg\to t\bar{t}H}^{(3)}\right) \end{pmatrix} \tag{7.21}$$

The resulting matrix element squared is

$$H_{22}^{gg\to t\bar{t}H,(0)} = \frac{1}{4}\left|\mathcal{M}^{(2)} + \mathcal{M}^{(3)}\right|^2 = C_A^2 H_{11}^{gg\to t\bar{t}H,(0)} \tag{7.22}$$

$$H_{33}^{gg\to t\bar{t}H,(0)} = \frac{1}{4}\left|2\mathcal{M}^{(1)} + \mathcal{M}^{(2)} - \mathcal{M}^{(3)}\right|^2 \tag{7.23}$$

$$H_{32}^{gg\to t\bar{t}H,(0)} = \frac{1}{4}\left(2\mathcal{M}^{(1)} + \mathcal{M}^{(2)} - \mathcal{M}^{(3)}\right)\left(\mathcal{M}^{(2)} + \mathcal{M}^{(3)}\right)^\dagger = C_A H_{31}^{gg\to t\bar{t}H,(0)} \tag{7.24}$$

with

$$\left(H_{IJ}^{gg\to t\bar{t}H,(0)}\right)^\dagger = H_{IJ}^{gg\to t\bar{t}H,(0)} \tag{7.25}$$

and

$$S_{IJ}^{gg\to t\bar{t}H,(0)} = \begin{pmatrix} 2C_F C_A^2 & 0 & 0 \\ 0 & C_F\left(C_A^2 - 4\right) & 0 \\ 0 & 0 & C_F C_A^2 \end{pmatrix} \tag{7.26}$$
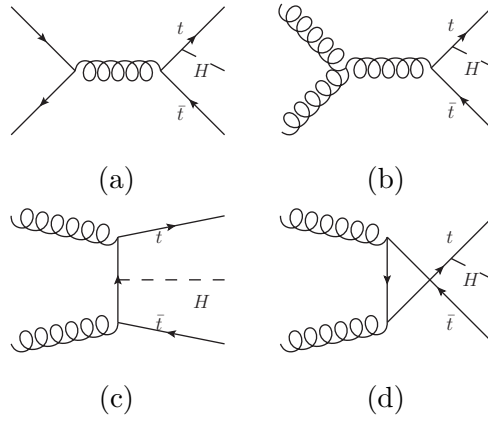
Figure 7.2: The four different types of Feynman diagrams involved in the $pp \to t\bar{t}H$. The quark initial state only has the s-channel contribution (a). For the gluon initial state there is the s-channel (b), t-channel (c) and u-channel (d). The Higgs boson can be emitted from any top quark meaning each type has multiple diagrams.

7.3 One-loop soft anomalous dimension

In this paragraph the method used to calculate the soft anomalous dimension matrix will be discussed. This will be done for the process $q\bar{q} \to Q\bar{Q}B$, with Q a heavy colored quark-like particle and B a (massive) colorless particle. This calculation is similar to the calculation of the soft anomalous dimension for $q\bar{q} \to Q\bar{Q}$. In addition the results for $gg \to Q\bar{Q}B$ will be presented. The results for the soft anomalous dimension matrix presented here can be used for the specific process $pp \to t\bar{t}H$. The computation of the soft anomalous dimension matrix is performed as in [88].

7.3.1 Gluon exchange diagrams

The computation of the soft anomalous dimension involves the calculation of all different diagrams that contain a gluon exchange between two different external particles and the self energy diagrams for the colored final state particles. The diagrams that need to be computed can be seen in Figure 7.3.

7.3.2 Color mixing matrix

The first step in calculating the soft anomalous dimension matrix is to find the color mixing matrix, C_{IJ}^{ab} with I and J color basis indices and a and b indices that indicate between which particles the gluon is exchanged. This matrix describes how the color structure is influenced due to a gluon emission.

In the color basis presented in Section 7.2.1 we can calculate the color mixing matrix. In order to calculate this matrix more easily we can define a matrix η_{IJ}^{ab} as:

$$\eta_{IJ}^{ab} \equiv c_I^\dagger c_K C_{KJ}^{ab} \equiv c_I^\dagger T^{C,b} c_J T^{C,a} \Delta \tag{7.27}$$

Here $T^{C,b}$ and $T^{C,a}$ are matrices belonging to the coupling between the gluon and particles b and a respectively and Δ is a delta function for the indices of the particles that do not have a
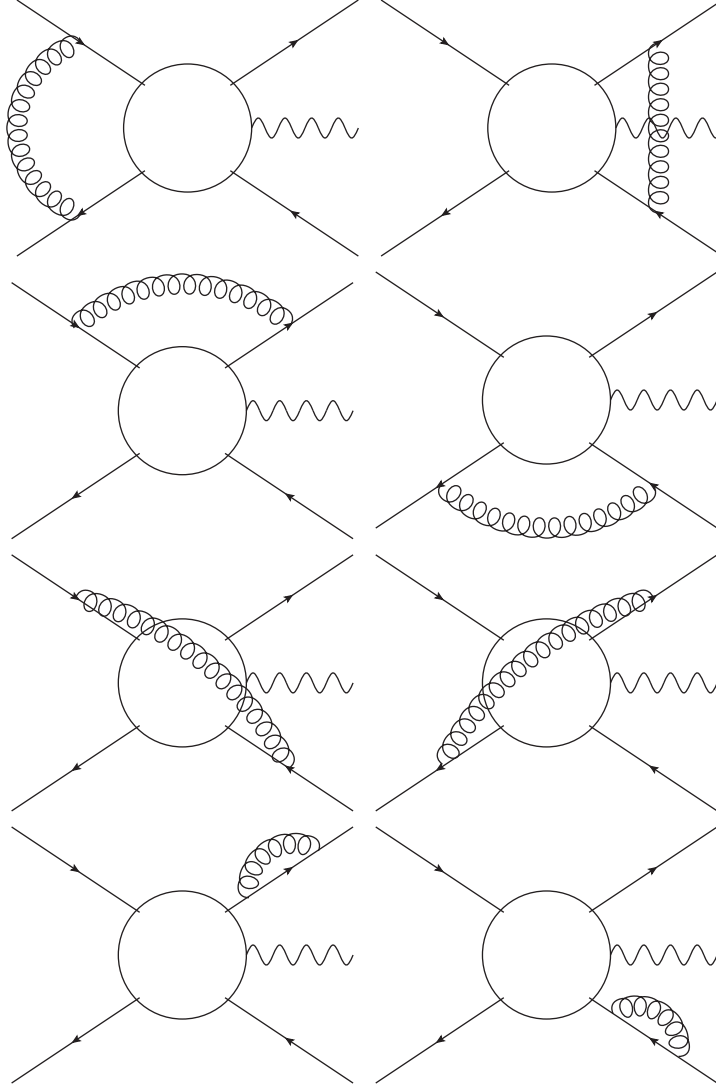
Figure 7.3: The one-loop Feynman diagrams contribute to the soft anomalous dimension for $q\bar{q} \to Q\bar{Q}X$.

gluon exchange. This new matrix can now be used to calculate the color mixing matrix in the following manner:

$$C_{IJ}^{ab} = \left(S_{IK}^{(0)}\right)^{-1} \eta_{KJ}^{ab} \tag{7.28}$$

For these computations the color package [112] for FORM [113] was used.

7.3.3 Eikonal integrals

The next step, in order to calculate the soft anomalous dimension matrix, is the calculation of the loop integrals. In order to compute these loop integrals we will use the eikonal rules derived in Section 4.1.1. We will write these in a general form for particle i as:

$$\frac{\Delta_i v_i^{\mu}}{\delta_i v_i \cdot k + i\epsilon} \tag{7.29}$$

with δ_i and Δ_i signs and $v_i^{\mu} = p_i^{\mu}\sqrt{2/\hat{s}}$, for $\hat{s}$ the center of mass energy squared.

Using the gluon propagator

$$D^{\mu\nu}(k) = \frac{-i}{k^2 + i\epsilon} N^{\mu\nu}(k), \qquad N^{\mu\nu}(k) = g^{\mu\nu} - \frac{n^{\mu}k^{\nu} + k^{\mu}n^{\nu}}{n \cdot k} + n^2 \frac{k^{\mu}k^{\nu}}{(n \cdot k)^2} \tag{7.30}$$

the integral is written as:

$$\omega^{ij} = g_s^2 \int \frac{d^d q}{(2\pi)^d} \frac{-i}{q^2 + i\epsilon} \left\{ \frac{\Delta_i \Delta_j v_i \cdot v_j}{(\delta_i v_i \cdot q + i\epsilon)(\delta_j v_j \cdot q + i\epsilon)} \right.$$

$$\left. - \frac{\Delta_i v_i \cdot n}{(\delta_i v_i \cdot q + i\epsilon)} \frac{P}{(n \cdot q)} - \frac{\Delta_j v_j \cdot n}{(\delta_j v_j \cdot q + i\epsilon)} \frac{P}{(n \cdot q)} + n^2 \frac{P}{(n \cdot q)^2} \right\} \tag{7.31}$$

with P, the principal value, used to deal with the poles and defined as:

$$\frac{P}{(n \cdot q)^{\beta}} = \frac{1}{2} \left(\frac{1}{(n \cdot q + i\epsilon)^{\beta}} + (-1)^{\beta} \frac{1}{(-n \cdot q + i\epsilon)^{\beta}} \right) \tag{7.32}$$

The integral can now be rewritten as:

$$\omega^{ij} = g_s^2 S_{ij} \left[I(\delta_i v_i, \delta_j v_j) - \frac{1}{2} I(\delta_i v_i, n) - \frac{1}{2} I(\delta_i v_i, -n) \right.$$

$$\left. - \frac{1}{2} I(\delta_j v_j, n) - \frac{1}{2} I(\delta_j v_j, -n) + \frac{1}{2} I(n, n) + \frac{1}{2} I(-n, -n) \right] \tag{7.33}$$

with an overall sign $S_{ij} = \Delta_i \Delta_j \delta_i \delta_j$. The general integral I can be rewritten using Feynman parametrization

$$\frac{1}{abc} = 2 \int_0^1 dx \int_0^{1-x} dy \, [a(1 - x - y) + bx + cy]^{-3} \tag{7.34}$$

This results in:

$$I(a, b) = \frac{-ia \cdot b}{(2\pi)^d} 2 \int_0^1 dx \int_0^{1-x} dy \int d^d q \, [q^2 x + a \cdot q(1 - y - x) + b \cdot qy + i\epsilon]^{-3}$$

$$= \frac{-ia \cdot b}{(2\pi)^d} 2 \int_0^1 dx \int_0^{1-x} dy \int d^d k \, [k^2 - \Delta]^{-3} x^{-3} \tag{7.35}$$

with $k = q + (1 - y - x)a/(2x) + yb/(2x)$ and $\Delta = ((1 - x - y)a/(2x) + yb/(2x))^2 - i\epsilon$. This integral results in:

$$I(a,b) = \frac{-a \cdot b}{(4\pi)^{d/2}} \int_0^1 dx \int_0^{1-x} dy \, [\Delta]^{-3+d/2} x^{-3} \Gamma\left(3 - \frac{d}{2}\right) \tag{7.36}$$

$$= \frac{-a \cdot b \Gamma\left(3 - \frac{d}{2}\right)}{(4\pi)^{d/2}} \int_0^1 dx \int_0^1 dw \left[((1 - w)a + wb)^2 - i\epsilon\right]^{-3+d/2} x^{3-d} 2^{6-d} (1 - x)^{-5+d}$$

with $w = y/(1 - x)$. The integral over x can be solved, however we only need the UV-divergent part. This coincides with the boundary $x \to 0$.

$$\int_0^1 dx x^{3-d}(1-x)^{-5+d} = \int_0^1 dx x^{-1+\varepsilon_{UV}}(1-x)^{-1-\varepsilon_{IR}} = \left[\frac{1}{\varepsilon_{UV}} - \frac{1}{\varepsilon_{IR}}\right] \tag{7.37}$$

with $d = 4 - \varepsilon$. This leaves the final integral:

$$I_{UV}(a,b) = \frac{-2^{6-d} a \cdot b \Gamma\left(3 - \frac{d}{2}\right)}{(4\pi)^{d/2} \varepsilon} \int_0^1 dw \left[((1 - w)a + wb)^2 - i\epsilon\right]^{-1+\varepsilon/2} \tag{7.38}$$

This integral needs to be solved in a case by case basis depending on what a^2 and b^2 are. If we take all these contributions into account the final results are:

$$\omega^{ab\left(v_a^2 \neq 0, v_b^2 \neq 0, a \neq b\right)} = S_{ab} \frac{\alpha_s}{\pi \varepsilon} [L_{\beta_{34}} + L_a + L_b - 1] \tag{7.39}$$

$$\omega^{aa\left(v_a^2 \neq 0\right)} = S_{aa} \frac{\alpha_s}{\pi \varepsilon} [2L_a - 2] \tag{7.40}$$

$$\omega^{ab\left(v_a^2 = 0, v_b^2 \neq 0\right)} = S_{ab} \frac{\alpha_s}{\pi \varepsilon} \left[-\frac{1}{2} \log\left(\frac{(v_a \cdot v_b)^2 s}{2m_b^2}\right) + L_b + \frac{1}{2} \log\left(\frac{(v_a \cdot n)^2}{|n|^2}\right) - 1\right] \tag{7.41}$$

$$\omega^{ab\left(v_a^2 = v_b^2 = 0\right)} = S_{ab} \frac{\alpha_s}{\pi \varepsilon} \left[-\log\left(\frac{v_a \cdot v_b}{2}\right) + \frac{1}{2} \log\left(\frac{(v_a \cdot n)^2}{|n|^2} \frac{(v_b \cdot n)^2}{|n|^2}\right) + i\pi - 1\right] \tag{7.42}$$

with the different variables defined as:

$$L_{\beta_{34}} = \frac{\kappa^2 + \beta_{34}^2}{2\kappa\beta_{34}} \left(\log\left(\frac{\kappa - \beta_{34}}{\kappa + \beta_{34}}\right) + i\pi\right) \tag{7.43}$$

with

$$\beta_{34} = \sqrt{1 - \frac{(m_3 + m_4)^2}{s_{34}}}$$

$$\kappa = \sqrt{1 - \frac{(m_3 - m_4)^2}{s_{34}}}$$

where m_3 and m_4 are the masses of the colored particles in the final state.

$$L_a = \frac{1}{2} [L_a(\delta_a v_a, n) + L_a(\delta_a v_a, -n)]$$

with

$$
\begin{aligned}
L_a \left(\delta_a v_a, \delta_n n \right) &= \frac{1}{2} \frac{v_a \cdot n}{\sqrt{(v_a \cdot n)^2 - 2m_a^2 n^2/s}} \\
&\times \left[\log \left(\frac{\delta_a \delta_n 2m_a^2/s - v_a \cdot n - \sqrt{(v_a \cdot n)^2 - 2m_a^2 n^2/s}}{\delta_a \delta_n 2m_a^2/s - v_a \cdot n + \sqrt{(v_a \cdot n)^2 - 2m_a^2 n^2/s}} \right) \right. \\
&+ \left. \log \left(\frac{\delta_a \delta_n n^2 - v_a \cdot n - \sqrt{(v_a \cdot n)^2 - 2m_a^2 n^2/s}}{\delta_a \delta_n n^2 - v_a \cdot n + \sqrt{(v_a \cdot n)^2 - 2m_a^2 n^2/s}} \right) - \delta_a \delta_n 2i\pi \right] \quad (7.44)
\end{aligned}
$$

7.3.4 The Soft Anomalous Dimension

We can now use the results from sections 7.3.2 and 7.3.3 to find the one-loop soft anomalous dimension matrix, $\bar{\Gamma}_{IJ}^{(1)}$, as defined in (4.79).

$$
\bar{\Gamma}_{ij\to kl,IJ}^{(1)} = -C_{IJ}^{ab}\mathrm{Res}\left\{\omega^{ab}\right\} - \frac{\alpha_s}{2\pi}\sum_{p=\{i,j\}} C_{2,p}\left(1 - \log\left(2\frac{(v_p \cdot n)^2}{|n|^2}\right) - i\pi\right)\delta_{IJ} \quad (7.45)
$$

where $C_{2,p}$ is $C_F = \left(N_C^2 - 1\right)/(2N_C)$ for a quark and N_C for a gluon with N_C the number of colors and Res stands for the residue. Using the equations from Section 7.3.2 the C_{IJ}^{ab} matrix can be computed. After including these the resulting soft anomalous dimension matrix is given by:

$$
\begin{aligned}
\bar{\Gamma}_{q\bar{q}\to Q\bar{Q}B,11}^{(1)} &= \mathrm{Res}\left\{-C_F\left(\omega^{12} + \omega^{34} + \frac{\omega^{33}}{2} + \frac{\omega^{44}}{2}\right)\right\} \\
&\quad -\frac{\alpha_s}{2\pi}C_F\left(2 - \log\left(4\frac{(v_1 \cdot n)^2}{|n|^2}\frac{(v_2 \cdot n)^2}{|n|^2}\right) - 2i\pi\right) \quad (7.46)
\end{aligned}
$$

$$
\bar{\Gamma}_{q\bar{q}\to Q\bar{Q}B,12}^{(1)} = \mathrm{Res}\left\{-\frac{C_F}{2N_C}\left(\omega^{13} + \omega^{14} + \omega^{23} + \omega^{24}\right)\right\} \quad (7.47)
$$

$$
\bar{\Gamma}_{q\bar{q}\to Q\bar{Q}B,21}^{(1)} = \mathrm{Res}\left\{-\left(\omega^{13} + \omega^{14} + \omega^{23} + \omega^{24}\right)\right\} \quad (7.48)
$$

$$
\begin{aligned}
\bar{\Gamma}_{q\bar{q}\to Q\bar{Q}B,22}^{(1)} &= \mathrm{Res}\left\{-C_F\left(\omega^{12} + \omega^{34} + \frac{\omega^{33}}{2} + \frac{\omega^{44}}{2} + 2\omega^{13} + 2\omega^{14} + 2\omega^{23} + 2\omega^{24}\right)\right. \\
&\quad \left. +\frac{N_C}{2}\left(\omega^{12} + \omega^{34} + \omega^{13} + 2\omega^{14} + 2\omega^{23} + \omega^{24}\right)\right\} \\
&\quad -\frac{\alpha_s}{2\pi}C_F\left(2 - \log\left(4\frac{(v_1 \cdot n)^2}{|n|^2}\frac{(v_2 \cdot n)^2}{|n|^2}\right) - 2i\pi\right) \quad (7.49)
\end{aligned}
$$

The self energy contributions, ω^{33} and ω^{44}, only contribute for half due to the definitions of the renormalization constant.

Next the results for ω^{ab} from Section 7.3.3 needs to be filled in. For this we use: $S_{12} = S_{24} = S_{34} = S_{13} = -S_{33} = -S_{44} = -S_{14} = -S_{23} = 1$ and $v_1 \cdot v_2 = 1$, $v_1 \cdot v_3 = -\tilde{t}_{13}/\hat{s}$, $v_2 \cdot v_4 = -\tilde{t}_{24}/\hat{s}$,

$v_1 \cdot v_4 = -\tilde{t}_{14}/\hat{s}$, $v_2 \cdot v_3 = -\tilde{t}_{23}/\hat{s}$, $v_3 \cdot v_4 = \left(s_{34} - m_3^2 - m_4^2\right)/\hat{s}$. This results in:

$$\bar{\Gamma}^{(1)}_{q\bar{q}\to Q\bar{Q}B,11} = -\frac{\alpha_s}{2\pi} 2C_F \left(L_{\beta_{34}} + 1\right) \tag{7.50}$$

$$\bar{\Gamma}^{(1)}_{q\bar{q}\to Q\bar{Q}B,12} = \frac{\alpha_s}{2\pi} \frac{2C_F}{N_C} \Omega_3 \tag{7.51}$$

$$\bar{\Gamma}^{(1)}_{q\bar{q}\to Q\bar{Q}B,21} = \frac{\alpha_s}{2\pi} 4\Omega_3 \tag{7.52}$$

$$\bar{\Gamma}^{(1)}_{q\bar{q}\to Q\bar{Q}B,22} = \frac{\alpha_s}{2\pi} \left[(N_C - 2C_F)\left(L_{\beta_{34}} + 1\right) + N_C \Lambda_3 + (8C_F - 3N_C)\,\Omega_3\right] \tag{7.53}$$

where Ω_3 and Λ_3 are defined as

$$\Omega_3 = (T_{13} + T_{24} - T_{14} - T_{23})/2 \tag{7.54}$$

$$\Lambda_3 = (T_{13} + T_{24} + T_{14} + T_{23})/2 \tag{7.55}$$

with

$$T_{ik} = \log\left(\frac{-\tilde{t}_{ik}}{m_k\sqrt{\hat{s}}}\right) + \frac{i\pi - 1}{2} \tag{7.56}$$

This can be reduced to the case of $q\bar{q} \to Q\bar{Q}$ by simply setting the kinematic variables to $t_{13} = t_{24} = t$, $t_{14} = t_{23} = u$ and $s_{34} = \hat{s}$ and agrees with the result presented in [88].

7.3.5 $gg \to Q\bar{Q}B$

The soft anomalous dimension for $gg \to Q\bar{Q}B$ can now be calculated in the same way as for $q\bar{q} \to Q\bar{Q}B$:

$$\bar{\Gamma}^{(1)}_{gg\to Q\bar{Q}B,11} = \text{Res}\left\{-N_C\omega^{12} - C_F\left(\omega^{34} + \frac{\omega^{33}}{2} + \frac{\omega^{44}}{2}\right)\right\}$$
$$- N_C\left(2 - \log\left(4\frac{(v_1 \cdot n)^2}{|n|^2}\frac{(v_2 \cdot n)^2}{|n|^2}\right) - 2i\pi\right) \tag{7.57}$$

$$\bar{\Gamma}^{(1)}_{gg\to Q\bar{Q}B,13} = \text{Res}\left\{-\frac{1}{2}\left(\omega^{13} + \omega^{14} + \omega^{23} + \omega^{24}\right)\right\} \tag{7.58}$$

$$\bar{\Gamma}^{(1)}_{gg\to Q\bar{Q}B,22} = \text{Res}\left\{-\frac{N_C}{2}\left(\omega^{12} + \frac{\omega^{13}}{2} - \frac{\omega^{14}}{2} - \frac{\omega^{23}}{2} + \frac{\omega^{24}}{2} - \omega^{34}\right)\right.$$
$$\left. - C_F\left(\omega^{34} + \frac{\omega^{33}}{2} + \frac{\omega^{44}}{2}\right)\right\}$$
$$- N_C\left(2 - \log\left(4\frac{(v_1 \cdot n)^2}{|n|^2}\frac{(v_2 \cdot n)^2}{|n|^2}\right) - 2i\pi\right) = \Gamma^{(1)}_{gg\to Q\bar{Q}B,33} \tag{7.59}$$

$$\bar{\Gamma}^{(1)}_{gg \to Q\bar{Q}B,23} = \mathrm{Res}\left\{-\frac{N_C}{4}\left(\omega^{13} + \omega^{14} + \omega^{23} + \omega^{24}\right)\right\} \tag{7.60}$$

$$\bar{\Gamma}^{(1)}_{gg \to Q\bar{Q}B,31} = \mathrm{Res}\left\{-\left(\omega^{13} + \omega^{14} + \omega^{23} + \omega^{24}\right)\right\} \tag{7.61}$$

$$\bar{\Gamma}^{(1)}_{gg \to Q\bar{Q}B,32} = \mathrm{Res}\left\{-\frac{N_C^2 - 4}{4N_C}\left(\omega^{13} + \omega^{14} + \omega^{23} + \omega^{24}\right)\right\} \tag{7.62}$$

$$\bar{\Gamma}^{(1)}_{gg \to Q\bar{Q}B,12} = \bar{\Gamma}^{(1)}_{gg \to Q\bar{Q}B,21} = 0 \tag{7.63}$$

After filling in ω^{ij} these result in:

$$\bar{\Gamma}^{(1)}_{gg \to Q\bar{Q}B,11} = -\frac{\alpha_s}{2\pi}2C_F\left(L_{\beta_{34}} + 1\right) \tag{7.64}$$

$$\bar{\Gamma}^{(1)}_{gg \to Q\bar{Q}B,13} = \frac{\alpha_s}{2\pi}2\Omega_3 \tag{7.65}$$

$$\bar{\Gamma}^{(1)}_{gg \to Q\bar{Q}B,22} = \bar{\Gamma}^{(1)}_{gg \to Q\bar{Q}B,33} = \frac{\alpha_s}{2\pi}\left[\frac{1}{N_C}\left(L_{\beta_{34}} + 1\right) + N_C\Lambda_3\right] \tag{7.66}$$

$$\bar{\Gamma}^{(1)}_{gg \to Q\bar{Q}B,23} = \frac{\alpha_s}{2\pi}N_C\Omega_3 \tag{7.67}$$

$$\bar{\Gamma}^{(1)}_{gg \to Q\bar{Q}B,31} = \frac{\alpha_s}{2\pi}4\Omega_3 \tag{7.68}$$

$$\bar{\Gamma}^{(1)}_{gg \to Q\bar{Q}B,32} = \frac{\alpha_s}{2\pi}\frac{N_C^2 - 4}{N_C}\Omega_3 \tag{7.69}$$

$$\bar{\Gamma}^{(1)}_{gg \to Q\bar{Q}B,12} = \bar{\Gamma}^{(1)}_{gg \to Q\bar{Q}B,21} = 0 \tag{7.70}$$

7.3.6 Diagonalization of the soft Anomalous dimension matrix

For the resummation the soft anomalous dimension matrix will be contained in a path ordered exponential. In order to calculate this exponential we need to diagonalize the matrix. For this diagonalization we will be mainly following the method of [90]. In this basis the hard matrix (H_{IJ}) and the soft matrix $(S^{(0)}_{IJ}$, the color matrix at LO) of Equation (4.66) also change:

$$\begin{aligned} \Gamma_R &= R^{-1}\Gamma R \\ H_R &= R^{-1}H\left(R^{-1}\right)^\dagger \\ S_R &= R^\dagger S R \end{aligned} \tag{7.71}$$

The transformation matrix R is comprised of the eigenvectors of the soft anomalous dimension matrix in order to diagonalize it in the R space.

Eigenspace for $q\bar{q} \to Q\bar{Q}B$ The general eigenvalues of a 2×2 matrix are:

$$\lambda_{1,2} = \frac{1}{2}\left[\Gamma_{11} + \Gamma_{22} \pm \sqrt{(\Gamma_{11} - \Gamma_{22})^2 + 4\Gamma_{12}\Gamma_{21}}\right] \tag{7.72}$$

these are accompanied by the eigenvectors:

$$v_i = \begin{pmatrix} \frac{\Gamma_{12}}{\lambda_i - \Gamma_{11}} \\ 1 \end{pmatrix}$$

From this we can conclude what R and R^{-1} are:

$$R = \begin{pmatrix} \frac{\Gamma_{12}}{\lambda_1 - \Gamma_{11}} & \frac{\Gamma_{12}}{\lambda_2 - \Gamma_{11}} \\ 1 & 1 \end{pmatrix} \tag{7.73}$$

$$R^{-1} = \frac{(\lambda_1 - \Gamma_{11})(\lambda_2 - \Gamma_{11})}{\Gamma_{12}(\lambda_2 - \lambda_1)} \begin{pmatrix} 1 & -\frac{\Gamma_{12}}{\lambda_2 - \Gamma_{11}} \\ -1 & \frac{\Gamma_{12}}{\lambda_1 - \Gamma_{11}} \end{pmatrix} \tag{7.74}$$

This allows us to calculate all the necessary matrices in the R space.

Eigenspace for $gg \to Q\bar{Q}B$ When writing the soft anomalous dimension matrix of $gg \to Q\bar{Q}X$ as

$$\Gamma^{(1)}_{gg \to Q\bar{Q}B} = \begin{pmatrix} \Gamma_{11} & 0 & \frac{\Gamma_{31}}{2} \\ 0 & \Gamma_{22} & \frac{N_C}{4}\Gamma_{31} \\ \Gamma_{31} & \frac{N_C^2 - 4}{4N_C}\Gamma_{31} & \Gamma_{22} \end{pmatrix} \tag{7.75}$$

its eigenvalues can be written as:

$$\lambda_1 = \frac{1}{3}\left[X^{1/3} - Y + \Gamma_{11} + 2\Gamma_{22} \right] \tag{7.76}$$

$$\lambda_{2,3} = \frac{1}{3}\left[-\frac{1}{2}\left(X^{1/3} - Y \right) + \Gamma_{11} + 2\Gamma_{22} \pm \frac{1}{2}i\sqrt{3}\left(X^{1/3} + Y \right) \right] \tag{7.77}$$

with

$$X = (\Gamma_{11} - \Gamma_{22})^3 - \frac{9}{16}\left(N_c^2 - 8 \right)\Gamma_{31}^2 (\Gamma_{11} - \Gamma_{22})$$

$$+ \frac{3\sqrt{3}}{4}\left[-\frac{(N_C^2 + 4)^3}{256}\Gamma_{31}^6 - (N_C^2 - 4)\Gamma_{31}^2 (\Gamma_{11} - \Gamma_{22})^4 \right.$$

$$\left. \frac{1}{8}\left((N_C^2 - 8)^2 - 12(N_C^2 - 2) \right)\Gamma_{31}^4 (\Gamma_{11} - \Gamma_{22})^2 \right]^{1/2} \tag{7.78}$$

and

$$Y = -\left[(\Gamma_{11} - \Gamma_{22})^2 + \frac{3}{16}\Gamma_{31}(N_C^2 + 4) \right] X^{-1/3}$$

which are accompanied by the eigenvectors:

$$v_i = \begin{pmatrix} \frac{\Gamma_{31}}{2(\lambda_i - \Gamma_{11})} \\ \frac{N_C \Gamma_{31}}{4(\lambda_i - \Gamma_{22})} \\ 1 \end{pmatrix}$$

From this we can conclude what R and R^{-1} are:

$$R = \begin{pmatrix} v_1^1 & v_2^1 & v_3^1 \\ v_1^2 & v_2^2 & v_3^2 \\ 1 & 1 & 1 \end{pmatrix} = \begin{pmatrix} \frac{\Gamma_{31}}{2(\lambda_1 - \Gamma_{11})} & \frac{\Gamma_{31}}{2(\lambda_2 - \Gamma_{11})} & \frac{\Gamma_{31}}{2(\lambda_3 - \Gamma_{11})} \\ \frac{N_C \Gamma_{31}}{4(\lambda_1 - \Gamma_{22})} & \frac{N_C \Gamma_{31}}{4(\lambda_2 - \Gamma_{22})} & \frac{N_C \Gamma_{31}}{4(\lambda_3 - \Gamma_{22})} \\ 1 & 1 & 1 \end{pmatrix} \tag{7.79}$$

$$R^{-1} = D^{-1}\begin{pmatrix} v_2^2 - v_3^2 & v_3^1 - v_2^1 & v_2^1 v_3^2 - v_3^1 v_2^2 \\ v_3^2 - v_1^2 & v_1^1 - v_3^1 & v_1^2 v_3^1 - v_1^1 v_3^2 \\ v_1^2 - v_2^2 & v_2^1 - v_1^1 & v_1^1 v_2^2 - v_1^2 v_2^1 \end{pmatrix} \tag{7.80}$$

with

$$D = \left(v_1^1 - v_3^1\right) v_2^2 - \left(v_1^1 - v_2^1\right) v_3^2 - \left(v_2^1 - v_3^1\right) v_1^2 \tag{7.81}$$

This allows us to calculate all the necessary matrices in the R space.

7.4 Absolute threshold resummation

In order to perform the absolute threshold resummation the soft anomalous dimension matrix will need to be approximated in the absolute threshold limit this will be presented in Section 7.4.1. In addition the inclusion of the matching coefficient will be explored in Section 7.4.2. Finally the numerical results will be presented in Section 7.4.3.

7.4.1 Absolute threshold for the soft anomalous dimension

After the absolute threshold approximation is used for the soft anomalous dimension we find using the definition in Equation (4.77):

$$D^{(1)}_{q\bar{q} \to Q\bar{Q}B,I} = \{0, -C_A\} = -C_I \tag{7.82}$$

$$D^{(1)}_{gg \to Q\bar{Q}B,I} = \{0, -C_A, -C_A\} = -C_I \tag{7.83}$$

this is also the same result as for heavy quark production.

7.4.2 Matching coefficient

For a $2 \to 3$ process the phase space is suppressed by β^4 instead of the usual β suppression, therefore contributions away from absolute threshold are more important. We will also include the matching coefficient contributions and look at the size of the difference due to their inclusion. For the computation we will make use of similar techniques to the ones used in Section 5.3, however now additional contributions to the dipole are required for massive colored final state particles. The final equation will not be derived here as this was done for squarks and gluinos in [68]. Instead the general method will be explained and the resulting final formula.

As before in Section 5.3 we will have two contributions, the virtual correction and the real correction through means of the dipole. The virtual contribution is extracted from `PowHeg-Box` [42] and confirmed using `aMC@NLO` [114]. In order to approach threshold numerically the Coulomb contribution is subtracted, as this is the only term that diverges near threshold. In the threshold limit and small s_{34} limit the matrix element is proportional to the LO matrix element. Therefore the cross section can be analyzed without integrating over any phase space variables. The only disadvantage of this method is that we cannot split the virtual contributions up into separate color channels, because the computations in `PowHeg-Box` and `aMC@NLO` are not split into the different color space contributions. The virtual corrections numerically result in:

$$\lim_{\beta \to 0} \left(\frac{\sum_I d\sigma^{fin}_{V,I}}{\sum_I d\sigma_{LO,I}} \right)_{gg} = \frac{\alpha_s}{\pi} \left[3.03 - 3.07 \log\left(\frac{\mu_0^2}{\mu_R^2}\right) - \frac{C_A}{2} \log^2\left(\frac{\mu_0^2}{\mu_R^2}\right) \right] \tag{7.84}$$

$$\lim_{\beta \to 0} \left(\frac{\sum_I d\sigma^{fin}_{V,I}}{\sum_I d\sigma_{LO,I}} \right)_{q\bar{q}} = \frac{\alpha_s}{\pi} \left[-2.92 - 2.18 \log\left(\frac{\mu_0^2}{\mu_R^2}\right) - \frac{C_F}{2} \log^2\left(\frac{\mu_0^2}{\mu_R^2}\right) \right] \tag{7.85}$$

with $d\sigma_{V,I}^{fin}$ the infrared finite part of the virtual correction with the coulomb subtracted:

$$d\sigma_V^{fin}\left(\mu_R^2\right) = d\sigma_V\left(\mu_R^2\right) + \sum_I \frac{\alpha_s \pi}{2\beta_{34}} \kappa_{ij \to klB,I} d\sigma_{LO,I} \tag{7.86}$$

where I indicates the color channel with $\kappa_{ij \to klB,I} = T_k T_l = \left(C_I - C_k - C_l\right)/2$ with C_i is the quadratic Casimir factor of the final state particles of color channel. A NLO cross section can have at most a single logarithm in the scale, therefore squared logarithmic dependence of the scale can be exactly predicted as it needs to cancel against the contributions from the dipole.

For the real emission cross section we need to take into account all integrated dipole contributions and the collinear counter terms. For the exact expressions used, [103] can be consulted. The only expression that does not need to be included is the final state emitter and final state spectator dipole. This dipole contribution if treated exactly vanishes at threshold. A discussion as to why the result in [103] is not exact can be found in [68]. The result of this computation in Mellin space with the logarithms of N and the infrared divergences subtracted is given by:

$$\begin{aligned}
\frac{\alpha_s}{\pi}\mathcal{C}_{ij \to t\bar{t}H}^{(1)} &= \lim_{\beta \to 0} \frac{\sum_I d\sigma_{V,I}^{fin}}{\sum_I d\sigma_{LO,I}} + \frac{\alpha_s}{\pi}\left[\sum_I C_I \left(\gamma_E - \log 2 + 1 + \frac{1}{2}\log\left(4\frac{\mu_R^2}{M^2}\right)\right)\frac{d\sigma_{LO,I}}{\sum_J d\sigma_{LO,J}} \right. \\
&\quad + \sum_{n=\{i,j\}} C_n \left\{\frac{1}{4}\log^2\left(4\frac{\mu_R^2}{M^2}\right) - \log\left(4\frac{\mu_R^2}{M^2}\right)\left(\log 2 - \frac{\gamma_n}{2C_n}\right)\right. \\
&\quad \left.\left. + \left(\gamma_E - \log 2\right)^2 + \frac{\pi^2}{12} - \left(\frac{\gamma_n}{2C_n} - \gamma_E\right)\log\left(4\frac{\mu_F^2}{M^2}\right)\right\}\right]
\end{aligned} \tag{7.87}$$

where the ratio $d\sigma_{LO,I}/\sum_J d\sigma_{LO,J}$ is given by $5/7$ the octet in the gluon initial state channel. Here a factor $(4\pi)^\epsilon/\Gamma\left(1-\epsilon\right)$ has been taken out of the brackets as is done in `PowHeg-Box`. The reason the Mellin space expression is the same regardless of the power β the LO cross section contains is because we can factorize the cross section from the dipole expression in Mellin space:

$$\begin{aligned}
\int_0^1 d\hat{\tau}\,\hat{\tau}^{N-1}\int_{\hat{\tau}}^1 dx\, \sigma_{LO}\left(\frac{\hat{\tau}}{x}\right)f\left(x\right) &= \int_0^1 dx \int_0^x d\hat{\tau}\,\hat{\tau}^{N-1}\sigma_{LO}\left(\frac{\hat{\tau}}{x}\right)f\left(x\right) \\
&= \int_0^1 dx\, x^N f\left(x\right)\int_0^1 dz\, z^{N-1}\sigma_{LO}\left(z\right) \\
&= \tilde{f}\left(N+1\right)\tilde{\sigma}_{LO}\left(N\right)
\end{aligned} \tag{7.88}$$

for any function f, in this case the dipole expression. As a $2 \to 3$ process has multiple combinations of the different mass scales when compared to $2 \to 2$, for example $s_{34} \to 4m_t^2$ and $\hat{s} \to (2m_t + m_H)^2$. However all scale combinations other than M are canceled.

The correct single logarithmic scale dependence of the matching coefficient can also be found through means of the renormalization. The renormalization scale dependence matches this dependence exactly and the factorization scale dependence agrees in the absolute threshold limit.

Finally, as was done for squarks and gluinos, we add the Coulomb separately. However, we will add the Coulomb in β-space and not in Mellin space. The Mellin transform is then performed numerically. This results in a total matching coefficient:

$$C_{ij \to t\bar{t}H} = 1 + \frac{\alpha_s}{\pi}\mathcal{C}_{ij \to t\bar{t}H}^{(1)} + \frac{\alpha_s}{\pi}\mathcal{C}_{ij \to t\bar{t}H}^{Coul,(1)}\left(s_{34}\right) \tag{7.89}$$
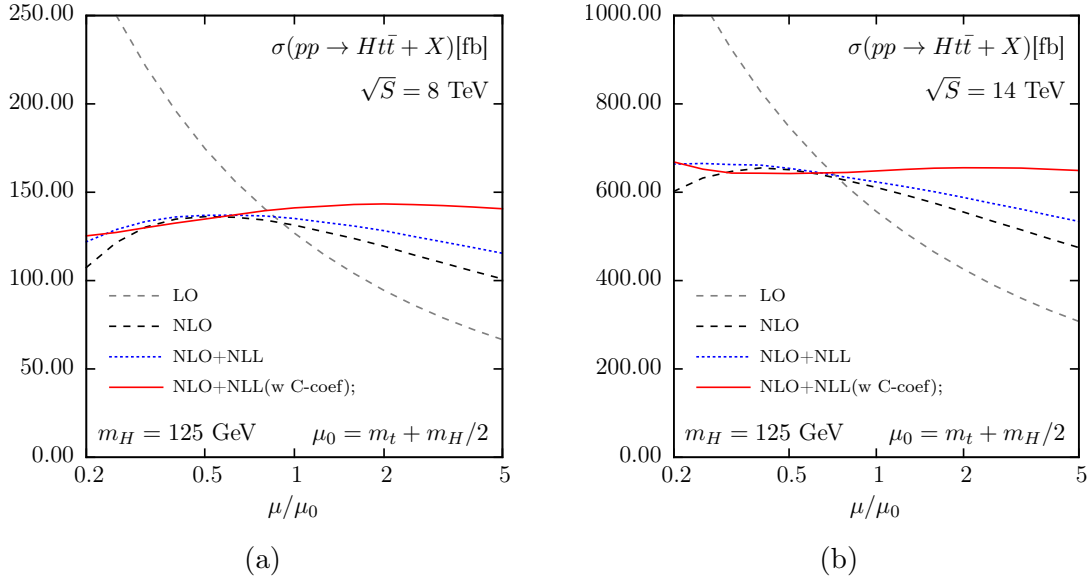
Figure 7.4: The scale dependence of the LO, NLO and NLO+NLL cross sections at $\sqrt{S} = 8$ TeV (a) and $\sqrt{S} = 14$ TeV (b) collision energies for the LHC. The results are obtained by simultaneously varying μ_F and μ_R.

with the Coulomb contribution

$$\mathcal{C}^{Coul,(1)}_{ij \to t\bar{t}H} = -\frac{\pi^2}{2} \frac{1}{\beta_{34}} \kappa_{ij \to klB,I} \tag{7.90}$$

7.4.3 Numerical results

Now that all of the different components for the absolute threshold resummation have been computed, the numerical results can be presented. The results presented here are also published in [115]. In the phenomenological analysis we use $m_t = 173$ GeV, $m_H = 125$ GeV and choose the central scale $\mu_0 = m_t + m_H/2$ as was used for [14]. The NLO cross section is computed using the aMC@NLO code [114]. The Mellin transform of the LO and the matching coefficient is done numerically. The analysis is performed using the MMHT2014 PDF [116] and the corresponding value of α_s. The results are presented using a matching coefficient including one loop effects, $C^{(1)}_{ij \to t\bar{t}H}$, and without , $C_{ij \to t\bar{t}H} = 1$.

The numerical study will be started by analyzing the scale dependence of the total cross section for $pp \to t\bar{t}H$ while simultaneously varying renormalization and factorization scale, μ_R and μ_F. These results for the center of mass energy $\sqrt{S} = 8$ TeV and $\sqrt{S} = 14$ TeV are presented in Figure 7.4 (a) and (b) respectively. Here it can be seen that the resummation corrections, NLO+NLL, stabilize the dependence on the scale $\mu = \mu_R = \mu_F$ with respect to the NLO result. At $\sqrt{S} = 8$ TeV the central value and scale uncertainty changes from $132^{+3.9\%}_{-9.3\%}$ at NLO to $141^{+1.4\%}_{-4.2\%}$ at NLO+NLL (with the $C^{(1)}_{ij \to t\bar{t}H}$ coefficient included), where the scale uncertainty is determined by varying the scales simultaneously between $\mu_0/2 \leq \mu \leq 2\mu_0$. Correspondingly the results are $613^{+6.2\%}_{-9.4\%}$ and $650^{+0.8\%}_{-1.2\%}$ for $\sqrt{S} = 14$ TeV. It can be seen that the matching coefficient have a significant impact, especially in the high scale region.

In order to explore the scale dependence in more detail we analyze the separate renormalization and factorization scale dependence. These results are presented in Figure 7.5. Here it can be
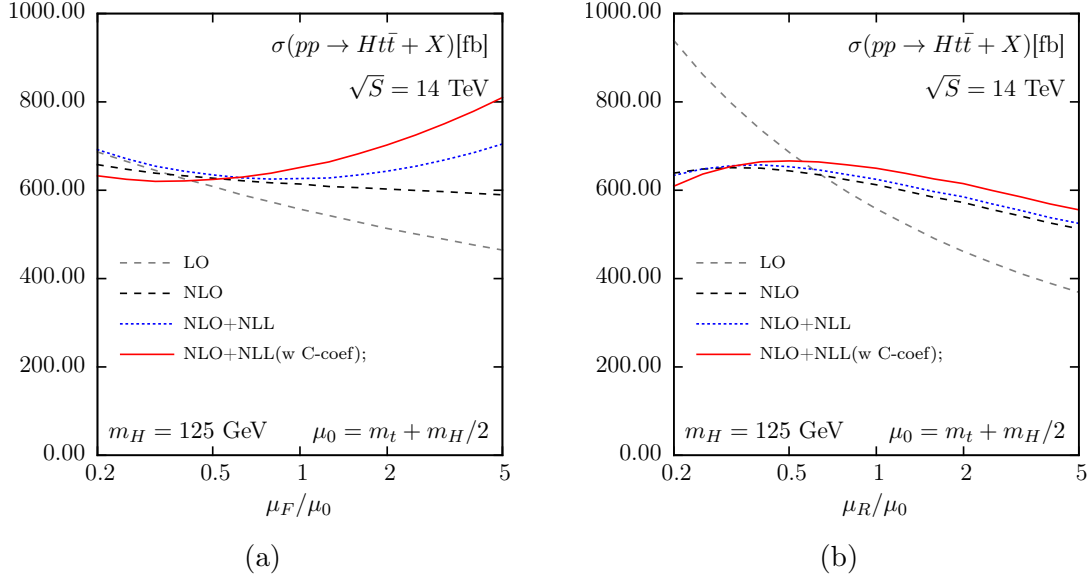
Figure 7.5: The factorization (a) and renormalization (b) scale dependence of the LO, NLO and NLO+NLL cross sections at $\sqrt{S} = 14$ TeV collision energy for the LHC where the other is fixed to μ_0.

seen that the small scale dependence for the simultaneous variation of the scales is a result of the cancellation between the factorization and renormalization scale dependence. A similar effect has previously been shown for the total cross section for Higgs production through gluon fusion [91]. The renormalization scale dependence can be explained by the usual dependence of α_s. For the factorization scale dependence it can be seen in Figure 7.5 (a) that the dependence for NLO+NLL around the central value is relatively small. The strong dependence of NLO+NLL with non-zero $C^{(1)}_{ij \to t\bar{t}H}$ coefficient included can be understood. The resummed expression takes into account cross terms between the matching coefficient and the higher order logarithms in N from the exponential. These effects are not taken into account in the running of the PDF. It is expected that this scale dependence will be significantly modified when the NNLO correction are known.

Due to the cancellation of the scales, we choose to estimate the scale uncertainty for the independent variation of the factorization and renormalization scale through means of the 7-point method. The 7-point method obtains the minimum and maximum values through means of seven combination of factorization and renormalization scale:

$$(\mu_R/\mu_0, \mu_F/\mu_0) = \{(0.5, 0.5), (0.5, 1), (1, 0.5), (1, 1), (1, 2), (2, 1), (2, 2)\} \tag{7.91}$$

. These results are presented in Table 7.1 for the LHC collision energies of 8, 13 and 14 TeV. The NLO+NLL predictions show a significant reduction in the scale uncertainty when compared to the NLO results. The positive and negative uncertainties are reduced by around 20% and 30% respectively for 13 and 14 TeV and by around 25% and 35% for 8 TeV. When the matching coefficient is included the lower uncertainty reduces further, however the upper bound instead increases. This increase can directly be traced back to the increased factorization scale dependence of the resummed predictions with matching coefficient included. However the total uncertainty is still reduced by around 7% for 8 TeV and 10% and 12% for 13 and 14 TeV with respect to the NLO uncertainties. However the scale uncertainties are still larger than the parton distribution uncertainty listed in Table 7.1. The parton distribution uncertainty is computed for the NLO predictions as the resummation only minimally influences the value of the parton distribution uncertainty.

$\sqrt{S}$ [TeV]	NLO [fb]	NLO+NLL		NLO+NLL with C		PDF uncertainty
		Value [fb]	K-factor	value [fb]	K-factor	
8	$132^{+3.9\%}_{-9.3\%}$	$135^{+3.0\%}_{-5.9\%}$	1.03	$141^{+7.7\%}_{-4.6\%}$	1.07	$^{+3.0\%}_{-2.7\%}$
13	$506^{+5.9\%}_{-9.4\%}$	$516^{+4.6\%}_{-6.5\%}$	1.02	$537^{+8.2\%}_{-5.5\%}$	1.06	$^{+2.3\%}_{-2.3\%}$
14	$613^{+6.2\%}_{-9.4\%}$	$625^{+4.6\%}_{-6.7\%}$	1.02	$650^{+7.9\%}_{-5.7\%}$	1.06	$^{+2.3\%}_{-2.2\%}$

Table 7.1: NLO and NLO+NLL total cross sections for $pp \rightarrow t\bar{t}H$ for various LHC collision energies. The uncertainty ranges given together with the NLO and NLO+NLL results indicate the scale variation from the variation of the renormalization and factorization scale independently for $\mu_0/2 \leq \mu_{R,F} \leq 2\mu_0$.

The large phase-space suppression near absolute threshold for the $2 \rightarrow 3$ results only in moderate increases of the cross section due to resummation. For NLO+NLL this results in a $2-3\%$ increase with respect to NLO. When the matching coefficient is included this results in a $6-7\%$ increase. This indicates that terms proportional to the born cross section with no additional threshold suppression or enhancement are important for this computation. Finally a check has been done in order to estimate the effect of the separation of the hard matching coefficient into separate color channels. In order to perform this check the central scale value of the averaged hard matching coefficient, $\mathcal{C}^{(1)}_{gg \rightarrow t\bar{t}H}$, is rescaled by $\mathcal{C}^{(1)}_{gg \rightarrow t\bar{t},I}/\mathcal{C}^{(1)}_{gg \rightarrow t\bar{t}}$ taken from [117]. This procedure is motivated by the similarity in the color structure between $pp \rightarrow t\bar{t}$ and $pp \rightarrow t\bar{t}H$. The rescaling procedure results in a per mille level difference at 14 TeV in the total cross section, and a 5% level effect on the correction. Therefore we do not expect the exact knowledge of the separated hard matching coefficients $\mathcal{C}^{(1)}_{gg \rightarrow t\bar{t}H,\mathbf{1}}$ and $\mathcal{C}^{(1)}_{gg \rightarrow t\bar{t}H,\mathbf{8}}$ to have a significant effect on the NLO+NLL predictions.

7.5 Threshold variables for resummation

In order to describe the differential notation we will use three different kinematic variables, which were chosen to describe the distance to threshold. These can serve as the weights of the resummation as described in Section 4.2. This will require relations between the hadronic and partonic weight variables in the soft and collinear limits for the emission.

7.5.1 Triplet-invariant mass (TIM) kinematics (z_5)

We will describe the threshold limit for the TIM kinematics by means of the variable z_5:

$$z_5 = \frac{\hat{s} - s_{345}}{\hat{s}} \tag{7.92}$$

The relevant kinematic variable for the TIM kinematics is s_{345}, the additional 4 kinematic variables can be chosen freely. The TIM kinematics can be used to describe cross section differential with respect to the invariant mass of the three final state particles, Q^2_{345}.

Next we can look at the relation between the hadronic threshold variable and the partonic,

neglecting terms of order Z_5^2:

$$
\begin{aligned}
Z_5 S &= S - Q_{345}^2 = (p_A + p_B)^2 - (x_1 p_A + x_2 p_B - k)^2 \\
&= (1 - x_1 x_2) S + 2 (p_1 + p_2) \cdot k - k^2 \\
&\approx (1 - x_1) S + (1 - x_2) S + z_5 \hat{s}
\end{aligned}
\tag{7.93}
$$

the approximation is near x_1 and x_2 are 1 and k is soft.

7.5.2 One-particle inclusive (1PI) kinematics (v_5)

The 1PI kinematics will be described by means of the threshold variable v_5:

$$
v_5 = \frac{(p_1 + p_2 - p_5)^2 - s_{34}}{\hat{s}} = \frac{\hat{s} + \tilde{t}_{15} + \tilde{t}_{25} + m_5^2 - s_{34}}{\hat{s}}
\tag{7.94}
$$

The relevant kinematic variables for the 1PI kinematics are $\tilde{t}_{15}$, $\tilde{t}_{25}$ and s_{34}. The final two kinematic variables can be chosen freely. The 1PI kinematics can be used to describe the cross section differential with respect to the momenta of one particle, in this case the fifth particle. The momentum can be described at the and of $\tilde{t}_{15}$ and $\tilde{t}_{25}$ or the transverse momentum $p_{T,5}$ and the rapidity y_5.

The relation between the hadronic threshold variable and the partonic is in this case described by:

$$
\begin{aligned}
V_5 S &= (p_A + p_B - p_5)^2 - Q_{34}^2 = (p_A + p_B - p_5)^2 - (x_1 p_A + x_2 p_B - p_5 - k)^2 \\
&= (1 - x_1 x_2) S - (1 - x_1) 2 p_A \cdot p_5 - (1 - x_2) 2 p_B \cdot p_5 + 2 (p_1 + p_2 - p_5) \cdot k - k^2 \\
&\approx (1 - x_1) \left(S + \tilde{T}_{A5} \right) + (1 - x_2) \left(S + \tilde{T}_{B5} \right) + v_5 \hat{s} \\
&\approx \left[(1 - x_1) \left(1 + \frac{\tilde{t}_{15}}{\hat{s}} \right) + (1 - x_2) \left(1 + \frac{\tilde{t}_{25}}{\hat{s}} \right) + v_5 \right] S \\
&\approx \left[(1 - x_1) \left(\frac{s_{34} - \tilde{t}_{25} - m_5^2}{s_{34} - \tilde{t}_{15} - \tilde{t}_{25} - m_5^2} \right) + (1 - x_2) \left(\frac{s_{34} - \tilde{t}_{15} - m_5^2}{s_{34} - \tilde{t}_{15} - \tilde{t}_{25} - m_5^2} \right) + v_5 \right] S
\end{aligned}
\tag{7.95}
$$

Note, the factors in front of $1 - x_i$ can also be described at the partonic level instead as the difference is a lower order in $1 - x_i$. In the final step we eliminate $\hat{s}$.

7.5.3 Two-particle inclusive (2PI) kinematics (s_5)

The 2PI kinematics will be described by means of the threshold variable s_5:

$$
s_5 = \frac{(p_1 + p_2 - p_3 - p_4)^2 - m_5^2}{\hat{s}} = \frac{\hat{s} + \tilde{t}_{1,34} + \tilde{t}_{2,34} + s_{34} - m_5^2}{\hat{s}}
\tag{7.96}
$$

The relevant kinematic variables for the 1PI kinematics are $\tilde{t}_{1,34}$, $\tilde{t}_{2,34}$ and s_{34}. The 2PI kinematics can be used to describe the cross section in terms of the momenta of the intermediate state that is a combination of two particles, in this case 34. This momentum can be described on the basis of the invariants $\tilde{t}_{1,34}$, $\tilde{t}_{2,34}$ and s_{34} or alternatively $p_{T,34}$, y_{34} and s_{34}.

weight	partonic invariants	hadronic invariants	process example
z_5	s_{345}	Q^2_{345}	$pp \to t\bar{t}H + X$
v_5	$\tilde{t}_{15}, \tilde{t}_{25}$ and s_{34}	$\tilde{T}_{A5}, \tilde{T}_{B5}$ and Q^2_{34}	$pp \to H + X\,[t\bar{t}]$
s_5	$\tilde{t}_{13}, \tilde{t}_{14}, \tilde{t}_{23}, \tilde{t}_{24}$ and s_{34}	$\tilde{T}_{A3}, \tilde{T}_{A4}, \tilde{T}_{B3}, \tilde{T}_{B4}$ and Q^2_{34}	$pp \to t\bar{t} + X\,[H]$

Table 7.2: An overview of the different kinematic schemes

The relation between the hadronic threshold variable and the partonic is in this case described by:

$$
\begin{aligned}
S_5 S &= (p_A + p_B - p_3 - p_4)^2 - p_5^2 = (p_A + p_B - p_3 - p_4)^2 - (x_1 p_A + x_2 p_B - p_3 - p_4 - k)^2 \\
&= (1 - x_1 x_2)\,S - (1 - x_1)\,2 p_A \cdot (p_3 + p_4) \\
&\quad - (1 - x_2)\,2 p_B \cdot (p_3 + p_4) + 2\,(p_1 + p_2 - p_3 - p_4) \cdot k - k^2 \\
&\approx (1 - x_1)\left(S + \tilde{T}_{A,34}\right) + (1 - x_2)\left(S + \tilde{T}_{B,34}\right) + s_5 \hat{s} \\
&\approx \left[(1 - x_1)\left(\frac{\hat{s} + \tilde{t}_{1,34}}{\hat{s}}\right) + (1 - x_2)\left(\frac{\hat{s} + \tilde{t}_{2,34}}{\hat{s}}\right) + s_5\right] S \qquad (7.97) \\
&\approx \left[(1 - x_1)\left(\frac{\tilde{t}_{2,34} + s_{34} - m_5^2}{\tilde{t}_{1,34} + \tilde{t}_{2,34} + s_{34} - m_5^2}\right) + (1 - x_2)\left(\frac{\tilde{t}_{1,34} + s_{34} - m_5^2}{\tilde{t}_{1,34} + \tilde{t}_{2,34} + s_{34} - m_5^2}\right) + s_5\right] S
\end{aligned}
$$

7.5.4 Overview kinematics

This method allows us to use 5 kinematic variables and in addition the threshold variable in the hard function. The variable $\hat{s}$ will be replaced in this case through the definition of the threshold variable. The final relation between the hadronic and partonic threshold variables will be defined as:

$$
\begin{aligned}
W &= (1 - x_1)\,c_1 + (1 - x_2)\,c_2 + \omega & (7.98) \\
&= \omega_1 c_1 + \omega_2 c_2 + \omega_s & (7.99)
\end{aligned}
$$

with W the hadronic weight and ω the partonic weight.

In Table 7.2 an overview is given of all the kinematic schemes and their variables.

7.5.5 Alternative understanding of the connection between the weights

An alternative way to better understand the connection between the different weights can be done by looking at different infrared limits. All different definitions of the weights approach zero in the soft limit, however for the collinear limit the way they approach zero is different.

Relation between z_5 and v_5 in collinear limits   In order to find the relation between z_5 and v_5 in the collinear limit we will write the momentum of the emitted gluon as:

$$
k = \begin{cases} \nu_1 p_1 & \text{Colinear to } p_1 \\ \nu_2 p_2 & \text{Colinear to } p_2 \end{cases} \qquad (7.100)
$$

This is allows us to rewrite z_5:

$$
\begin{aligned}
z_5 &= \frac{\hat{s} - (p_3 + p_4 + p_5)^2}{\hat{s}} = \frac{(p_1 + p_2)^2 - (p_1 + p_2 - k)^2}{\hat{s}} = \frac{2(p_1 + p_2) \cdot k + k^2}{\hat{s}} \\
&= \frac{2\nu_i (p_1 + p_2) \cdot p_i}{\hat{s}} = \nu_i
\end{aligned} \tag{7.101}
$$

Next we need to rewrite v_5 in the same manner:

$$
\begin{aligned}
v_5 &= \frac{(p_1 + p_2 - p_5)^2 - (p_3 + p_4)^2}{\hat{s}} = \frac{(p_1 + p_2 - p_5)^2 - (p_1 + p_2 - p_5 - k)^2}{\hat{s}} \\
&= \frac{2(p_1 + p_2 - p_5) \cdot k + k^2}{\hat{s}} = \nu_i \frac{2(p_1 + p_2 - p_5) \cdot p_i}{\hat{s}} = \begin{cases} z_5 \frac{\hat{s} + \tilde{t}_{15}}{\hat{s}} & i = 1 \\ z_5 \frac{\hat{s} + \tilde{t}_{25}}{\hat{s}} & i = 2 \end{cases}
\end{aligned} \tag{7.102}
$$

This gives us the final result

$$
\omega_{v_5} = \omega_1 \frac{\hat{s} + \tilde{t}_{15}}{\hat{s}} + \omega_2 \frac{\hat{s} + \tilde{t}_{25}}{\hat{s}} + \omega_s \tag{7.103}
$$

if

$$
\omega_{z_5} = \omega_1 + \omega_2 + \omega_s \tag{7.104}
$$

Relation between z_5 and s_5 in collinear limits   The same steps can be followed for s_5:

$$
\begin{aligned}
s_5 &= \frac{(p_1 + p_2 - p_3 - p_4)^2 - m_5^2}{\hat{s}} = \frac{(p_5 + k)^2 - M^2}{\hat{s}} = \frac{2p_5 \cdot k + k^2}{\hat{s}} \\
&= \nu_i \frac{2p_5 \cdot p_i}{\hat{s}} = \nu_i \frac{2(p_1 + p_2 - p_3 - p_4) \cdot p_i}{\hat{s}} = \begin{cases} z_5 \frac{\hat{s} + \tilde{t}_{1,34}}{\hat{s}} & i = 1 \\ z_5 \frac{\hat{s} + \tilde{t}_{2,34}}{\hat{s}} & i = 2 \end{cases}
\end{aligned} \tag{7.105}
$$

This gives us the final weights

$$
\omega_{s_5} = \omega_1 \frac{\hat{s} + \tilde{t}_{1,34}}{\hat{s}} + \omega_2 \frac{\hat{s} + \tilde{t}_{2,34}}{\hat{s}} + \omega_s \tag{7.106}
$$

7.6 Differential distributions

If Equation (4.66) is combined with the definitions of the weights the final resummation results in:

$$
\frac{d\sigma_{h_1 h_2 \to c+X}}{d\Pi_3} = \sum_{i,j} \int_{x_1^-}^1 dx_1 \int_{x_2^-}^1 dx_2 \, f_{i/h_1}\left(x_1, \mu^2\right) f_{j/h_2}\left(x_2, \mu^2\right) \int \frac{dN}{2\pi i} e^{N\omega} \tilde{\omega}_{ij \to c+X}\left(N, \hat{\Pi}_3\right) \tag{7.107}
$$

with $\omega = \left(x_1 x_2 S - s\left(\hat{\Pi}_3\right)\right)/(x_1 x_2 S)$ the weight and s a function of the partonic kinematics that depends on the choice of the weight and is equal to $\hat{s}$ in the threshold limit. The resummed partonic cross section is defined as:

$$
\begin{aligned}
\tilde{\omega}_{ij \to klB+X}\left(N, \hat{\Pi}_3\right) &= \text{Tr}\left\{ H\left(\hat{\Pi}_3\right) \bar{\text{P}} \exp\left[\int_\mu^{s/N} \frac{dq}{q} \Gamma_{ij \to kl}^\dagger\left(\alpha_s\left(q^2\right)\right)\right] S \right. \\
&\qquad \left. \times \text{P} \exp\left[\int_\mu^{s/N} \frac{dq}{q} \Gamma_{ij \to kl}\left(\alpha_s\left(q^2\right)\right)\right]\right\} \bar{\Delta}_i\left(c_1 N\right) \bar{\Delta}_j\left(c_2 N\right)
\end{aligned} \tag{7.108}
$$

H is the hard matrix in color space and is dependent on the choice of kinematics through the Jacobian, this is given at LO by:

$$H_{IJ} = \frac{1}{s}\frac{1}{2s}\frac{1}{(2\pi)^5}J\left(\hat{\Pi}_3\right)c_{ij}M_{IJ} \tag{7.109}$$

with c_{ij} encompassing the couplings and averaging over color and spin of the initial state and M_{IJ} the squared matrix element in the color basis. The Jacobian is given by $J\left(\hat{\Pi}_3\right)$. Here the soft anomalous dimension needs to be fully taken into account and we cannot move the pure initial state contribution to the collinear contributions.

$$\begin{aligned}\Gamma^{(1)}_{ij\to kl,IJ} &= \bar{\Gamma}^{(1)}_{ij\to kl,IJ} + \frac{\alpha_s}{2\pi}\sum_{p=\{i,j\}}C_p\left(1-\log\left(2\frac{(v_i\cdot n)^2}{|n|^2}\right)-i\pi\right)\delta_{IJ}\\ &= \bar{\Gamma}^{(1)}_{ij\to kl,IJ} + \frac{\alpha_s}{2\pi}\sum_{p=\{i,j\}}C_p\left(1-i\pi\right)\delta_{IJ}\end{aligned}$$

therefore $\bar{\Delta}_i$ is the initial state collinear emission with the purely soft contribution removed

$$\begin{aligned}\bar{\Delta}_i\left(N\right) &= \Delta_i\left(N\right)\exp\left[-\frac{C_i}{\pi}\int_\mu^{s/N}\frac{dq}{q}\alpha_s\left(q^2\right)\right]\\ &= \Delta_i\left(N\right)\exp\left[-h_2\left(b_0\alpha_s\log N\right)|_{D^{(1)}_{q\bar{q}\to Q\bar{Q}B,I}\to C_i}\right] \tag{7.110}\end{aligned}$$

at NLL order. Where we have chosen the gauge vector $n = p_1 + p_2$. If the soft anomalous dimension matrix is now diagonalized the result becomes:

$$\begin{aligned}\tilde{\omega}_{ij\to klB+X}\left(N,\hat{\Pi}_3\right) &= \left\{H^R_{IJ}\left(\hat{\Pi}_3\right)\exp\left[\int_\mu^{s/N}\frac{dq}{q}\lambda^*_{ij\to klB,J}\left(\alpha_s\left(q^2\right)\right)\right]S^R_{JI}\right.\\ &\quad\left.\times\exp\left[\int_\mu^{s/N}\frac{dq}{q}\lambda_{ij\to klB,I}\left(\alpha_s\left(q^2\right)\right)\right]\right\}\bar{\Delta}_i\left(c_1N\right)\bar{\Delta}_j\left(c_2N\right) \tag{7.111}\end{aligned}$$

with $\lambda_{ij\to kl,I}$ the eigenvalues of the soft anomalous dimension matrix.

We can use the Mellin transform instead resulting in

$$\begin{aligned}\frac{d\sigma_{h_1h_2\to klB+X}}{d\Pi_3} &= \sum_{i,j}\int_{x_1^-}^1 dx_1\int_{x_2^-}^1 dx_2\, f_{i/h_1}\left(x_1,\mu^2\right)f_{j/h_2}\left(x_2,\mu^2\right)\\ &\quad\int\frac{dN}{2\pi i}\left(\frac{s}{x_1x_2S}\right)^{-N}\omega_{ij\to klB+X}\left(N+1,\hat{\Pi}_3\right) \tag{7.112}\end{aligned}$$

7.6.1 Integration limits and Jacobian

Finally the integration limits of the different kinematic variables and the Jacobian need to be determined. These need to be computed for every choice of weight individually.

Triplet-invariant mass (TIM) kinematics (z_5)   As we have a free choice for four kinematic variables, we will choose the same variables as in [37]: Q_{34}^2, the polar angle of the fifth particle in the initial state center-of-mass frame (θ_5^{CM}) and the solid angle of the third particle in the rest frame of particles 3, 4 using the direction of flight of particles 3, 4 in the initial state center-of-mass frame as the z-axis, Ω_3^*. This choice of kinematics results in the Jacobian:

$$J\left(\hat{\Pi}_3\right) = \frac{\lambda^{1/2}\left(s_{34}, m_3^2, m_4^2\right)}{8s_{34}} \frac{\lambda^{1/2}\left(\hat{s}, s_{34}, m_5^2\right)}{8\hat{s}} 2\pi \sin\left(\theta_5^{CM}\right) \sin\left(\theta_3^*\right) \tag{7.113}$$

with $\lambda\left(x, y, z\right) = \left(x - y - z\right)^2 - 4yz$.

The limits on the kinematic variables are computed by means of:

$$x_1 x_2 S - Q_{345}^2 \geq 0 \tag{7.114}$$

This results in the limit for x_2

$$x_2^- = \frac{Q_{345}^2}{x_1 S} \tag{7.115}$$

and for x_1

$$x_1^- = \frac{Q_{345}^2}{S} \tag{7.116}$$

The limits for Q_{345}^2 are given by:

$$\left(m_3 + m_4 + m_5\right)^2 \leq Q_{345}^2 \leq S \tag{7.117}$$

Finally the limits of Q_{34}^2 are given by

$$\left(m_3 + m_4\right)^2 \leq Q_{34}^2 \leq \left(\sqrt{Q_{345}^2} - m_5\right)^2 \tag{7.118}$$

The limits for the angles are given by $\theta_5^{CM} \in [0, \pi]$, $\theta_3^* \in [0, \pi]$ and $\phi_3^* \in [0, 2\pi]$.

What can be seen is that the two particle variant of the TIM kinematics (Pair Invariant Mass (PIM) kinematics) is the same as the Q-approach presented in Chapter 5.

One-particle inclusive (1PI) kinematics (v_5)   For the free choice of kinematic variables, we will use the same variables as for TIM kinematics. The difference is that we replace Q_{345}^2 and θ_5^{CM} by the necessary kinematic variables $\tilde{T}_{A5}$ and $\tilde{T}_{B5}$. This choice results in the Jacobian:

$$J\left(\hat{\Pi}_3\right) = \frac{\lambda^{1/2}\left(s_{34}, m_3^2, m_4^2\right)}{8s_{34}} \frac{\pi}{2\hat{s}} \sin\left(\theta_3^*\right) x_1 x_2 \tag{7.119}$$

The kinematic limits are found on the basis of the definition of the weight:

$$x_1 x_2 S + x_1 \tilde{T}_{A5} + x_2 \tilde{T}_{B5} + m_5^2 - Q_{34}^2 \geq 0 \tag{7.120}$$

This results in the limits for x_1 and x_2:

$$x_2^- = \frac{Q_{34}^2 - x_1 \tilde{T}_{A5} - m_5^2}{x_1 S + \tilde{T}_{B5}} \tag{7.121}$$

and

$$x_1^- = \frac{Q_{34}^2 - \tilde{T}_{B5} - m_5^2}{S + \tilde{T}_{A5}} \tag{7.122}$$

The denominators of these limits are always positive as, for example:

$$x_2\left(x_1 S + \tilde{T}_{B5}\right) = 2p_2 \cdot (p_1 - p_5) = 2p_2 \cdot (p_3 + p_4 + k - p_2)$$

$$= 2p_2 \cdot (p_3 + p_4 + k) \geq 0 \tag{7.123}$$

For limits of the hadronic Lorentz invariant variables we will use:

$$S + \tilde{T}_{A5} + \tilde{T}_{B5} + m_5^2 - Q_{34}^2 \geq 0 \tag{7.124}$$

$$\Delta_{3,h}\left(p_A, p_B, p_5\right) \geq 0 \tag{7.125}$$

with

$$\Delta_{3,h}\left(p_A, p_B, p_5\right) = \mathrm{Det}\left[\frac{1}{8}\begin{pmatrix} 0 & S & -\tilde{T}_{A5} \\ S & 0 & -\tilde{T}_{B5} \\ -\tilde{T}_{A5} & -\tilde{T}_{B5} & 2m_5^2 \end{pmatrix}\right]$$

$$= \frac{1}{4}\left(\tilde{T}_{A5}\tilde{T}_{B5} - Sm_5^2\right) \tag{7.126}$$

This results in the limits:

$$Q_{34}^2 - S - \tilde{T}_{B5} - m_5^2 \leq \tilde{T}_{A5} \leq \frac{Sm_5^2}{\tilde{T}_{B5}} \tag{7.127}$$

and

$$\tilde{T}_{B5}^- \leq \tilde{T}_{B5} \leq \tilde{T}_{B5}^+ \tag{7.128}$$

with

$$\tilde{T}_{B5}^{\pm} = \frac{1}{2}\left(Q_{34}^2 - m_5^2 - S \pm \lambda^{1/2}\left(S, Q_{34}^2, m_5^2\right)\right) \tag{7.129}$$

Finally the limits for Q_{34}^2 are given by

$$(m_3 + m_4)^2 \leq Q_{34}^2 \leq \left(\sqrt{S} - m_5\right)^2 \tag{7.130}$$

Two-particle inclusive (2PI) kinematics (s_5)   As the 2PI kinematics are used to describe the kinematics of the $t\bar{t}$-pair we can consider a different set of kinematics more similar to the 1PI kinematics. For this alternative choice we will use $\tilde{T}_{A,34}$ and $\tilde{T}_{B,34}$, where 34 indicates the combined momenta of particles 3 and 4. For the free choice of kinematic variables, we will use the same variables as for 1PI kinematics. This choice results in the same Jacobian:

$$J\left(\hat{\Pi}_3\right) = \frac{\lambda^{1/2}\left(s_{34}, m_3^2, m_4^2\right)}{8s_{34}}\frac{\pi}{2\hat{s}}\sin\left(\theta_3^*\right)x_1 x_2 \tag{7.131}$$

The kinematic limits are found on the basis of the definition of the weight:

$$x_1 x_2 S + x_1 \tilde{T}_{A,34} + x_2 \tilde{T}_{B,34} + Q_{34}^2 - m_5^2 \geq 0 \tag{7.132}$$

This results in the limits for x_1 and x_2:

$$x_2^- = \frac{m_5^2 - x_1 \tilde{T}_{A,34} - Q_{34}^2}{x_1 S + \tilde{T}_{B5}} \tag{7.133}$$

and

$$x_1^- = \frac{m_5^2 - \tilde{T}_{B,34} - Q_{34}^2}{S + \tilde{T}_{A,34}} \tag{7.134}$$

For limits of the hadronic Lorentz invariant variables we will use:

$$S + \tilde{T}_{A,34} + \tilde{T}_{B,34} + Q_{34}^2 - m_5^2 \geq 0 \tag{7.135}$$

$$\Delta_{3,h}(p_A, p_B, p_5) \geq 0 \tag{7.136}$$

with

$$\Delta_{3,h}(p_A, p_B, p_5) = \mathrm{Det}\left[\frac{1}{8}\begin{pmatrix} 0 & S & -\tilde{T}_{A,34} \\ S & 0 & -\tilde{T}_{B,34} \\ -\tilde{T}_{A,34} & -\tilde{T}_{B,34} & 2m_5^2 \end{pmatrix}\right]$$

$$= \frac{1}{4}\left(\tilde{T}_{A,34}\tilde{T}_{B,34} - Sm_5^2\right) \tag{7.137}$$

This results in the limits:

$$m_5^2 - S - \tilde{T}_{B,34} - Q_{34}^2 \leq \tilde{T}_{A,34} \leq \frac{Sm_5^2}{\tilde{T}_{B,34}} \tag{7.138}$$

and

$$\tilde{T}_{B5}^- \leq \tilde{T}_{B5} \leq \tilde{T}_{B5}^+ \tag{7.139}$$

with

$$\tilde{T}_{B5}^{\pm} = \frac{1}{2}\left(m_5^2 - Q_{34}^2 - S \pm \lambda^{1/2}\left(S, Q_{34}^2, m_5^2\right)\right) \tag{7.140}$$

Finally the limits for Q_{34}^2 are given by

$$(m_3 + m_4)^2 \leq Q_{34}^2 \leq \left(\sqrt{S} - m_5\right)^2 \tag{7.141}$$

Alternative kinematics   Alternatively we can change the invariants into other hadronic kinematic variables. For this example the 1PI kinematics will be used with the transverse momentum $(p_{T,5})$ and rapidity (y_5) variables of the fifth particle. We can write these in terms of the invariants as:

$$p_{T,5}^2 = \frac{\tilde{T}_{A5}\tilde{T}_{B5}}{S} - m_5^2 \tag{7.142}$$

$$y_5 = \frac{1}{2}\log\left(\frac{\tilde{T}_{A5}}{\tilde{T}_{B5}}\right) \tag{7.143}$$

If we inverse these changes in variables this results in:

$$\tilde{T}_{A5} = -\sqrt{S}\sqrt{p_{T,5}^2 + m_5^2}\,e^{y_5} \tag{7.144}$$

$$\tilde{T}_{A5} = -\sqrt{S}\sqrt{p_{T,5}^2 + m_5^2}\,e^{-y_5} \tag{7.145}$$

This leads to a Jacobian

$$|\det(J)| = 2Sp_{T,5} \tag{7.146}$$

This set of variables leads to the integration limits:

$$S + \tilde{T}_{A5} + \tilde{T}_{B5} + m_5^2 \geq Q_{34}^2 \geq (m_3 + m_4)^2 \tag{7.147}$$

where $\tilde{T}_{A5}$ and $\tilde{T}_{B5}$ are defined by means of $p_{T,5}$ and y_5. The remaining limits are given by:

$$\left[\frac{\left(S + m_5^2 - (m_3 + m_4)^2 \right)^2}{4S \cosh^2 (y_5)} - m_5^2 \right]^{1/2} \geq p_{T,5} \geq 0 \tag{7.148}$$

and

$$\frac{S + m_5^2 - (m_3 + m_4)^2}{2\sqrt{S} m_5} \geq \cosh (y_5) \tag{7.149}$$

Alternatively we can define the limits in the opposite order

$$\frac{S + m_5^2 - (m_3 + m_4)^2}{2\sqrt{S}\sqrt{p_{T,5}^2 + m_5^2}} \geq \cosh (y_5) \tag{7.150}$$

and

$$\left[\frac{\left(S + m_5^2 - (m_3 + m_4)^2 \right)^2}{4S} - m_5^2 \right]^{1/2} \geq p_{T,5} \geq 0 \tag{7.151}$$

The advantage of these kinematic variables is that they allow us to directly calculate differential distributions. These kinematics can be used in in similar manner for the secondary kinematics of 2PI, but with the momenta of particle 5 replaced with intermediate state 34.

8 Conclusion and Discussion

Gluon-induced Higgs strahlung For $gg \to ZH$ we explored two different approaches to threshold for the soft-gluon resummation: absolute threshold (M-approach) and invariant mass threshold (Q-approach). In the Q-approach logarithms relative to the threshold of the production of a ZH pair with invariant mass Q are resummed and in the M-approach logarithms relative to the absolute production threshold of the ZH system with a total mass $M = m_H + m_Z$ are resummed. Of these, it was argued that the Q-approach is the more stable and more "natural" choice due to the more appropriate choice of the renormalization and factorization scale: $\mu_R = \mu_F = Q$.

After the inclusion of the resummation corrections, the NLO+NLL result showed a strongly reduced scale dependence relative to the NLO result. In addition the central value was increased. The stability with respect to higher order corrections was checked through means of NNLL corrections. These points motivate the re-evaluation of the total inclusive $pp \to ZH$ cross section, including all the previously known NNLO corrections. The central value of the new prediction for $pp \to ZH$ is slightly larger than the value that is currently suggested by LHC-HXSWG [17] and the theoretical uncertainty due to the scale variation is reduced by roughly a factor of two.

The main source of uncertainty for the gluon-induced ZH production process is the validity of the heavy top mass limit used for the NLO corrections. Specifically it may not hold well in the boosted Higgs, $p_{T,H} > 200$ GeV, which is of some experimental interest. However, the main way to determine this precision would be by completing the full computation, which is beyond the current capabilities of the fixed order calculations.

Squark and gluino production For the squark and gluino production processes, we have studied the inclusion of absolute threshold logarithmic corrections up to the NNLL order in resummation. This includes the one loop hard matching coefficient and Coulomb corrections up to the second order. The inclusion of these correction resulted in a significant increase in the inclusive cross section, which will shift the current experimental SUSY mass exclusion limits to higher values.

In addition, the scale dependence around the central value has decreased for most processes. The only exception is gluino pair production. This increase in scale dependence can be traced back to two contributions. In the low scale region, this can be explained by the Coulomb corrections and for high scales this is due to the the scale dependent terms in the resummed exponential. The reason this effect is dominant for gluino production is likely due to the large color factors involved in this process, making the resummation more important. This could also potentially be partially caused by the incompleteness of the two-loop matching coefficient. In order to test this theory the full NNLO result would need to be computed first.

Further studies can be done on the inclusion of Coulomb resummation by performing the Mellin transform numerically. In addition other bound state effects can also be included. Once the results for the full computation are complete a public code can be created as an update to

`NLL-fast`. This will allow the major experiments easy access to the numbers for use for the latest Run 2 SUSY results. Finally a full study to compare the results with the SCET collaboration [78,79] can be done in order to confirm the validity of both results and to see agreement between the different methods.

Three particle final state processes   In the final project we aimed to extend the general resummation from the case of a $2 \to 2$ process to $2 \to 3$ processes. The demonstration of this was done by means of the absolute threshold resummation for the process $pp \to t\bar{t}H$. For this process there are small corrections to the total inclusive cross section. The size of these corrections and the reduction of the scale dependence is strongly influenced by the inclusion of the first order matching coefficients. The total scale uncertainty is reduced by a modest amount after the resummation with the one-loop matching coefficients are included.

In addition the theoretical framework for the resummation of differential cross sections was presented. Here three different types of threshold parameters were presented that allow for differential distributions in different kinematic variables. Additional studies need to be performed for the numerical behavior of this framework in order to obtain final numerical results for a specific process.

For the absolute threshold resummation of $t\bar{t}H$ further studies can go into the computation of the virtual correction split up into color channels in order to compute the color split hard matching coefficients for the gluon initial state, though the expected differences to the cross section are small. The resummed exponential can be increased to include NNLL effects. Finally, higher order Coulomb or even Coulomb resummation can be included.

Closing remarks   The method that has been the focus of this thesis is soft-gluon resummation, which takes into account the dominant logarithmic terms near threshold. Different definitions of the threshold variable can be used for the resummation and the main focus has been absolute threshold and invariant mass threshold. The resummation techniques have been applied to three types of processes: $gg \to ZH$, squark and gluino production and $2 \to 3$ type processes. The precision for both the $gg \to ZH$ and the squark and gluino production cross sections has been improved. In addition we have successfully performed the absolute threshold resummation for a $2 \to 3$ process in the Mellin space formalism and established the theoretical framework for the computation of resummation for differential cross section in different threshold limits.

Bibliography

[1] S. Weinberg, *A Model of Leptons*, Phys. Rev. Lett. **19** (1967) 1264.

[2] S. L. Glashow, *Partial Symmetries of Weak Interactions*, Nucl. Phys. **22** (1961) 579.

[3] A. Salam, *Weak and Electromagnetic Interactions*, Conf. Proc. C **680519** (1968) 367.

[4] H. Fritzsch, M. Gell-Mann and H. Leutwyler, *Advantages of the Color Octet Gluon Picture*, Phys. Lett. B **47** (1973) 365.

[5] D. J. Gross and F. Wilczek, *Asymptotically Free Gauge Theories. 1*, Phys. Rev. D **8** (1973) 3633.

[6] S. Weinberg, *Nonabelian Gauge Theories of the Strong Interactions*, Phys. Rev. Lett. **31** (1973) 494.

[7] P. W. Higgs, *Broken Symmetries and the Masses of Gauge Bosons*, Phys. Rev. Lett. **13** (1964) 508.

[8] F. Englert and R. Brout, *Broken Symmetry and the Mass of Gauge Vector Mesons*, Phys. Rev. Lett. **13** (1964) 321.

[9] G. S. Guralnik, C. R. Hagen and T. W. B. Kibble, *Global Conservation Laws and Massless Particles*, Phys. Rev. Lett. **13** (1964) 585.

[10] G. Aad *et al.* [ATLAS Collaboration], *Observation of a new particle in the search for the Standard Model Higgs boson with the ATLAS detector at the LHC*, Phys. Lett. B **716** (2012) 1 [arXiv:1207.7214 [hep-ex]].

[11] S. Chatrchyan *et al.* [CMS Collaboration], *Observation of a new boson at a mass of 125 GeV with the CMS experiment at the LHC*, Phys. Lett. B **716** (2012) 30 [arXiv:1207.7235 [hep-ex]].

[12] J. Wess and B. Zumino, *A Lagrangian Model Invariant Under Supergauge Transformations*, Phys. Lett. B **49** (1974) 52.

[13] H. P. Nilles, *Supersymmetry, Supergravity and Particle Physics*, Phys. Rept. **110** (1984) 1.

[14] S. Dittmaier *et al.* [LHC Higgs Cross Section Working Group Collaboration], *Handbook of LHC Higgs Cross Sections: 1. Inclusive Observables*, arXiv:1101.0593 [hep-ph].

[15] S. Dittmaier, C. Mariotti, G. Passarino, R. Tanaka, S. Alekhin, J. Alwall and E. A. Bagnaschi *et al.*, *Handbook of LHC Higgs Cross Sections: 2. Differential Distributions*, arXiv:1201.3084 [hep-ph].

[16] S. Heinemeyer *et al.* [LHC Higgs Cross Section Working Group Collaboration], *Handbook of LHC Higgs Cross Sections: 3. Higgs Properties*, arXiv:1307.1347 [hep-ph].

[17] `https://twiki.cern.ch/twiki/bin/view/LHCPhysics/LHCHXSWG`

[18] V. Khachatryan *et al.* [CMS Collaboration], *Precise determination of the mass of the Higgs boson and tests of compatibility of its couplings with the standard model predictions using proton collisions at 7 and 8 TeV*, arXiv:1412.8662 [hep-ex].

[19] G. Aad *et al.* [ATLAS Collaboration], *Measurement of Higgs boson production in the diphoton decay channel in pp collisions at center-of-mass energies of 7 and 8 TeV with the ATLAS detector*, Phys. Rev. D **90** (2014) 11, 112015 [arXiv:1408.7084 [hep-ex]].

[20] G. Aad *et al.* [ATLAS Collaboration], *Measurements of Higgs boson production and couplings in the four-lepton channel in pp collisions at center-of-mass energies of 7 and 8 TeV with the ATLAS detector*, Phys. Rev. D **91** (2015) 1, 012006 [arXiv:1408.5191 [hep-ex]].

[21] G. Aad *et al.* [ATLAS Collaboration], *Observation and measurement of Higgs boson decays to WW^* with the ATLAS detector*, arXiv:1412.2641 [hep-ex].

[22] G. Aad *et al.* [ATLAS Collaboration], *Search for the $b\bar{b}$ decay of the Standard Model Higgs boson in associated $(W/Z)H$ production with the ATLAS detector*, JHEP **1501** (2015) 069 [arXiv:1409.6212 [hep-ex]].

[23] G. Aad *et al.* [ATLAS Collaboration], *Evidence for the Higgs-boson Yukawa coupling to tau leptons with the ATLAS detector*, arXiv:1501.04943 [hep-ex].

[24] T. Han and S. Willenbrock, *QCD correction to the $pp \rightarrow WH$ and ZH total cross-sections* Phys. Lett. B **273** (1991) 167.

[25] H. Baer, B. Bailey and J. F. Owens, *$\mathcal{O}(\alpha_s)$ Monte Carlo approach to $W + Higgs$ associated production at hadron supercolliders*, Phys. Rev. D **47** (1993) 2730.

[26] J. Ohnemus and W. J. Stirling, *Order α_s corrections to the differential cross-section for the WH intermediate mass Higgs signal*, Phys. Rev. D **47** (1993) 2722.

[27] R. Hamberg, W. L. van Neerven and T. Matsuura, *A Complete calculation of the order α_s^2 correction to the Drell-Yan K factor*, Nucl. Phys. B **359** (1991) 343 [Erratum-ibid. B **644** (2002) 403].

[28] R. V. Harlander and W. B. Kilgore, *Next-to-next-to-leading order Higgs production at hadron colliders*, Phys. Rev. Lett. **88** (2002) 201801 [hep-ph/0201206].

[29] O. Brein, A. Djouadi and R. Harlander, *NNLO QCD corrections to the Higgs-strahlung processes at hadron colliders*, Phys. Lett. B **579** (2004) 149 [hep-ph/0307206].

[30] O. Brein, R. Harlander, M. Wiesemann and T. Zirke, *Top-Quark Mediated Effects in Hadronic Higgs-Strahlung*, Eur. Phys. J. C **72** (2012) 1868 [arXiv:1111.0761 [hep-ph]].

[31] M. L. Ciccolini, S. Dittmaier and M. Krämer, *Electroweak radiative corrections to associated WH and ZH production at hadron colliders*, Phys. Rev. D **68** (2003) 073003 [hep-ph/0306234].

[32] L. Altenkamp, S. Dittmaier, R. V. Harlander, H. Rzehak and T. J. E. Zirke, *Gluon-induced Higgs-strahlung at next-to-leading order QCD*, JHEP **1302** (2013) 078 [arXiv:1211.5015 [hep-ph]].

[33] Z. Kunszt, *Associated Production of Heavy Higgs Boson with Top Quarks*, Nucl. Phys. B **247** (1984) 339.

[34] J. F. Gunion, *Associated top anti-top Higgs production as a large source of W H events: Implications for Higgs detection in the lepton neutrino gamma gamma final state*, Phys. Lett. B **261** (1991) 510.

[35] W. J. Marciano and F. E. Paige, *Associated production of Higgs bosons with t anti-t pairs*, Phys. Rev. Lett. **66** (1991) 2433.

[36] W. Beenakker, S. Dittmaier, M. Krämer, B. Plumper, M. Spira and P. M. Zerwas, *Higgs radiation off top quarks at the Tevatron and the LHC*, Phys. Rev. Lett. **87** (2001) 201805 [hep-ph/0107081].

[37] W. Beenakker, S. Dittmaier, M. Krämer, B. Plumper, M. Spira and P. M. Zerwas, *NLO QCD corrections to t anti-t H production in hadron collisions*, Nucl. Phys. B **653** (2003) 151 [hep-ph/0211352].

[38] L. Reina and S. Dawson, *Next-to-leading order results for t anti-t h production at the Tevatron*, Phys. Rev. Lett. **87** (2001) 201804 [hep-ph/0107101].

[39] S. Dawson, L. H. Orr, L. Reina and D. Wackeroth, *Associated top quark Higgs boson production at the LHC*, Phys. Rev. D **67** (2003) 071503 [hep-ph/0211438].

[40] R. Frederix, S. Frixione, V. Hirschi, F. Maltoni, R. Pittau and P. Torrielli, *Scalar and pseudoscalar Higgs production in association with a top-antitop pair*, Phys. Lett. B **701** (2011) 427 [arXiv:1104.5613 [hep-ph]].

[41] M. V. Garzelli, A. Kardos, C. G. Papadopoulos and Z. Trocsanyi, *Standard Model Higgs boson production in association with a top anti-top pair at NLO with parton showering*, Europhys. Lett. **96** (2011) 11001 [arXiv:1108.0387 [hep-ph]].

[42] H. B. Hartanto, B. Jager, L. Reina and D. Wackeroth, *Higgs boson production in association with top quarks in the POWHEG BOX*, arXiv:1501.04498 [hep-ph].

[43] S. Frixione, V. Hirschi, D. Pagani, H. S. Shao and M. Zaro, *Weak corrections to Higgs hadroproduction in association with a top-quark pair*, JHEP **1409** (2014) 065 [arXiv:1407.0823 [hep-ph]].

[44] Y. Zhang, W. G. Ma, R. Y. Zhang, C. Chen and L. Guo, *QCD NLO and EW NLO corrections to $t\bar{t}H$ production with top quark decays at hadron collider*, Phys. Lett. B **738** (2014) 1 [arXiv:1407.1110 [hep-ph]].

[45] S. P. Martin, *A Supersymmetry primer*, Adv. Ser. Direct. High Energy Phys. **21** (2010) 1 [hep-ph/9709356].

[46] J. Ellis, J. R. Espinosa, G. F. Giudice, A. Hoecker and A. Riotto, *The Probable Fate of the Standard Model*, Phys. Lett. B **679** (2009) 369 [arXiv:0906.0954 [hep-ph]].

[47] J. Elias-Miro, J. R. Espinosa, G. F. Giudice, G. Isidori, A. Riotto and A. Strumia, *Higgs mass implications on the stability of the electroweak vacuum*, Phys. Lett. B **709** (2012) 222 [arXiv:1112.3022 [hep-ph]].

[48] G. Degrassi, S. Di Vita, J. Elias-Miro, J. R. Espinosa, G. F. Giudice, G. Isidori and A. Strumia, *Higgs mass and vacuum stability in the Standard Model at NNLO*, JHEP **1208** (2012) 098 [arXiv:1205.6497 [hep-ph]].

[49] U. Amaldi, W. de Boer and H. Furstenau, *Comparison of grand unified theories with electroweak and strong coupling constants measured at LEP*, Phys. Lett. B **260** (1991) 447.

[50] R. Haag, J. T. Lopuszanski and M. Sohnius, *All Possible Generators of Supersymmetries of the s Matrix*, Nucl. Phys. B **88** (1975) 257.

[51] S. R. Coleman and J. Mandula, *All Possible Symmetries of the S Matrix*, Phys. Rev. **159** (1967) 1251.

[52] G. Aad *et al.* [ATLAS Collaboration], *Search for squarks and gluinos with the ATLAS detector in final states with jets and missing transverse momentum using $\sqrt{s} = 8$ TeV proton–proton collision data*, JHEP **1409** (2014) 176 [arXiv:1405.7875 [hep-ex]].

[53] S. Chatrchyan *et al.* [CMS Collaboration], *Search for supersymmetry in hadronic final states with missing transverse energy using the variables α_T and b-quark multiplicity in pp collisions at $\sqrt{s} = 8$ TeV*, Eur. Phys. J. C **73** (2013) 9, 2568 [arXiv:1303.2985 [hep-ex]].

[54] M. Krämer, A. Kulesza, R. van der Leeuw, M. Mangano, S. Padhi, T. Plehn and X. Portell, *Supersymmetry production cross sections in pp collisions at $\sqrt{s} = 7$ TeV*, arXiv:1206.2892 [hep-ph].

[55] http://pauli.uni-muenster.de/~akule_01/nllwiki/index.php/NLL-fast

[56] W. Beenakker, R. Hopker, M. Spira and P. M. Zerwas, *Squark and gluino production at hadron colliders*, Nucl. Phys. B **492** (1997) 51 [hep-ph/9610490].

[57] W. Beenakker, M. Krämer, T. Plehn, M. Spira and P. M. Zerwas, *Stop production at hadron colliders*, Nucl. Phys. B **515** (1998) 3 [hep-ph/9710451].

[58] W. Beenakker, M. Klasen, M. Krämer, T. Plehn, M. Spira and P. M. Zerwas, *The Production of charginos / neutralinos and sleptons at hadron colliders*, Phys. Rev. Lett. **83** (1999) 3780 [Erratum-ibid. **100** (2008) 029901] [hep-ph/9906298].

[59] M. Spira, *Higgs and SUSY particle production at hadron colliders*, hep-ph/0211145.

[60] T. Plehn, *Measuring the MSSM Lagrangean*, Czech. J. Phys. **55** (2005) B213 [hep-ph/0410063].

[61] W. Beenakker, R. Hopker, M. Spira and P. M. Zerwas, *Squark production at the Tevatron*, Phys. Rev. Lett. **74** (1995) 2905 [hep-ph/9412272].

[62] W. Beenakker, R. Hopker, M. Spira and P. M. Zerwas, *Gluino pair production at the Tevatron*, Z. Phys. C **69** (1995) 163 [hep-ph/9505416].

[63] A. Kulesza and L. Motyka, *Threshold resummation for squark-antisquark and gluino-pair production at the LHC*, Phys. Rev. Lett. **102** (2009) 111802 [arXiv:0807.2405 [hep-ph]].

[64] A. Kulesza and L. Motyka, *Soft gluon resummation for the production of gluino-gluino and squark-antisquark pairs at the LHC*, Phys. Rev. D **80** (2009) 095004 [arXiv:0905.4749 [hep-ph]].

[65] W. Beenakker, S. Brensing, M. Krämer, A. Kulesza, E. Laenen and I. Niessen, *Soft-gluon resummation for squark and gluino hadroproduction*, JHEP **0912** (2009) 041 [arXiv:0909.4418 [hep-ph]].

[66] W. Beenakker, S. Brensing, M. Krämer, A. Kulesza, E. Laenen and I. Niessen, *Supersymmetric top and bottom squark production at hadron colliders*, JHEP **1008** (2010) 098 [arXiv:1006.4771 [hep-ph]].

[67] W. Beenakker, S. Brensing, M. n. Krämer, A. Kulesza, E. Laenen, L. Motyka and I. Niessen, *Squark and Gluino Hadroproduction*, Int. J. Mod. Phys. A **26** (2011) 2637 [arXiv:1105.1110 [hep-ph]].

[68] W. Beenakker, T. Janssen, S. Lepoeter, M. Krämer, A. Kulesza, E. Laenen, I. Niessen and S. Thewes *et al.*, *Towards NNLL resummation: hard matching coefficients for squark and gluino hadroproduction*, JHEP **1310** (2013) 120 [arXiv:1304.6354 [hep-ph]].

[69] M. Beneke, P. Falgari and C. Schwinn, *Threshold resummation for pair production of coloured heavy (s)particles at hadron colliders*, Nucl. Phys. B **842** (2011) 414 [arXiv:1007.5414 [hep-ph]].

[70] P. Falgari, C. Schwinn and C. Wever, *NLL soft and Coulomb resummation for squark and gluino production at the LHC*, JHEP **1206** (2012) 052 [arXiv:1202.2260 [hep-ph]].

[71] U. Langenfeld and S. O. Moch, *Higher-order soft corrections to squark hadroproduction*, Phys. Lett. B **675** (2009) 210 [arXiv:0901.0802 [hep-ph]].

[72] U. Langenfeld, S. O. Moch and T. Pfoh, *QCD threshold corrections for gluino pair production at hadron colliders*, JHEP **1211** (2012) 070 [arXiv:1208.4281 [hep-ph]].

[73] W. Beenakker, S. Brensing, M. Krämer, A. Kulesza, E. Laenen and I. Niessen, *NNLL resummation for squark-antisquark pair production at the LHC*, JHEP **1201** (2012) 076 [arXiv:1110.2446 [hep-ph]].

[74] T. Pfoh, *Phenomenology of QCD threshold resummation for gluino pair production at NNLL*, JHEP **1305** (2013) 044 [Erratum-ibid. **1310** (2013) 090] [arXiv:1302.7202 [hep-ph]].

[75] A. Broggio, A. Ferroglia, M. Neubert, L. Vernazza and L. L. Yang, *NNLL Momentum-Space Resummation for Stop-Pair Production at the LHC*, JHEP **1403** (2014) 066 [arXiv:1312.4540 [hep-ph]].

[76] P. Falgari, C. Schwinn and C. Wever, *Finite-width effects on threshold corrections to squark and gluino production*, JHEP **1301** (2013) 085 [arXiv:1211.3408 [hep-ph]].

[77] W. Beenakker, C. Borschensky, M. Krämer, A. Kulesza, E. Laenen, V. Theeuwes and S. Thewes, *NNLL resummation for squark and gluino production at the LHC*, JHEP **1412** (2014) 023 [arXiv:1404.3134 [hep-ph]].

[78] M. Beneke, P. Falgari, J. Piclum, C. Schwinn and C. Wever, *Higher-order soft and Coulomb corrections to squark and gluino production at the LHC*, PoS RADCOR **2013** (2013) 051 [arXiv:1312.0837 [hep-ph]].

[79] M. Beneke, P. Falgari, J. Piclum, C. Schwinn and C. Wever, *Higher-order soft and Coulomb corrections to squark and gluino production at the LHC*, PoS LL **2014** (2014) 060.

[80] S. Catani and L. Trentadue, *Resummation of the QCD Perturbative Series for Hard Processes*, Nucl. Phys. B **327** (1989) 323.

[81] G. Luisoni and S. Marzani, *QCD resummation for hadronic final states*, arXiv:1505.04084 [hep-ph].

[82] H. Contopanagos, E. Laenen and G. F. Sterman, *Sudakov factorization and resummation*, Nucl. Phys. B **484** (1997) 303 [hep-ph/9604313].

[83] R. K. Ellis, W. J. Stirling and B. R. Weber, *QCD and Collider Physics*, (Cambridge University Press, 1996)

[84] G. F. Sterman, *Summation of Large Corrections to Short Distance Hadronic Cross-Sections*, Nucl. Phys. B **281** (1987) 310.

[85] L. Magnea, *All Order Summation and Two Loop Results for the Drell-Yan Cross-section*, Nucl. Phys. B **349** (1991) 703.

[86] J. Kodaira and L. Trentadue, *Summing Soft Emission in QCD*, Phys. Lett. B **112** (1982) 66.

[87] N. Kidonakis, G. Oderda and G. F. Sterman, *Threshold resummation for dijet cross-sections*, Nucl. Phys. B **525** (1998) 299 [hep-ph/9801268].

[88] N. Kidonakis and G. F. Sterman, *Resummation for QCD hard scattering*, Nucl. Phys. B **505** (1997) 321 [hep-ph/9705234].

[89] N. Kidonakis, E. Laenen, S. Moch and R. Vogt, *Sudakov resummation and finite order expansions of heavy quark hadroproduction cross-sections*, Phys. Rev. D **64** (2001) 114001 [hep-ph/0105041].

[90] N. Kidonakis, *Resummation for heavy quark and jet cross-sections*, Int. J. Mod. Phys. A **15** (2000) 1245 [hep-ph/9902484].

[91] S. Catani, D. de Florian, M. Grazzini and P. Nason, *Soft gluon resummation for Higgs boson production at hadron colliders*, JHEP **0307** (2003) 028 [hep-ph/0306211].

[92] S. Catani, M. L. Mangano, P. Nason and L. Trentadue, *The Resummation of soft gluons in hadronic collisions*, Nucl. Phys. B **478** (1996) 273 [hep-ph/9604351].

[93] A. Vogt, *Efficient evolution of unpolarized and polarized parton distributions with QCD-PEGASUS*, Comput. Phys. Commun. **170** (2005) 65 [hep-ph/0408244].

[94] A. D. Martin, W. J. Stirling, R. S. Thorne and G. Watt, *Parton distributions for the LHC*, Eur. Phys. J. C **63** (2009) 189 [arXiv:0901.0002 [hep-ph]].

[95] R. D. Ball *et al.* [NNPDF Collaboration], *Parton distributions for the LHC Run II*, JHEP **1504** (2015) 040 [arXiv:1410.8849 [hep-ph]].

[96] A. Kulesza, G. F. Sterman and W. Vogelsang, *Joint resummation in electroweak boson production*, Phys. Rev. D **66** (2002) 014011 [hep-ph/0202251].

[97] R. V. Harlander, A. Kulesza, V. Theeuwes and T. Zirke, *Soft gluon resummation for gluon-induced Higgs Strahlung*, JHEP **1411** (2014) 082 [arXiv:1410.0217 [hep-ph]].

[98] D. de Florian and M. Grazzini, *Higgs production through gluon fusion: Updated cross sections at the Tevatron and the LHC*, Phys. Lett. B **674** (2009) 291 [arXiv:0901.2427 [hep-ph]].

[99] D. de Florian and M. Grazzini, *Higgs production at the LHC: updated cross sections at $\sqrt{s} = 8$ TeV*, Phys. Lett. B **718** (2012) 117 [arXiv:1206.4133 [hep-ph]].

[100] S. Catani and M. H. Seymour, *A General algorithm for calculating jet cross-sections in NLO QCD*, Nucl. Phys. B **485** (1997) 291 [Erratum-ibid. B **510** (1998) 503] [hep-ph/9605323].

[101] O. Brein, R. V. Harlander and T. J. E. Zirke, *vh@nnlo - Higgs Strahlung at hadron colliders*, Comput. Phys. Commun. **184** (2013) 998 [arXiv:1210.5347 [hep-ph]].

[102] M. Beneke, P. Falgari and C. Schwinn, *Soft radiation in heavy-particle pair production: All-order colour structure and two-loop anomalous dimension*, Nucl. Phys. B **828** (2010) 69 [arXiv:0907.1443 [hep-ph]].

[103] S. Catani, S. Dittmaier, M. H. Seymour and Z. Trocsanyi, *The Dipole formalism for next-to-leading order QCD calculations with massive partons*, Nucl. Phys. B **627** (2002) 189 [hep-ph/0201036].

[104] M. J. Strassler and M. E. Peskin, *The Heavy top quark threshold: QCD and the Higgs*, Phys. Rev. D **43** (1991) 1500.

[105] M. R. Kauth, A. Kress and J. H. Kuhn, *Gluino-Squark Production at the LHC: The Threshold*, JHEP **1112** (2011) 104 [arXiv:1108.0542 [hep-ph]].

[106] M. Beneke, M. Czakon, P. Falgari, A. Mitov and C. Schwinn, *Threshold expansion of the $gg(q\bar{q}) \rightarrow Q\bar{Q} + X$ cross section at $\mathcal{O}(\alpha_s 4)$*, Phys. Lett. B **690** (2010) 483 [arXiv:0911.5166 [hep-ph]].

[107] J. R. Ellis and S. Rudaz, *Search for Supersymmetry in Toponium Decays*, Phys. Lett. B **128** (1983) 248.

[108] J. Beringer *et al.* [Particle Data Group Collaboration], *Review of Particle Physics (RPP)*, Phys. Rev. D **86** (2012) 010001.

[109] R. Bonciani, S. Catani, M. L. Mangano and P. Nason, *Sudakov resummation of multiparton QCD cross-sections*, Phys. Lett. B **575** (2003) 268 [hep-ph/0307035].

[110] S. M. Aybat, L. J. Dixon and G. F. Sterman, *The Two-loop anomalous dimension matrix for soft gluon exchange*, Phys. Rev. Lett. **97** (2006) 072001 [hep-ph/0606254].

[111] S. M. Aybat, L. J. Dixon and G. F. Sterman, *The Two-loop soft anomalous dimension matrix and resummation at next-to-next-to leading pole*, Phys. Rev. D **74** (2006) 074004 [hep-ph/0607309].

[112] T. van Ritbergen, A. N. Schellekens and J. A. M. Vermaseren, *Group theory factors for Feynman diagrams*, Int. J. Mod. Phys. A **14** (1999) 41 [hep-ph/9802376].

[113] J. Kuipers, T. Ueda, J. A. M. Vermaseren and J. Vollinga, *FORM version 4.0*, Comput. Phys. Commun. **184** (2013) 1453 [arXiv:1203.6543 [cs.SC]].

[114] J. Alwall *et al.*, *The automated computation of tree-level and next-to-leading order differential cross sections, and their matching to parton shower simulations*, JHEP **1407** (2014) 079 [arXiv:1405.0301 [hep-ph]].

[115] A. Kulesza, L. Motyka, T. Stebel and V. Theeuwes, *Soft gluon resummation for associated $t\bar{t}H$ production at the LHC*, arXiv:1509.02780 [hep-ph].

[116] L. A. Harland-Lang, A. D. Martin, P. Motylinski and R. S. Thorne, *Parton distributions in the LHC era: MMHT 2014 PDFs*, Eur. Phys. J. C **75** (2015) 5, 204 [arXiv:1412.3989 [hep-ph]].

[117] M. Czakon and A. Mitov, *On the Soft-Gluon Resummation in Top Quark Pair Production at Hadron Colliders*, Phys. Lett. B **680** (2009) 154 [arXiv:0812.0353 [hep-ph]].

Acknowledgments

Curriculum Vitae

Personal Information

Name: Vincent Michel Theeuwes
Place and date of birth: Nijmegen, July 18 1988
Nationality: Dutch

Education

November 2012 - now
PhD in Physics, *Institute for Theoretical Physics, WWU Münster*, Germany.
Thesis Supervisor: Jun. Prof. Dr. Anna Kulesza
Thesis Subject: Soft Gluon Resummation for Heavy Particle Production at the LHC
Main focus: Soft-gluon resummation for different processes

2010 - 2012
Master Physics and Astronomy, *Radboud University Nijmegen*, The Netherlands.
Cum Laude
Thesis Supervisor: Prof. Dr. Wim Beenakker
Thesis Subject: Radiative corrections to the dark matter relic density.
Main focus: Massive Sommerfeld and Sudakov corrections

July 2011 - September 2011
Summer Student, *CERN*, Geneva, Switzerland.
Supervisors: Dr. Nicola Giacinto Piacquadio and Dr. Andrea Messina
Subject: Testing next to leading order simulators for production of W-boson and two b-quarks

2007 - 2010
Bachelor Physics and Astronomy, *Radboud University Nijmegen*, The Netherlands.
Thesis Supervisor: Prof. Dr. Nicolo de Groot
Thesis Subject: Majorana neutrinos at the LHC.
Main focus: Monte Carlo simulator to calculate the cross section of a process involving a Majorana neutrino.

2000 - 2007
Bilingual VWO, *Kandinsky College*, Nijmegen, The Netherlands.
Bilingual in English and Dutch
VWO is the highest level of middle and high school in the Netherlands